INTEGRATING MASS SPECTROMETRY AND COMPUTATIONAL CHEMISTRY

INTEGRATING MASS SPECTROMETRY AND COMPUTATIONAL CHEMISTRY : A STUDY OF DISSOCIATION REACTIONS OF RADICAL CATIONS IN THE GAS PHASE

By

Richard Lee, B. Sc.

A Thesis

Submitted to the School of Graduate Studies

In Partial Fulfillment of the Requirements

for the Degree

Master of Science

McMaster University

MASTER OF SCIENCE
(Chemistry)

McMaster University
Hamilton, Ontario

TITLE : Integrating mass spectrometry and computational chemistry : a study of dissociation reactions of radical cations in the gas phase.

AUTHOR : Richard Lee (McMaster University)

SUPERVISOR : Dr. Johan K. Terlouw

NUMBER OF PAGES : x, 104

ABSTRACT

The organic ions studied in this thesis were generated in the rarefied gas phase of the mass spectrometer by electron ionization of selected precursor molecules. The characterization of their structure and reactivity was probed by using a variety of tandem mass spectrometry techniques. These include metastable ion spectra to probe the dissociation chemistry of the low energy ions and collision experiments to establish the atom connectivity of the ions. The technique of neutralization-reionization mass spectrometry (NRMS) was used to probe the structure and stability of the neutral counterparts of the ions. Computational results involving the CBS-QB3 model chemistry formed an integral component in the interpretation of the experimental findings.

The above approach was used to study proton-transport catalysis in the formaldehyde elimination from low energy 1,3-dihydroxyacetone radical cations. Solitary ketene-water ions, $CH_2=C(=O)OH_2^{\bullet+}$, do not readily isomerize into its more stable isomer, $CH_2=C(OH)_2^{\bullet+}$. A mechanistic analysis using the CBS-QB3 model chemistry shows that metastable 1,3-dihydroxyacetone radical cations will rearrange into hydrogen-bridged radical cations $[CH_2C(=O)O(H)\text{–}H\bullet\bullet\bullet OCH_2]^{\bullet+}$, where the $CH_2=O$ will catalyze the transformation of $CH_2=C(=O)OH_2^{\bullet+}$ into $CH_2=C(OH)_2^{\bullet+}$.

Metastable pyruvic acid radical cations, $CH_3C(=O)COOH^{\bullet+}$, have been shown to undergo decarboxylation to yield m/z 44 ions, $C_2H_4O^{\bullet+}$, in competition with the formation of $CH_3C{\equiv}O^+ + COOH^{\bullet}$ by direct bond cleavage. Collision induced dissociation experiments agree with an earlier report that oxycarbene ions $CH_3COH^{\bullet+}$ are formed but they also suggest the more stable isomer $CH_3C(H)=O^{\bullet+}$ may be co-generated. Using the CBS-QB3 model chemistry, a mechanism is proposed to rationalize these results.

Next, the isomeric ions $CH_3O\text{-}P=S^{\bullet+}$ and $CH_3S\text{-}P=O^{\bullet+}$ were characterized and differentiated by tandem mass spectrometry. Metastable $CH_3O\text{-}P=S^{\bullet+}$ and $CH_3S\text{-}P=O^{\bullet+}$ ions both spontaneously lose water to yield m/z 74 cyclic product ion $[\text{-}S\text{-}CH=]P^{\bullet+}$. Using the CBS-QB3 model chemistry a mechanism is proposed for the water loss from $CH_3O\text{-}P=S^{\bullet+}$

and $CH_3S\text{-}P{=}O^{\bullet+}$. Our calculations also show that these two isomers communicate via a common intermediate, the distonic ion $CH_2S\text{-}P\text{-}OH^{\bullet+}$, prior to the loss of water.

The final component of this work details the computational study addressing the long standing question on the mechanism for the water elimination from metastable ethyl acetate radical cations. The CBS-QB3 results show that low energy ethyl acetate ions isomerize into ionized 4-hydroxy-2-butanone prior to the loss of water.

ACKNOWLEDGEMENTS

A number of people have been part of my graduate studies as friends and teachers. First and foremost, I would like to thank my supervisor, Prof. Terlouw. He is a brilliant and passionate professor who is dedicated to the work of his graduate students. Prof. Terlouw, thank you for believing in me and for always guiding me down the right path.

I would also like to thank our collaborators, Dr. P.C. Burgers and Dr. P.J.A. Ruttink, who have helped in my studies.

In the lab I was surrounded by a number of friendly and knowledgeable faces. I would like to thank the entire Mass Spec Group for their help over the past two years. This includes Kirk Green, Tadek Olech, Leah Allan, Gina Dimopoulos, and Karl Jobst.

I have been lucky to have a number of good friends who have been supportive and encouraged me through some tough times. There are too many to name individually so I thank you all.

Finally, I would like to thank those who are closest to me. To my parents, I am grateful for their love and encouragement that has guided me through the many years. To my sister Jackie and brother-in-law Dave, thank you for having an open ear. Most of all, I would like to thank Karin for all her love and support. I could not imagine going through graduate school without your support.

TABLE OF CONTENTS

LIST OF FIGURES

LIST OF ABBREVIATIONS

B	=	magnetic sector
B3LYP	=	hybrid Hartree-Fock/density functional theory
CCSD(T)	=	coupled cluster singles doubles and triples
CI	=	chemical ionization
CID	=	collision-induced dissociation
CIDI	=	collision-induced dissociative ionization
CBS-QB3	=	complete basis set model chemistry
CBS-APNO	=	complete basis set model chemistry
DFT	=	density functional theory
EI	=	electron ionization
ESA (E)	=	electrostatic analyzer
eV	=	electron Volt (1 eV=23.061 kcal mol^{-1} or 96.487 kJ mol^{-1})
ffr	=	field-free region
G2	=	Gaussian-2 theoretical method
G3	=	Gaussian-3 theoretical method
$\Delta_f H$	=	enthalpy of formation
HF	=	Hartree-Fock
IE	=	ionization energy
KER	=	kinetic energy release
MI	=	metastable ion
MP	=	Möller-Plesset(perturbation theory)
MS	=	mass spectrometry
NDMA	=	N,N-dimethylaniline
m/z	=	mass to charge ratio
NR(MS)	=	neutralization-reionization(mass spectrometry)
PA	=	proton affinity
q	=	charge
r,R	=	radius
T	=	kinetic energy release (value)
TS	=	transition state
ZAB-R	=	BEE three-sector mass spectrometer
ZPVE	=	zero-point vibrational energy

Chapter 1

1.1 Introduction, scope of this thesis

The gas phase ion chemistry described in this thesis focuses on the study of relatively small organic ions. To generate these ionic species a mass spectrometer is used. The techniques used to probe their structure and reactivity are tandem mass spectrometry and computational chemistry. The ions that are generated in the mass spectrometer are radical cations. In certain cases the ions can be generated in the source by direct electron ionization (EI) of its gaseous neutral counterpart. An alternative method to direct EI is dissociative electron ionization of a judiciously selected precursor molecule. An important detail of these experiments is the pressure in the ion source. The source pressure must be kept low to ensure that the ions do not interact with molecules via ion-molecule reactions. This implies that the chemistry and reactivity of the ions is observed in a "solvent-free" environment.

Radical cations generally have stable isomers of conventional or unconventional structure. Radical cations of unconventional structure include the following : (i) distonic ions, where the charge and radical are located on separate atoms within the same ion, (ii) ion-dipole complexes, ionic species which are stabilized by the charge of the ionic component and the dipole of the neutral component and (iii) hydrogen-bridged radical cations (HBRC's), species where the ionic and neutral components interact through a hydrogen bond. The methanol radical cation, $CH_3OH^{\bullet+}$, has a only one stable isomer of unconventional structure : the distonic ion $^{\bullet}CH_2OH_2^{+}$ [**1**]. In contrast, ionized formic acid $H\text{-}C(=O)OH^{\bullet+}$, has four stable isomers : the ion-dipole complex, $[H_2O\bullet\bullet\bullet CO]^{\bullet+}$, the hydrogen-bridged radical cations $[OC\bullet\bullet\bullet H\bullet\bullet\bullet OH]^{\bullet+}$ and $[CO\bullet\bullet\bullet H\bullet\bullet\bullet OH]^{\bullet+}$, and the ionized carbene, $HO\text{-}C\text{-}OH^{\bullet+}$ [**2**].

The radical cations which are generated in the low pressure experiments do not necessarily retain their structure connectivity. The internal energy content of these ions may be so high that isomerization into one or more stable isomers takes place, frequently via a H-shift rearrangement. In contrast, there are many systems where the energy barrier for unimolecular H-shifts are too high for interconversion to another isomer to occur. However, recent studies by our group and other research laboratories have shown that such high rearrangement barriers can be lowered if the ion is allowed to form an encounter complex with a carefully chosen neutral molecule. In our experimental arrangement this is achieved by carrying out the reaction under chemical ionization (CI) conditions, where the source pressure is greater by a factor of c. 10 000 compared to a conventional electron ionization experiment. This reaction, where a single (solvent) molecule assisted isomerization of a given radical cation into a more stable isomer takes place, has been coined "proton-transport catalysis" and is further discussed in detail in Section. 1.

Chapter 2 describes the above situation. It focuses on the metastable dissociation of the 1,3-dihydroxacetone radical cation, $HOCH_2C(=O)CH_2OH^{\bullet+}$. Upon dissociation it yields $C_2H_4O_2^{\bullet+}$ ions via loss of formaldehyde. These ions were determined to have the structure connectivity of the enol of acetic acid, $CH_2=C(OH)_2^{\bullet+}$. Our calculations indicate that the initial complex that is formed is the hydrogen-bridged radical cation $[O=C\text{-}CH_2OH\bullet\bullet\bullet H\bullet\bullet\bullet OCH_2]^{\bullet+}$. Solitary $CH_2=C(=O)OH_2^{\bullet+}$ ions do not readily communicate with their more stable isomer $CH_2=C(OH)_2^{\bullet+}$ because the interconversion barrier lies too high but prior to dissociation, the $CH_2=O$ molecule catalyzes the rearrangement.

Chapter 2 also deals with the dissociation of low-energy (metastable) pyruvic acid radical cations, $CH_3C(=O)\text{-}C(OH)=O^{\bullet+}$. The most prominent reaction is a decarboxylation which yields $C_2H_4O^{\bullet+}$ ions. The identity of these ions was determined to be the ionized carbene $CH_3COH^{\bullet+}$ rather than its more stable isomer $CH_3C(H)=O^{\bullet+}$, ionized acetaldehyde. Our computational study on the mechanism for the dissociation of ionized pyruvic acid suggests that the HBRC $CH_3CO\text{-}H^{\bullet+}\bullet\bullet\bullet O=C=O$ is initially formed. In contrast to the CH_2O mediated isomerization in dihydroxyacetone, the carbon dioxide molecule in the above

HBRC cannot accomodate the transformation of $CH_3COH^{\bullet+}$ into $CH_3C(H)=O^{\bullet+}$. The barrier for the isomerization is significantly lowered but it does not become low enough for efficient proton transport catalysis.

The characterization and behaviour of $CH_3S\text{-}P=O^{\bullet+}$ and $CH_3O\text{-}P=S^{\bullet+}$ is discussed in Chapter 3. Experiments involving collision-induced dissociation (CID) and neutralization-reionization (NR) mass spectrometry are used to probe the structure, stability and reactivity of these ions in the gas phase. Both isomers spontaneously lose H_2O to form the same cyclic product ion, $[\text{-}S\text{-}CH=]P^{\bullet+}$ and computational results suggest that these two ions communicate through a common intermediate. The dehydration reaction of $CH_3S\text{-}P=O^{\bullet+}$ involves a double hydrogen transfer, while the water loss from $CH_3O\text{-}P=S^{\bullet+}$ requires a skeletal rearrangement.

Chapter 4 describes the unimolecular chemistry of the ethyl acetate radical cation and in particular the generation of ionized methyl vinyl ketone, $CH_3C(=O)CH=CH_2^{\bullet+}$ via the spontaneous loss of water from low-energy (metastable) ethyl acetate ions. The mechanism of this reaction has been shrouded in mystery for the past 20 years although a great number of studies have been conducted. It will be shown that this reaction occurs via the potential energy surface of ionized 4-hydroxy-2-butanone, $CH_3C(=O)CH_2CH_2OH^{\bullet+}$. This Chapter is an example of theory and experiment working in concert to elucidate a complex yet transparent mechanism which involves 7 steps to describe the water elimination from ionized ethyl acetate.

The next two sections of this Chapter provides the non-expert reader with the background information on the mass spectrometry based techniques and the computational chemistry methods employed in the studies reported in this thesis.

Section 1.2 gives a brief introduction to the instrumentation used in the various experiments ; a state-of-the-art tandem magnetic sector mass spectrometer. This section will also discuss the various techniques used to generate and characterize the ions and the computational chemistry used to assist in the interpretation of the experimental results.

Section 1.3 presents a brief overview of the methods to perform ion-molecule reactions under chemical ionization conditions. It focuses on the importance of the

various parameters that influence molecule-assisted isomerization reactions of radical cations.

1.2 The generation and characterization of ions by tandem mass spectrometry

The VG Analytical ZAB-R Mass Spectrometer

Several sophisticated mass spectrometric techniques used in conjunction with computational chemistry allowed for the characterization of ions generated in the ion source of the mass spectrometer.

A schematic diagram illustrating the various components of our ZAB-R mass spectrometer is shown in Fig. 1. The instrument is a multi-sector mass spectrometer and is comprised of an ion source and three mass analyzers : a magnetic sector (B) followed by two electrostatic analyzers (E). This mass spectrometer is of reverse geometry, with a BEE configuration in that the magnetic sector precedes the electrostatic analyzers. The sectors are separated by field-free regions (ffr) where there is no external field to alter the flight path of the ion-beam. Within these regions are collision cells, which can be pressurized by various gases to perform sophisticated experiments such as collision-induced dissocation (CID) and neutralization-reionization (NR) mass spectrometry.

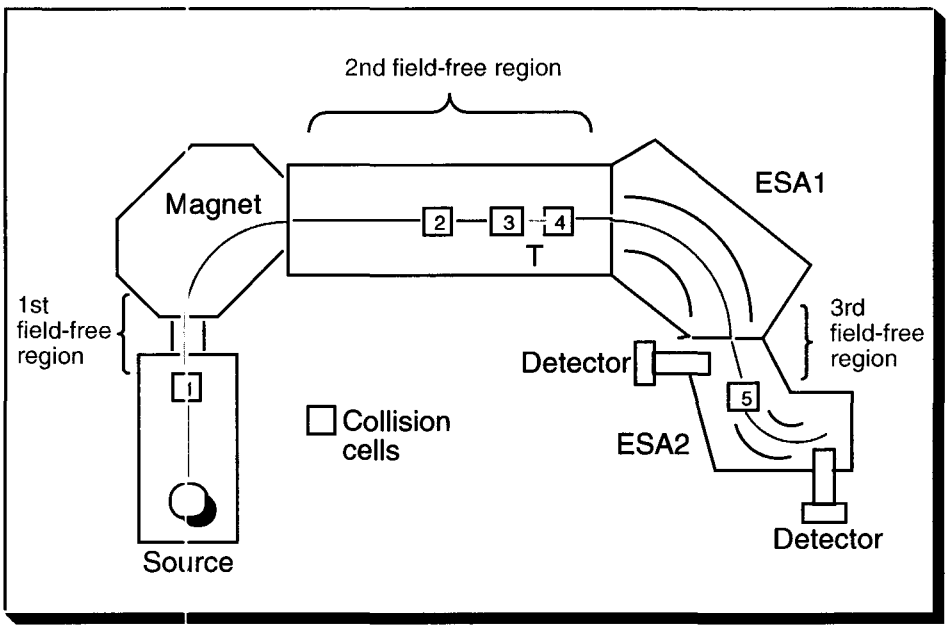

Fig. 1. Schematic diagram of the VG ZAB-R Mass Spectrometer.

The compound of interest is introduced into the ion source as a vapour directly via a leak valve or a direct insertion probe. Electrons which are generated from a tungsten filament are accelerated into the source by a potential difference of c. 70 V between the filament and the ion source [3]. Ions are generated by the "collision" of the accelerated electrons and the neutral vapour molecules as the electrons travel towards the trap, an electrode with a slightly higher potential. Ionization occurs by direct contact or close contact of the electrons with the neutral molecule. Removal of an electron from the neutral sample molecule leads to the formation of an ion. This method of ion generation is termed electron (impact) ionization (EI). The ion that is generated is positively charged and the process occurs as : $M + e^- \rightarrow M^{\bullet+} + 2e^-$, where M is the neutral sample molecule, e^- is an electron and $M^{\bullet+}$ represents the radical cation that is generated. The resulting $M^{\bullet+}$ species is an odd-electron ion because almost all organic molecules contain an even number of electrons.

Electron ionization takes place within 10^{-16} sec, which is much faster than the movement of the nuclei in the molecule : the fastest molecular vibrations require 10^{-14} sec. [3]. Therefore, during the ionization process the nuclei can be viewed as stationary.

This situation can be described as a vertical ionization process that is governed by the Frank-Condon principle. If there is excess energy from the ionization process, i.e. the energy imparted by the electron is greater than the ionization energy of the molecule, the excess energy materializes as internal energy in the form of transitions to excited vibrational, rotational and electronic states. The excess energy imparted by the electrons is different for every ion that is generated, resulting in a wide range of internal energies. Consequently only a fraction of the ions dissociate, by direct bond cleavage or rearrangement, whereas the others remain intact.

The incipient ions reside in the source for c. 1 μs and takes them c. 10 μs to reach to the detector. For molecular ions to dissociate in the source, they must do so within 1 μs which is equivalent to a minimum rate constant, k, of 10^6 sec^{-1}. The internal energy content of a given ion dictates the type of reactions it can undergo. For example, rearrangement reactions generally have a maximum rate constant of 10^{10} sec^{-1} compared to direct bond cleavage reactions which have a maximum rate constant of 10^{14} sec^{-1}. Ions which dissociate in the source – the "unstable" ions - do so with a rate constant of $10^6 < k < 10^{14}$ sec^{-1}. Ions that do not dissociate prior to reaching the detector because their internal energy is insufficient are deemed to be "stable". Such ions are characterized by a rate constant of $k < 10^4$ sec^{-1}. The fraction of ions that dissociates with a rate constant in the range of $10^4 < k < 10^6$ sec^{-1} has just enough internal energy to dissociate en route to the detector. These low-energy ions are termed metastable ions and their dissociation chemistry can be studied in the field-free regions of the mass spectrometer.

Two well established statistical theories describe the relationship between the rate constant, k, to the internal energy of an ion : the Quasi-Equilibrium Theory (QET) and the Rice, Rampsberger, Kassel and Marcus (RRKM) Theory. In the most basic representation of the QET, the dissociation reactions of ions can be described by the following equation : $k = \nu[\varepsilon_i - \varepsilon_o/\varepsilon_i]^{s-1}$, where ν is the frequency factor, ε_i is the internal energy of the dissociating ion, ε_o is the activation energy and s represents the number of effective oscillators of the ion [3].

Metastable Ion spectra

Metastable ion (MI) spectra are generated by mass selecting the ion of interest with the magnet. As the beam of ions traverse through the magnet from the ion source, a magnetic field is imposed on the beam in a direction that is perpendicular to the flight path of the ions [3]. The path of the ions through the magnet can be represented by the following equation : r = mv/Be, where r is the radius of the circular path, m mass of the ion, v the velocity of the ion, e the charge, and B the strength of the magnetic field. The radius of the path can be viewed as proportional to the momentum. The magnet can be viewed as a momentum separator. The magnetic field separates the ions by the following relationship : $m/z = B^2r^2/2v$ [3]. Once the precursor ions, $m_1^{\bullet+}$, are selected, they are transmitted into the 2ffr where a small fraction spontaneously dissociates into the products $m_2^{\bullet+}$ and m_3. The translational energy of the precursor ion, $m_1^{\bullet+}$, is distributed among the products based on their mass, by the following mass- weighted relationship : $(m_2/m_1)V_{acc}$, where V_{acc} is the accelerating voltage. This allows for the first ESA to function as a mass analyzer based on the translational energy of the product ions. The initial main beam of ions contains a mixture of stable and metastable ions, and generally not more than 1 % of the main beam contributes to the overall intensity of the peaks in the MI spectrum.

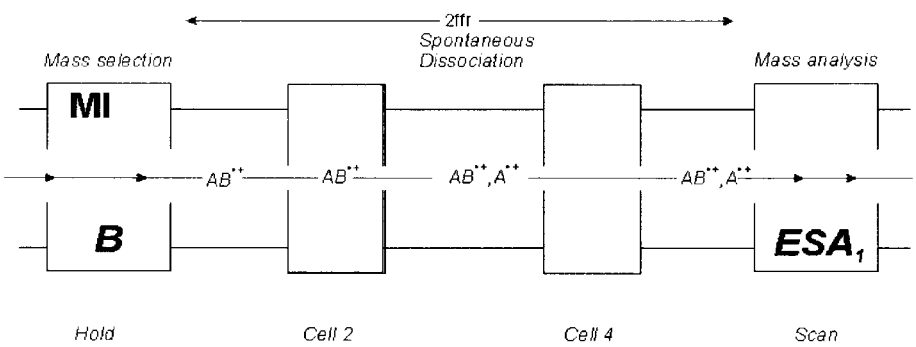

Fig. 2. A schematic diagram demonstrating the events in a metastable ion experiment.

A general observation in MI mass spectra is the broadening of the fragment ion peak with respect to the main beam of non-dissociating ions [3]. The broadening of the peaks is caused by the conversion of internal energy of the precursor ion $m_1^{\bullet+}$ into kinetic energy of the products $m_2^{\bullet+}$ and m_3. Figure 2 illustrates the dissociation of metastable ions in the second field-free region.

A reverse activation energy may also contribute to the kinetic energy content of the products. The energy diagram of Fig. 3 depicts an endothermic dissociation reaction with a barrier for the reverse reaction. The minimum amount of internal energy required to observe the dissociation of $m_1^{\bullet+}$ in the metastable time-frame is represented by ε_{min} [3]. To satisfy the energetic requirements, ε_{min} must be larger than the forward activation energy, ε_o. The excess energy, ε_{excess}, is the difference between the ε_{min} and ε_o. The energy for the reverse barrier is represented by ε_{rev}. The difference between the enthalpy of formation of the reaction products and the activated complex is equal to the barrier. The reverse activation energy, along with the excess energy contributes to the kinetic energy of the products.

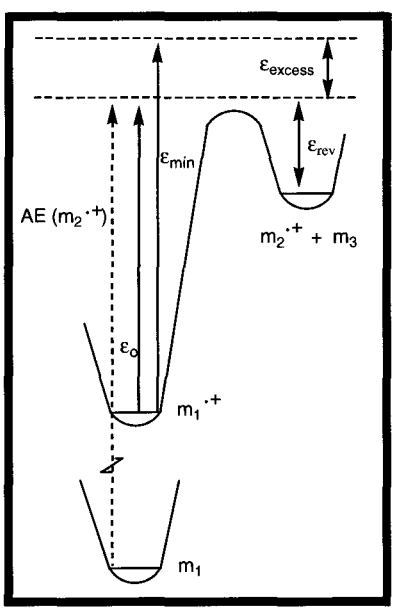

Fig. 3. A potential energy diagram for an endothermic reaction in the gas phase.

During the energy conversion, from internal energy to translational energy, a kinetic energy release (KER) may result [3]. The kinetic energy release is a result of contributions from the reverse activation energy and excess energy of the activated complex. Direct bond cleavage reactions are generally not associated with a significant reverse activation energy. Reactions that do have a significant reverse activation energy are rearrangements reactions, where the products are a stable ionic species and a neutral molecule [3]. The broadening of the metastable peaks relative to the main beam can be observed in the MI spectrum. Metastable peaks associated with a large kinetic energy release may have a flat-topped or dish shaped peak but reactions with a small kinetic energy release are characterized by peaks of a Gaussian shape [3]. Metastable peak shapes can provide information on the structure of the fragmenting ion, as well as the distribution of the internal energy of the fragmenting ion into translational energy of its products [5]. The kinetic energy release can be calculated by the following relationship : $T_{0.5} = (m_1^2/16m_2m_3)(V_{acc})[(\Delta E_{0.5})^2/E^2]$, where V_{acc} is the accelerating voltage, $\Delta E_{0.5}$ is the width of the metastable peak at half height, and E represents the sector voltage of the transmitted ions.

Collision-Induced Dissociation spectra

Collision-induced dissociation reactions provide valuable information on the structure (atom connectivity) of the precursor ion. To generate a CID spectrum, the ions of interest are accelerated from the ion source by 8 kV and then they are mass selected by the magnet. The selected beam of ions is then transmitted into the 2ffr, where one of the collision chambers is pressurized with a suitable collision gas such as helium or oxygen. Figure 4 shows the collision events during a CID experiment. A portion of the fast moving ions collides with a gas molecule and, as it does so, a small fraction of the ion's translational energy is converted into internal energy. The internal energy distribution of the collisionally activated ions is fairly broad. This generally leads to a range of dissociation reactions and more often than not, direct bond cleavage reactions dominate

over rearrangement reactions. Thus the CID spectrum of a given ion is generally characterized by a number of direct bond cleavage reactions and/or rearrangement reactions whereas its MI spectrum may only display one or two low energy rearrangement processes.

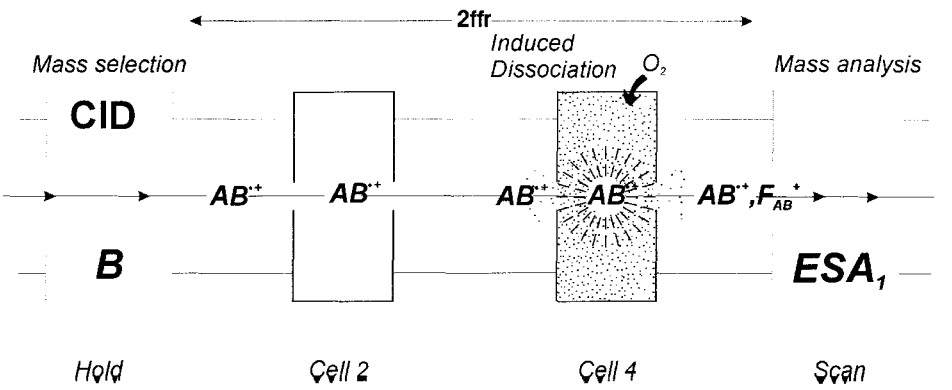

Fig. 4. Schematic diagram illustrating the events in a collision-induced dissociation experiment.

The intensity distribution of the peaks in a CID mass spectrum depends on a number of factors such as the type of collision gas, its pressure and also the translational energy of the ions. Typical collision gases are helium, argon, nitrogen and oxygen. Of these helium is most commonly used because it does not readily neutralize the ions and it causes less scattering. All experiments reported in this thesis use oxygen as the collision gas. CID mass spectra generated with oxygen are similar in appearance to those obtained using helium. However, they sometimes display weak peaks resulting from high energy reactions that are not seen in CID spectra obtained with other collision gases [6].

As mentioned earlier, the pressure of the collision cell can affect the CID experiment. The pressure of the collision gas dictates if the ion undergoes a single collision or multiple collisions. In the experiments conducted in this thesis, the pressure of the collision gas was kept sufficiently low to ensure that only single collision reactions take place. A remote ionization gauge located outside the collision was used to monitor the pressure of the collision gas. Monitoring the main beam intensity can provide an estimate of the pressure within the collision cell. To avoid multiple collision reactions, the optimal conditions are set to reduce the main beam to c. 60 – 70 % [7]. If the collision

cell pressure is too high and multiple collision reactions occur, structure-specific information may be lost [7].

As noted earlier, the translational energy of the collisionally activated ions can also affect the appearance of the CID spectrum. As the translational energy of an ion is increased, the range of internal energy also increases, resulting in more collision induced fragmentation [7]. An estimate of the energy transferred during a collision can be obtained from the following relationship : $E_{max} = h/a(2eV/m)^{1/2}$, where h denotes Plank's constant, a represents the interaction distance, eV is the ion's translational energy and m is the mass of the ion [7]. The size of the collision gas can also affect the appearance of the CID spectrum.

Neutralization-Reionization spectra

Neutralization-reionization (NR) mass spectrometry has become an important technique in studying the stability of elusive and highly reactive neutrals that are normally difficult to generate because of their propensity toward unimolecular dissociation or bimolecular rearrangement [8a]. Below in Fig. 5, the major elements of a NR experiment are shown.

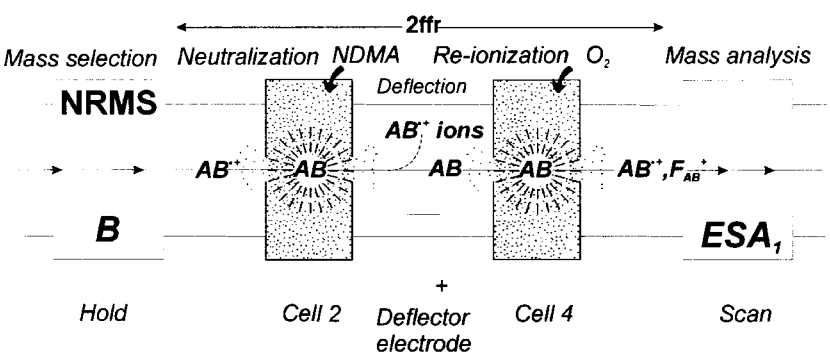

Fig. 5. Schematic diagram illustrating the events in a neutralization-reionization experiment.

To conduct a NR study, ions are first generated in the source from an appropriate precursor ion. The ions of interest are then selected by the magnet and allowed to enter

the 2ffr. The fast moving ions are then subjected to two consecutive collisions with the appropriate target gases. The first collision cell is pressurized with the neutralizing gas, N,N,-dimethylaniline (or Xe), that neutralizes the ions by electron transfer. Ions that are not neutralized are deflected away by a positively charged deflector electrode, positioned between the two collision cells in the 2ffr. The fast moving neutral molecules are then reionized as they travel through the second collision cell which is pressurized with oxygen gas. Some of the reionized ions will fragment in this collision cell. The reionized ions are then analyzed by the first ESA and detected by the first photomultiplier detector. If the NR spectrum displays a peak corresponding to the original mass-selected ion, then the neutral counterpart of the ion is deemed to be a stable species on the μs timescale.

As previously mentioned, xenon can be used effectively for neutralization despite the fact it has a rather high ionization energy (12.2 eV). Implying that the neutralization process is often an endothermic process. This does not inhibit the neutralization process because the translational energy of the ions compensates for the energy deficiency [8b]. Typically a "hard" target gas such as helium is used for the collisional reionization process : $AB + He \rightarrow AB^+ + He + e^-$. However, using such a hard target gas can result in extensive dissociation during the reionization process. Oxygen is a softer target gas which causes less fragmentation. The reionization process with O_2 involves the following reaction : $AB + O_2 \rightarrow AB^+ + O_2^-$. One aspect of using helium as the collision gas is the large amount of information on the structure (atom connectivity) of the neutral species compared to oxygen, but oxygen does allow for a higher yield of "survivor" ions.

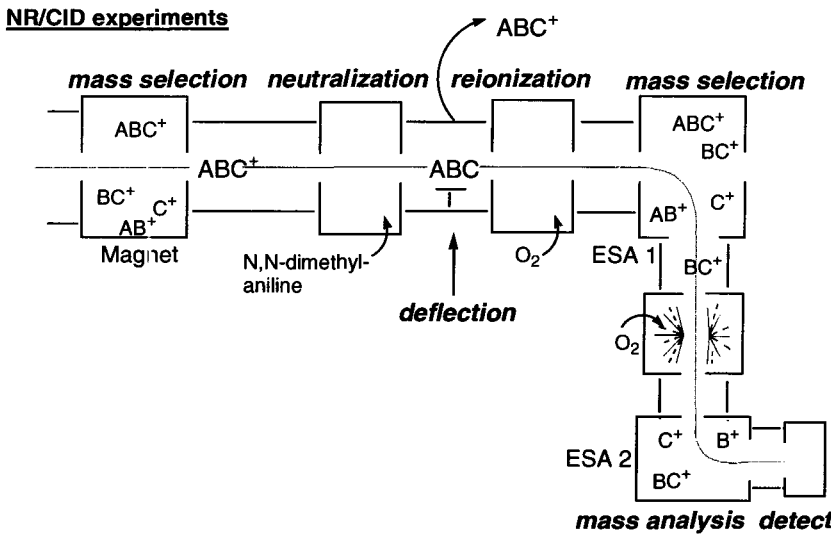

Fig. 6. A schematic diagram illustrating the events in a neutralization-reionization/collision-induced dissociation experiment.

A NR/CID experiment can provide information on whether the neutral species has retained its original structure connectivity or that it has rearranged into a more stable isomer prior to reionization. To perform a NR/CID experiment, the reionized species, the "survivor ions", are mass selected with the first ESA and transmitted into the 3ffr. The collision cell in this ffr is pressurized with oxygen and the mass selected ions are induced to dissociate by high energy collisions. The dissociating ions are then separated according to their m/z values by scanning the second ESA.

To determine whether the neutral species has retained its structure, the NR/CID spectrum is compared to the 3ffr CID spectrum of the source generated ions. If the two spectra are closely similar, there is strong evidence that the neutral molecule has retained its structural identity. If, on the other hand, there is a discrepancy between the spectra, it may be tentatively concluded that the neutral has isomerized into a more stable isomer. Definitive evidence that a given neutral has rearranged into a more stable isomer comes from a comparison with a reference CID spectrum of the more stable isomer. It should be noted in this context that NR/CID and CID spectra will also be different if the source generated ions consist of a mixture of isomers and/or contain isobaric impurities [9]

Collision-Induced Dissociative Ionization spectra

Another method to probe the stability of a neutral species is to perform a collision-induced dissociative ionization (CIDI) experiment. In this experiment neutrals generated from a spontaneous dissociation reaction are studied. A precursor ion is transmitted into the 2ffr by mass selecting it by the magnet. A small fraction of the selected ions undergoes unimolecular dissociation en route to the collision chamber [10]. The precursor ions $m_1^{\bullet+}$ and the product ions $m_2^{\bullet+}$ are deflected away by the deflector electrode so that only the fast moving neutral species enter the collision cell. The collision cell is pressurized with O_2 which reionizes the neutral species. The reionized neutrals and their dissociation products are then separated according to their m/z values by scanning the first ESA to generate a CIDI spectrum. The structure of the ionized neutrals can be further probed by mass selecting the ionized neturals with ESA1 and transmitting these ions into the 3ffr, where they are collisionally induced to dissociate by pressurizing the 3ffr collision cell with O_2.

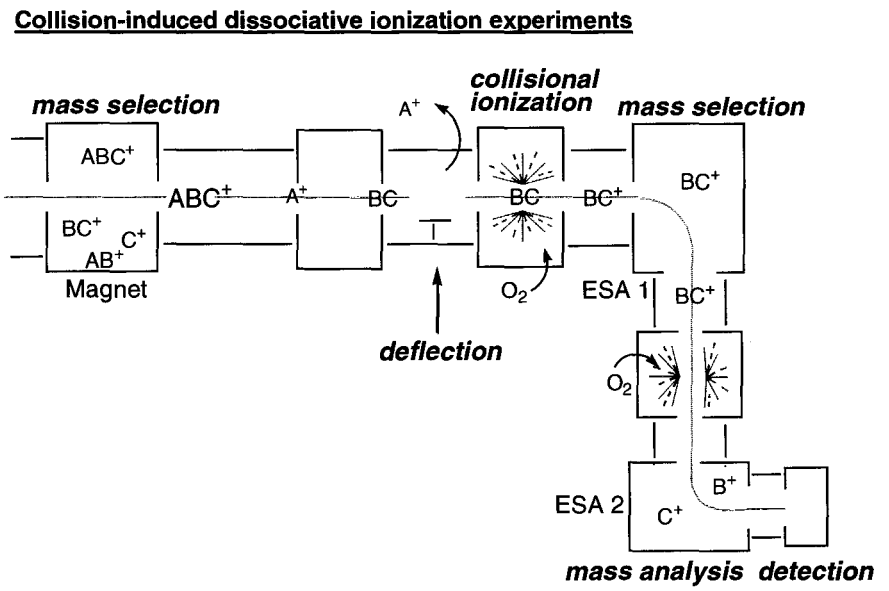

Fig. 7. A schematic diagram illustrating the events in a collision-induced dissociative ionization experiment.

Computational Chemistry

In conjunction with the results from a mass spectrometric analysis, computational chemistry is often used as a complementary aid in determining the structure of a species and the mechanism of its formation [11].

Several types of model chemistries are available but the one used in the studies of this thesis is the CBS-QB3 method [12]. This model chemistry allows for the calculation of the absolute enthalpies of formation for minima and transition states. The CBS-QB3 method is a Complete Basis Set Quadratic (CBS-Q) configuration interaction model chemistry with an empirical correction/pair correlation energy extrapolation function that incorporates density functional theory, B3LYP (B3), to optimize the geometry. The B3LYP geometry optimization uses the extensive 6-311G(2d,d,p) basis set to describe the orbitals. This model chemistry involves a composite approach comprised of four calculations at varying levels of theory to determine the final energy of the structure that is examined.

The first part of the calculation involves the optimization in terms of bond angles and bond lengths of the input geometry (the initial guess) of an ion or neutral of a given atom connectivity. In this step, density functional (B3LYP) theory is used to search for the geometry that corresponds with the lowest energy on the potential energy surface (PES). The structure is optimized once all the forces converge to zero [13]. The converged structure may correspond to a minimum or a transition state.

The energy calculated at this point is not used but rather the optimized structure is used for the subsequent steps to determine its absolute heat of formation at 0 K and 298 K. In this step, the vibrational frequencies of the optimized structure are also calculated. For any non-linear polyatomic molecule or ion there are 3N-6 vibrational frequencies, where N is the number of atoms. In a transition state, one of these frequencies corresponds to the negative imaginary frequency of the transition state vibration. The zero point energy (ZPE) of the neutral molecule, ion or transition state can be determined from the frequencies [14].

The subsequent steps in the CBS-QB3 method involve calculating the energy by electron correlation methods. The second step following the geometry optimization calculates the energy by coupled-cluster theory, CC. Coupled-cluster theory is the highest order electron correlation method used in the CBS-QB3 model. This is a many body perturbation theory approach [15] which takes into account the single, double and triple excitations, CCSDT. The next two steps incorporate the so-called Møller-Plesset (MP) level of theory. Within MP type calculations there are various orders of electron-correlation [16]. The third and fourth steps of the CBS-QB3 method, utilize the MP4 and MP2 levels of theory respectively.

The final energy is then calculated and presented as E(CBS-QB3) in the output file. The E(CBS-QB3) value uses the MP2 generated energy which is corrected with the energy determined from the CCSD(T) and MP4 steps. This final energy represents the total energy of the species at 0 K. To determine the heat of formation at 298 K, $\Delta_f H^0_{298}$, the following relationship must be used :

$$\Delta_f H_{298} = \Delta_f H_0(\text{exp}) - E_{AT} + E(\text{CBS-QB3}) + E_{thermal} - ZPE - \Delta H_{298}(\text{exp})$$

where $\Delta_f H_0(\text{exp})$ represents the sum of all the experimental $\Delta_f H_0$ values of each atom in the molecule or ion, E_{AT} denotes the total atomization energies for each type of atom in the structure, $E_{thermal}$ is the thermal energy correction, ZPE is the zero point vibrational energy and $\Delta H_{298}(\text{exp})$ represents the sum of the experimentally derived values for each of the atoms in the species. A list of $\Delta_f H_0(\text{exp})$ and $\Delta H_{298}(\text{exp})$ values for first and second-row elements has been compiled by Nicolaides et al. [17].

A validation study on the accuracy of the CBS-QB3 method for ionic dissociations has been reported [18]. It proposes that the calculated heats of formation are reliable to 1-2 kcal mol^{-1} for minima and 2-5 kcal mol^{-1} for transition states. The accuracy of the energies can be affected by the so-called spin contamination. Spin contamination can be viewed as a mixture of spin states resulting from too much spin polarization [19b]. The inclusion of spin contamination generally results in a higher energy due to the addition of a higher spin state. A large spin contamination can also result in a change of the geometry. The total spin value, S^2, can be found in the output file. If there is no spin

contamination this value should be equal to s(s + 1), where s denotes the number of unpaired electrons multiplied by ½. An acceptable level of spin contamination is that the value lies within 10 % of the s(s + 1) value [19b].

All calculations were performed with the Gaussian suite of programs implemented on both a desktop PC as well as on the SharcNet (McMaster University) cluster of computers.

1.3 Ion-Molecule Reactions and Proton-Transport Catalysis

The study of bimolecular reactions of ions and neutrals in the gas phase is an extensive field of research [20]. To study such reactions chemical ionization (CI) conditions must be used. In CI experiments the source pressure typically ranges from 10^{-4} to 10^{-5} Torr to ensure that the species of interest experience multiple collisions prior to exiting the source [4]. To pressurize the source, a reagent gas, R, is introduced which is initially ionized by collision with fast moving electrons. Once the reagent gas is ionized, it has the option to react with other reagent molecules or sample molecules, M, to generate various ionic species [4]. Shown below are the possible routes of reaction and the potential encounter complexes :

$$R + e^- \rightarrow R^{\bullet+} + 2e^-$$

$$R^{\bullet+} + M \rightarrow [R\bullet\bullet\bullet M]^{\bullet+} \quad \text{(ion-dipole complex)}$$

$$R^{\bullet+} + R \rightarrow [R\bullet\bullet\bullet R]^{\bullet+} \quad \text{(dimer radical cation)}$$

$$R^{\bullet} + R \rightarrow RH + [R\text{-}H]^{\bullet}$$

$$RH^+ + M \rightarrow [R\bullet\bullet H\bullet\bullet M]^+ \quad \text{(proton bound mixed dimer)}$$

$$RH^+ + M \rightarrow [R\bullet\bullet H\bullet\bullet R]^+ \quad \text{(proton bound dimer)}$$

$$R^{\bullet+} + M \rightarrow [R\bullet\bullet H\bullet\bullet (M\text{-}H)]^{\bullet+} \quad \text{(hydrogen-bridged radical cation)}$$

Encounter complexes of ions and neutrals result when the two species interact via electrostatic forces and/or hydrogen bonding. An ion-dipole complex is an encounter complex between an ion and the dipole of a neutral molecule that is stabilized by the electrostatic forces. Proton-bound dimers (PBDs) $[R\bullet\bullet\bullet H\bullet\bullet\bullet R]^+$ and $[R\bullet\bullet\bullet H\bullet\bullet\bullet M]^+$ are generated from the interaction of the protonated reagent RH^+ with a neutral molecule. When a reagent ion interacts with a hydrogen atom of a neutral molecule, a hydrogen-bridged radical cation (HBRC) of the type $[R\bullet\bullet\bullet H\bullet\bullet\bullet(M\text{-}H)]^{\bullet+}$ can be formed, where the two species are connected by a bridging hydrogen. The dimer radical cations formed between a reagent radical cation and a neutral molecule are either ion-dipole complexes or HBRCs.

Stabilization Energy

Before the widespread adoption of computational chemistry, the heat of formation of proton-bound dimers was experimentally determined through an empirical relationship between the proton affinity (PA) of the separate molecules and the bond dissociation energies of the PBD.

A proton-bound dimer is an even electron ion because neither of its components has lost an electron but is bound together by a proton. When the two bridged molecules are the same then a symmetrical PBD is generated, such as the proton bound dimer of water, $[H_2O\bullet\bullet\bullet H\bullet\bullet\bullet OH_2]^+$. In an asymmetrical PBD, the two bridged species are different, such as the proton-bound dimer of water and methanol, $[H_2O\bullet\bullet\bullet H\bullet\bullet\bullet O(H)CH_3]^+$.

An empirical relationship for the heat of formation of $O\bullet\bullet\bullet H\bullet\bullet\bullet O$ proton-bound dimers has been developed by Meot-Ner [22] along with Larson and McMahon [21]. These researchers were able to study the exchange equilibria of a great number of PBDs with carefully selected bases in high pressure CI type experiments. Gibbs free energy and bond dissociation energies can also be obtained from the solvent-exchange equilibria.

The empirical relationships developed by the two groups are not exactly the same, as the PBD species studied were different. For the stabilization energy (SE) of a PBD,

Meot-Ner [22] derived the empirical relationship SE(kcal mol^{-1}) = 30.4 – 0.30[ΔPA] whereas Larson and McMahon [21] derived SE(kcal mol^{-1}) = 30.8 – 0.46[ΔPA]. The first term represents the average bond dissociation energy of a set of symmetrical PBDs. In both equations the first term is slightly different due to the different PBD species studied. The second term denotes the slope of the bond dissociation vs. ΔPA plots.

The determination of the stabilization energy of a symmetrical PBD differs from that of an asymmetric proton-bound dimer. If the PBD is symmetric the stabilization energy is obtained from the expression : $\Delta H_f(product_1) + \Delta H_f(product_2) - \Delta H_f(PBD^+)$. In a symmetrical PBD like for example $[H_2O{\bullet\bullet\bullet}H{\bullet\bullet\bullet}OH_2]^+$, there is only one possibility for the products, $H_3O^+ + H_2O$, and their heats of formation are well established. The PA is the same for each component water molecule so ΔPA is zero and as a result the stabilization energy is 30.0 kcal mol^{-1}. This value can be used to obtain the $\Delta_f H$ of the proton-bound dimer.

When the PBD is asymmetrical, as in $[H_2O{\bullet\bullet\bullet}H{\bullet\bullet\bullet}O(H)CH_3]^+$, the proton-bound dimer between water and methanol, there are two possible combinations of dissociation products, $H_3O^+ + CH_3OH$ and $H_2O + CH_3OH_2^+$. In this situation, the lowest energy combination is used to derive the enthalpy of formation of the PBD, as indicated in the Figure below :

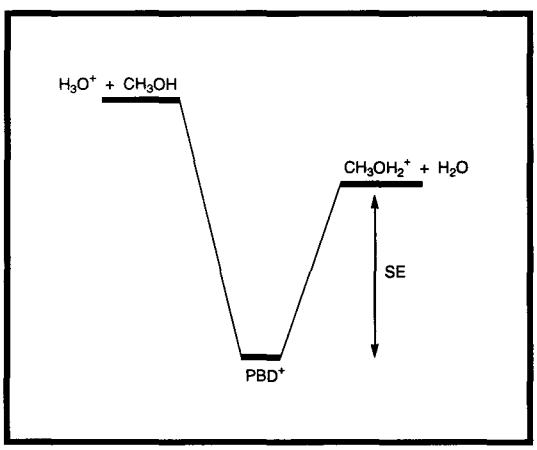

Meot-Ner has also studied $[N\bullet\bullet\bullet H\bullet\bullet\bullet O]^+$ and $[N\bullet\bullet\bullet H\bullet\bullet\bullet N]^+$ proton-bound dimers [22]. For these, the expressions for the stabilization energy (kcal mol^{-1}) are 30.0 – 0.26[ΔPA] and 23.2 – 0.25[ΔPA] respectively.

The empirically derived expressions for the stabilization energy of proton-bound dimers have also been applied to hydrogen-bridged radical cations. An example of a HBRC is the radical cation $[CH_3O\bullet\bullet\bullet H\bullet\bullet\bullet OH_2]^{\bullet+}$, where the hydroxyl hydrogen of methanol provides the bridging hydrogen. Employing the same empirical expression, SE = 30.0 – 0.30[ΔPA], a good estimate of the enthalpy of formation of this O•••H•••O bridged HBRC can be calculated. For HBRCs the ΔPA term represents the difference in proton affinity of the radical ($CH_3O^{\bullet}$) and the molecule (H_2O). As with asymmetric PBDs, there are two combinations of dissociation products in HBRCs of which the lowest energy pair is used to determine its heat of formation..

Catalyzed Isomerization Reactions

A great number of studies have been reported which demonstrate that the interconversion of isomeric ions can be catalyzed by interaction with a suitable neutral molecule [20]. These catalyzed isomerization reactions often involve distonic ions. Distonic ions are radical cations in which the charge and the radical reside on different atoms [20]. They tend to be more stable than their conventional counterparts but the two types of ions are often separated by a large energy barrier. This high energy barrier enables independent observation of the two isomeric species. The archetypal example of this type of reaction is the rearrangement of ionized methanol, $CH_3OH^{\bullet+}$, into the more stable methylene oxinium ion, $^{\bullet}CH_2OH_2^+$ [23,24]. As solitary ions these two isomers cannot interconvert because of a prohibitively high 1,2-H shift barrier. Nevertheless, this reaction readily occurs with a single water molecule acting as the catalyst.

This type of reaction is termed proton-transport catalysis (PTC) [25]. The mechanism for the rearrangement of a convention radical cation, $[H\text{-}X\text{-}Y]^{\bullet+}$, into its more stable counterpart, $[X\text{-}Y\text{-}H]^{\bullet+}$, occurs via a three step proton transfer process :

$$B + [H\text{-}XY]^{\bullet+} \rightarrow B\bullet\bullet\bullet H^{+}\bullet\bullet\bullet [XY]^{\bullet}$$

$$B\bullet\bullet\bullet H^{+}\bullet\bullet\bullet[XY]^{\bullet} \rightarrow B\bullet\bullet\bullet H^{+}\bullet\bullet\bullet [YX]^{\bullet}$$

$$B\bullet\bullet\bullet H^{+}\bullet\bullet\bullet[YX]^{\bullet} \rightarrow B + [H\text{-}YX]^{\bullet+}$$

The neutral molecule, B, acts as a "base" to abstract a proton from $[H\text{-}XY]^{\bullet+}$. The second step in the mechanism illustrates how the base acts as a catalyst to "transport" the proton from the high energy site to the low energy site. In order for this reaction to proceed the PA of the base must be higher than the PA of $XY^{\bullet}$ at the X site but lower than at the Y site. The weakly bound complex, $B\bullet\bullet\bullet H^{+}\bullet\bullet\bullet[XY]^{\bullet}$, allows for the rotation of the XY molecule within the ion. In the case where the PA[B] is lower than the PA[$XY^{\bullet}$] at X, the $B\bullet\bullet\bullet H^{+}\bullet\bullet\bullet[YX]^{\bullet}$ encounter complex cannot be formed. If, on the other hand, PA[B] is greater than the PA[$XY^{\bullet}$] at Y, the intermediate complex, $B\bullet\bullet\bullet H^{+}\bullet\bullet\bullet[XY]^{\bullet}$, will dissociate into undesirable products, HB^{+} and $[X\text{-}Y]^{\bullet}$. Based on extensive computational studies, Radom and co-workers have developed a criterion for efficient PTC : the PA[B] must be intermediate between PA[X] and PA[Y] for successful PTC [20b].

References

[1] (a) L. Radom, W.J. Bouma, R.H. Nobes, B.F. Yates, Pure Appl. Chem. 56 (1984) 1831 ; (b) W.J. Bouma, J.K. MacLeod, L. Radom, J. Am. Chem. Soc. 104 (1982) 2930 ; (c) J.L. Holmes, F.P. Lossing, J.K. Terlouw, P.C. Burgers, J. Am. Chem. Soc. 104 (1982) 2931 ; (d) B.F. Yates, W.J. Bouma, L. Radom, J. Am. Chem. Soc. 109 (1987) 2250 ; (e) J.W. Gauld, L. Radom, J. Phys. Chem. 98 (1994) 777.

[2] E. Uggerud, W. Koch, H. Schwarz., Int. J. Mass Spectrom. Ion Proc. 73 (1986) 187.

[3] R.G. Cooks, J.H. Beynon, R.M. Caprioli, G.R. Lester. *Metastable Ions.* Elsevier Scientific Pub. Com. Amsterdam 1973.

[4] F.W. McLafferty, F. Turecek. *Interpretation of Mass Spectra.* Fourth Edition. University Science Books. California. 1993.

[5] J.L. Holmes , J.K. Terlouw, Org. Mass Spectrom. 15 (1980) 383.

[6] (a) R. Flammang, V. Henrotte, P. Gerbaux, M.T. Nguyen. Eur. J. Mass Spectrom. 6 (2000) 3; (b) G.A. McGibbon, P.C. Burgers, J. K. Terlouw. Int. J. Mass Spectrom. Ion Process. 136 (1994) 191.

[7] J.L. Holmes. Org. Mass Spectrom. 20 (1985) 169.

[8] (a) C.A. Schalley, G. Hornung, D. Schröder, H. Schwarz. Chem. Soc. Rev. 27 (1998) 91; (b) F. Cacace. Chem. Eur. J. 8 (2002) 3838.

[9] L.N. Heydorn, C.Y. Wong, R. Srinivas, J.K. Terlouw Int. J. Mass Spectro. 225 (2003) 11.

[10] J.K. Terlouw, H. Schwarz. Angew. Chem. Int. Ed. Engl. 26 (1987) 805.

[11] P.C. Burgers and J.K. Terlouw. *In* Encyclopedia of mass spectrometry. Vol. 4. *Edited by* N.M.M. Nibbering. Elsevier, Amsterdam. 2005. p. 173.

[12] (a) J.A. Montgomery, Jr., M.J. Frisch, J.W. Ochterski, G.A. Petersson. J. Chem. Phys. 112 (2000) 6532; (b) J.A. Montgomery,Jr., M.J. Frisch, J.W. Ochterski, G.A. Petersson. J. Chem. Phys. 110 (1999) 2822.

[13] J.B. Foresman, A. Frisch. *Exploring Chemistry with Electronic Structure Methods.* Second Edition. Gaussian, Inc. Pennsylvania.1995-6.

[14] (a) A.D. Becke. J. Chem. Phys. 98 (1993) 5648; (b) A.D. Becke. J. Chem. Phys. 98 (1993) 1372.

[15] (a) R.J. Bartlett, Ann. Rev. Phys. Chem. 32 (1981) 59 ; (b) N. Oliphant, L. Adamowicz, J. Chem. Phys. 95 (1991) 6645

[16] W.J. Hehre, L. Radom, R.v.R. Schleyer, J.A. Pople, *Ab Initio Molecular Orbital Theory*, Wiley, New York, 1986.

[17] A. Nicolaides, A. Rauk, M.N. Glukhovstev, L. Radom. J. Phys. Chem. 100 (1996) 17640.

[18] L.N. Heydorn, Y. Ling, G. de Oliveira, J.M.L. Martin, C. Lifshitz, J.K. Terlouw. Zeitschrift für Physikalische Chemie. 215 (2001) 141.

[19] (a) F. Jensen. *Introduction to Computational Chemistry.* John Wiley and Sons. New York. 1999; (b) D. Young. *Computational Chemistry; A Practical Guide for Applying Techniques to Real World Problems.* John Wiley and Sons. New York. 2001.

[20] (a) D.K. Böhme. Int. J. Mass Spectrom Ion Processes. 115 (1992) 95; (b) J.W. Gauld, L. Radom. J. Am. Chem. Soc. 119 (1987) 9831; (c) M.A. Trikoupis, J.K. Terlouw, P.C. Burgers. J. Am. Chem. Soc. 120 (1998) 12131.

[21] J.W. Larson, T.B. McMahon. J. Am. Chem. Soc. 104 (1982) 6255.

[22] M. Meot-Ner. J. Am. Chem. Soc. 106 (1984) 1257.

[23] L. Radom, W.J. Bouma, R.H. Nobes, B.F. Yates. Pure & Appl. Chem. 56 (1984) 1831.

[24] J.L. Holmes, F.P. Lossing, J.K. Terlouw, P.C.Burgers. J. Am. Chem. Soc. 104 (1982) 2931.

[25] M.A. Trikoupis, P.C. Burgers, P.J.A. Ruttink, J.K. Terlouw. Int. J. Mass Spectrom. 217 (2002) 97 and references cited therein.

Chapter 2a

Formaldehyde mediated proton-transport catalysis in the ketene-water radical cation $CH_2=C(=O)OH_2^{\bullet+}$

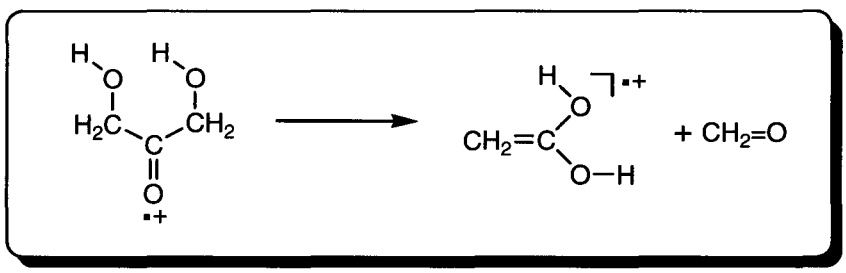

Abstract

Previous studies have shown that the solitary ketene-water ion $CH_2=C(=O)OH_2^{\bullet+}$ (**1**) does not isomerize into $CH_2=C(OH)_2^{\bullet+}$ (**2**), its more stable hydrogen shift isomer. Tandem mass spectrometry based collision experiments reveal that this isomerization does take place in the $CH_2=O$ loss from *low energy* 1,3-dihydroxyacetone ions $(HOCH_2)_2C=O^{\bullet+}$.

A mechanistic analysis using the CBS-QB3 model chemistry shows that such molecular ions rearrange into hydrogen-bridged radical cations $[CH_2C(=O)O(H)–H\bullet\bullet\bullet OCH_2]^{\bullet+}$ in which the CH_2O molecule catalyzes the transformation **1** → **2** prior to dissociation. The barrier for the unassisted reaction, 29 kcal mol^{-1}, is reduced to a mere 0.6 kcal mol^{-1} for the catalysed transformation. Formaldehyde is an efficient catalyst because its proton affinity meets the criterion for facile proton-transport catalysis.

1. Introduction

A very recent review elegantly demonstrates that the application of mass spectrometric techniques to the study of elementary ion reactions has led to remarkable progress in the characterization of detailed aspects of the kinetics, thermodynamics, and mechanisms of **molecular** transformations catalyzed by **ions** in the gas-phase [1].

This active field of research has greatly benefited from the selected-ion flow tube (SIFT) studies of D.K. Böhme and his research group [1]. This is also true for the related area of research which studies **ionic** transformations catalyzed by **molecules** in the gas-phase. As pointed out in Böhme's early review on this topic [2], a pair of solitary ionic isomers whose interconversion barrier is prohibitively high may be induced to interconvert via proton transfer in an encounter complex with a neutral molecule having the correct proton affinity (PA). This process is commonly called proton-transport catalysis (PTC). As a result the higher energy isomer may be transformed into its thermodynamically more stable counterpart.

For example [3], a large 1,2-H shift barrier prevents the conversion of ionized hydroxycarbene into ionized formaldehyde: $HCOH^{\bullet+}$ —//→ $CH_2{=}O^{\bullet+}$. The barrier exceeds the energy required for loss of $H^{\bullet}$ by direct bond cleavage, so even high energy ions will dissociate rather than interconvert. However, when a neutral molecule is allowed to interact with $HCOH^{\bullet+}$, proton-transport catalysis (PTC) may promote its isomerization into the lower energy $CH_2{=}O^{\bullet+}$ isomer. The molecule may act as a base (B) and accept a proton from one site of the $HCOH^{\bullet+}$ substrate, and then donate it back to a different site, as illustrated in Eq. 1: $HCOH^{\bullet+} + B \rightarrow HCO\text{-}H^{\bullet+}{\bullet\bullet\bullet}B$ (**a**) $\rightarrow HC{=}O^{\bullet}{\bullet\bullet\bullet}HB^{+} \rightarrow O{=}C(H)^{\bullet}{\bullet\bullet\bullet}HB^{+}$ $\rightarrow O{=}C(H)\text{-}H^{\bullet+}{\bullet\bullet\bullet}B$ (**b**) $\rightarrow CH_2{=}O^{\bullet+} + B$ (1).

Criteria for successful proton-transport catalysis have been further developed by Radom and co-workers [4]. The most important criterion states that a smooth isomerization for the reaction of Eq. 1 occurs if the PA of the base B lies between the PA of $HCO^{\bullet}$ at O and at C. If PA(B) is too low, proton abstraction will not take place. If PA(B) is too high, the incipient ion BH^{+} will not release the proton: dissociation to $HCO^{\bullet}$ + BH^{+} will ensue instead. As reported recently [5], the criterion can be significantly

extended downwards to include bases of lower PA with a concomitant increase of the barrier height.

Several examples of ion-molecule reactions in the gas phase are now available [6] where interaction of a radical cation with a single, judiciously chosen, "solvent" molecule leads to its transformation into a more stable isomer. Key intermediates in these reactions are hydrogen-bridged radical cations (HBRCs) [7] of the type (**a**) and (**b**) in Eq. 1. However, we note that not all such catalyzed transformations involve transport of a proton rather than a hydrogen atom [6c] and also that these transformations may take place in the dissociative ionization of molecules [3].

In the context of studies on proton transport catalysis, the Böhme group presented intriguing experimental and computational results on the water-catalyzed hydrolysis of the ketene radical cation at the 2004 Trent Conference in Mass Spectrometry [8]. Ketene ions were allowed to react with water in the SIFT mass spectrometer and one aspect of their study dealt with the water catalyzed isomerization of the incipient ketene-water ion, $CH_2=C(=O)OH_2^{\bullet+}$ (**1**), into its thermodynamically more stable isomer $CH_2=C(OH)_2^{\bullet+}$ (**2**), the enol ion of ionized acetic acid, CH_3-$C(=O)OH^{\bullet+}$ (**3**).

The criterion for efficient PTC for the transformation $CH_2=C(=O)OH_2^{\bullet+}$ (**1**)$\rightarrow$ $CH_2=C(OH)_2^{\bullet+}$ (**2**) stipulates[*] that the base has a PA in the range of 166–183 kcal mol^{-1} and hence water (PA = 167 kcal mol^{-1}) is a suitable catalyst. The PA of the formaldehyde molecule, 170 kcal mol^{-1} [10b], also satisfies the PTC criterion. Thus it may be expected that formaldehyde can also efficiently catalyse the isomerization.

This information inspired us to re-examine the generation of **1** as the product ion of the dissociative ionization of 1,3-dihydroxyacetone: $(HOCH_2)_2C=O^{\bullet+}$ (**DHA-1**) $\rightarrow$ $CH_2=C(=O)OH_2^{\bullet+}$ (**1**) + $CH_2=O$. In 1986, Postma et al. [9] provided experimental and supporting computational evidence that the *source* generated $C_2H_4O_2^{\bullet+}$ ions of this dissociation have the connectivity of ketene-water type ions **1**. The ion undergoes one major unimolecular dissociation, loss of H_2O to yield $CH_2=C=O^{\bullet+}$. This process is associated with a very small kinetic energy release, indicative of a species in which a

water molecule is attached to ionized ketene by an ion-dipole bond. Loss of water also wholly dominates the collision induced dissociation (CID) mass spectrum, which is characteristically different from that of any other $C_2H_4O_2^{\bullet+}$ isomer, including $CH_2=C(OH)_2^{\bullet+}$ (**2**). Thus, there is little doubt that the *source* generated m/z 60 $C_2H_4O_2^{\bullet+}$ ions from **DHA-1** are (largely) ketene-water type ions **1**.

Appearance energy measurements of the m/z 60 ion [9] yielded an apparent heat of formation of 138 kcal mol^{-1} which was interpreted to correspond to the formation of **1** at the thermochemical threshold. This implies that the abundant loss of $CH_2=O$ from low-energy ions **DHA-1** – the MI spectrum of **DHA-1** is dominated by a simple Gaussian shaped peak [11] at m/z 60 corresponding with a $T_{0.5}$ value of 25 meV – would also yield $C_2H_4O_2^{\bullet+}$ ions of structure **1**.

This proposal could be verified by analyzing the CID mass spectrum of the m/z 60 ions generated from *metastable* **DHA-1** ions. Such an experiment could not be performed with the instrumentation of the study of ref. 9 but our three-sector ZAB-R magnetic deflection instrument does have this capability.

The result of this experiment is shown in Figure 1a. The spectrum is virtually identical with that of enol ions $CH_2=C(OH)_2^{\bullet+}$ (**2**) , see Figure 1b. It is incompatible with the formation of the ketene-water isomer $CH_2=C(=O)OH_2^{\bullet+}$ (**1**) whose ^{18}O isotopomer $CH_2=C(=O^{18})OH_2^{\bullet+}$ yields the spectrum of Fig. 1c. This spectrum shows a specific loss of $H_2{}^{16}O$, confirming that ions **1** do not communicate with ions **2** prior to dissociation.

Thus, the formaldehyde loss from low-energy **DHA-1** ions does **not** yield ketene-water ions **1** but rather enol ions **2**, possibly by a formaldehyde-catalyzed isomerization **1** $\rightarrow$ **2**. The derived heat of formation of 138 kcal mol^{-1} for the m/z 60 product ion generated in the formaldehyde loss (see above) is not compatible with the threshold formation of **2** (122 kcal mol^{-1}, see Table 1) but could result from an energy barrier in the rearrangement.

---

*using Δ_fH [$^{\bullet}CH_2COOH$] = -61.6 kcal mol^{-1} [10a], Δ_fH (**1a**) = 138.5 kcal mol^{-1} (Table 1), Δ_fH (**2**) = 121.8 kcal mol^{-1} (Table 1).

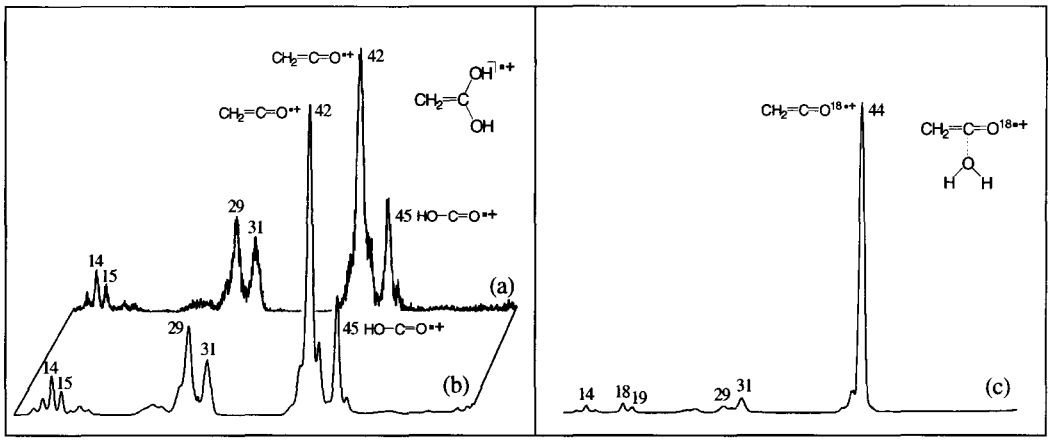

Fig. 1. CID mass spectra of (a) the $C_2H_4O_2^{\bullet+}$ ions generated by loss of CH_2=O from metastable 1,3-dihydroxy-acetone ions ; (b) the enol ion of acetic acid, $CH_2=C(OH)_2^{\bullet+}$; (c) the ^{18}O labelled ketene-water ion $CH_2=C(=O^{18})OH_2^{\bullet+}$.

This intriguing result prompted us to explore the mechanism of the formaldehyde loss from low-energy 1,3-dihydroxyacetone ions using computational chemistry. During the past five years we have successfully used the CBS-QB3 method [12] in mechanistic studies of proton-transport catalysis in various organic radical cations [13]. We therefore decided to use this CBS variant, which uses density functional geometries and frequencies in the calculations, as the primary computational tool in probing the mechanism for the formaldehyde elimination from metastable ions **DHA-1**.

It will be shown that proton-transport catalysis indeed accounts for the formation of enol ions **2** in the formaldehyde loss from low-energy 1,3-dihydroxacetone radical cations.

2. Experimental and theoretical methods

The experiments were performed with the VG Analytical ZAB-R mass spectrometer of BEE geometry (B, magnet; E, electric sector) [14] using an electron ionization source at an accelerating voltage of 8 kV. Metastable ion (MI) mass spectra were recorded in the second field free region (2ffr). The CID mass spectra of the 2ffr metastable peaks were obtained in the 3ffr using O_2 as collision gas (Transmittance, T = 70%). The reference CID mass spectrum of the enol ion of acetic acid of Fig. 2b was

obtained via the dissociative ionization of butyric acid. The spectrum of Fig. 2c was obtained in the context of a previously reported study of ionized oxalacetic acid : it pertains to the decarbonylation of metastable α-hydroxy(^{18}OH) acrylic acid ions into $CH_2=C(=O^{18})OH_2^{\bullet+}$ as indicated in Scheme 3 of ref. 15. All spectra were recorded using a PC-based data system developed by Mommers Technologies Inc. (Ottawa).

The 1,3-dihydroxyacetone sample was of research grade (Aldrich) and used without further purification.

The calculations were performed with the CBS-QB3 model chemistry [12] using Gaussian 2003, Rev C.02 [16] and (for selected transition state searches) GAMESS-UK [17]. In this model chemistry the geometries of minima and connecting transition states are obtained from B3LYP density functional theory in combination with the 6-311G(2d,d,p) basis set (also denoted as the CBSB7 basis set). The resulting total energies and enthalpies of formation for minima and connecting transition states (TS) in the 1,3-dihydroxy acetone system of ions are presented in Table 1. Spin contaminations were within an acceptable range. Figure 3 displays the optimized geometries for the principal species.

Table 1. Enthalpies of formation (kcal mol^{-1}) and total energies (Hartree) derived from CBS-QB3 calculations.

Isomer	E_{total} (0 K)	$\Delta_fH^0_{298}$	Isomer	E_{total} (0 K)	$\Delta_fH^0_{298}$	
DHA-1	-342.75044	92.9	**1a**	-228.38018	138.5	
DHA-2	-342.73670	102.2	**1b**	-228.38058	138.4	
DHA-3	-342.74391	98.6	**1c**	-228.34425	160.4	
DHA-4	-342.75694	89.7	**2**	-228.40494	121.8	[a]
DHA-5	-342.76572	83.9	**3**	-228.37212	142.5	[b]
DHA-6a	-342.78428	72.3	**4**	-229.54435	136.7	
DHA-6b	-342.78676	70.6	TS **1a→2**	-228.33042	168.5	
DHA-7	-342.73078	107.6	TS **1a→3**	-228.30139	187.0	
TS **DHA-1→2**	-342.73165	104.8	TS **2 →3**	-228.33128	167.8	
TS **DHA-2→3**	-342.71951	113.0	TS **1a→1c**	-228.34001	162.8	
TS **DHA-3→4**	-342.74307	99.2	TS **1a→1b**	-228.38110	137.6	
TS **DHA-4→5**	-342.75310	91.7	$CH_2=C=O^{\bullet+}$	-152.02212	210.2	[c]
TS **DHA-5→6**	-342.76421	84.5	H_2O	-76.33382	-58.3	
TS **DHA-2→7**	-342.71562	115.7	$CH_2=O$	-114.34411	-27.3	

[a] lowest energy conformer ; experimental value = 120 kcal mol^{-1} [10c] ; [b] lowest energy conformer ; experimental value = 142.5 kcal mol^{-1} [10c] ; [c] experimental value = 210.2 kcal mol^{-1} [10c]

3. Results and discussion

3.1. The structure and stability of the ketene-water ion and the relationship with its hydrogen-shift isomers $CH_2=C(OH)_2^{\bullet+}$ (2) and $CH_3-C(=O)OH^{\bullet+}$ (3).

In the early ab initio calculations of Postma et al. [9], the standard 4-31G basis set was used to optimize the geometries of various configurations of the ketene-water ion. Our CBS-QB3 calculations agree with their findings that ion **1a** and the hydrogen-bridged radical cation **1b**, whose optimized geometries are shown in Fig.3, represent the most stable configurations. The two ions have similar energies and our calculations further agree that the barrier for the interconversion **1a/ 1b** is negligible (see Table 1). At internal energies in excess of only a few kcal mol^{-1} above **1a/b**, the water molecule can freely move from carbon to carbon. The sum of the product energies relative to **1a** was calculated to be 15 kcal mol^{-1} [9] which reasonably agrees with our CBS-QB3 result of 13.4 kcal mol^{-1}.

The optimized geometry of **1a** shown in Figure 3a points to a description of the ion as a (ketene)ion – (water)dipole complex. Using the simple equation for the ion-dipole stabilization energy – SE (kcal mol^{-1}) = 68.8 μ / r^2 , with μ = dipole moment (D) and r = distance (Å) between the charge and the dipole) – one obtains SE (**1a**) = 27 kcal mol^{-1}, much larger than the CBS-QB3 derived value of 13.4 kcal mol^{-1}. However, the above equation does not account for repulsive effects associated with an ion-dipole interaction. That such a repulsive destabilizing effect operates in **1a** follows from an inspection of the geometries of the ketene ion in **1a** and **1b**, see Fig. 3a. In **1b** the ketene ion has a linear configuration but in **1a** repulsion of the oxygen atoms' lone pairs causes the ion to adopt an energetically less favourable "bent" structure. In a Valence Bond type of description, structure **1a** suffers from some contribution of the distonic form $^{\bullet}CH_2$-$C(OH_2^+)$=O, raising the total energy.

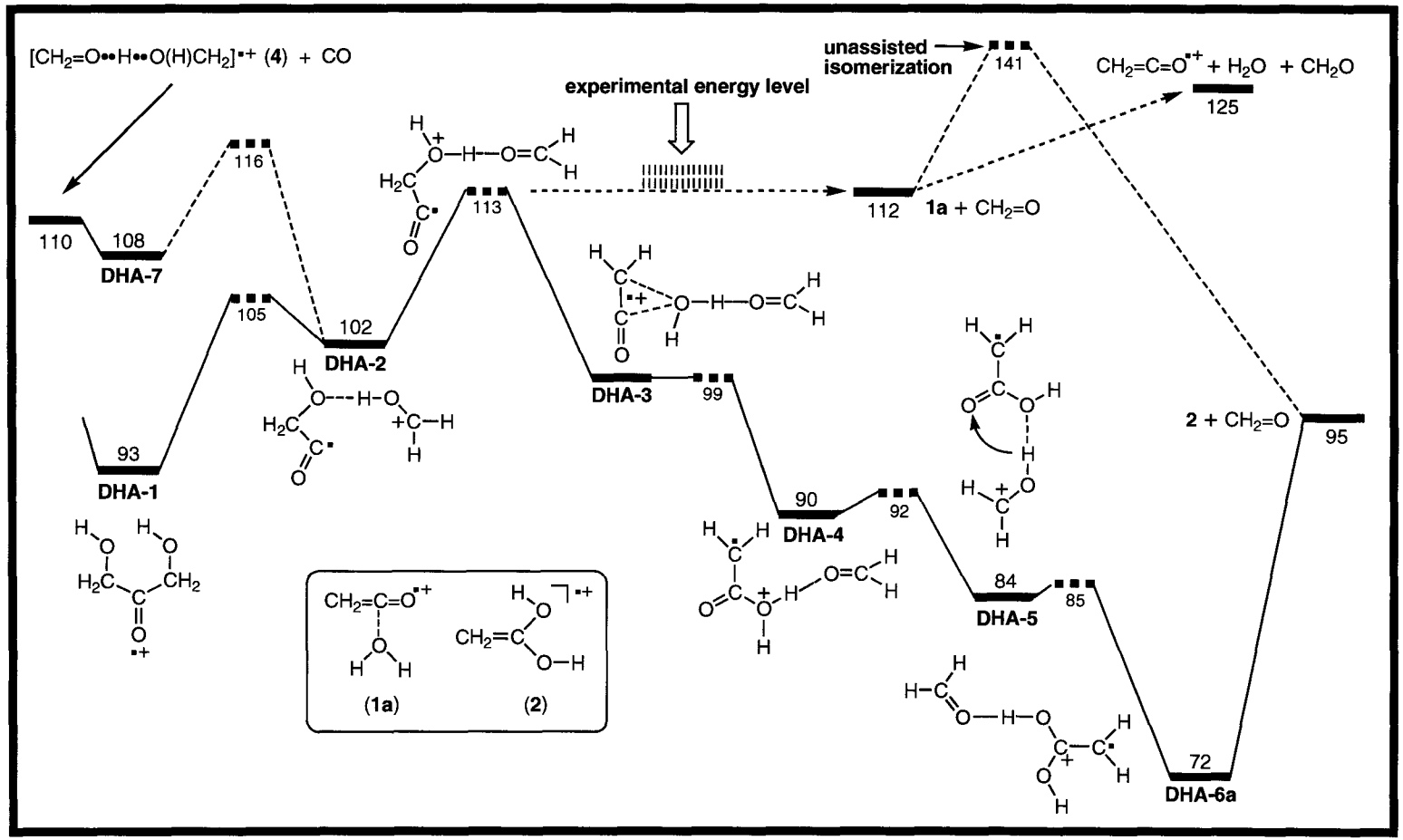

Fig.2 Energy level diagram derived from CBS-QB3 calculations describing the formation of enol ions **2** via loss of $CH_2=O$ from metastable 1,3-dihydroxy-acetone ions.

Postma et al. [9] further reported that point calculations for other geometries related to H_2O motion about the ends of the ketene ion showed barriers to such motion. One such motion leads to an isomer of the connectivity H_2O----CH_2=C=O$^{\bullet+}$ having an O---C bond length of 2.839 Å, which was calculated to lie ~ 6 kcal mol^{-1} above **1a**. This structure is probably not a minimum on the PES: when we optimized its geometry with the CBS-QB3 method, a minimum was located with corresponds with the distonic ion H_2O-CH_2=C=O$^{\bullet+}$ (**1c**), having an O---C bond of 1.533 Å (see Figure 3). This ion is only marginally stable – it lies 22 kcal mol^{-1} higher in energy than **1a** and requires only 2.5 kcal mol^{-1} to rearrange into energy rich ions **1a** which subsequently dissociate – but it does play a role in the mechanism discussed in the next section.

Our computational results, see Table 1, further show that the unassisted isomerization of ions **1a** into the enol of acetic acid ion **2** is prohibitively high : the associated energy barrier of 29 kcal mol^{-1} lies well above the energy required for dissociation by direct bond cleavage into CH_2=C=O$^{\bullet+}$ + H_2O. The same holds true for the isomerization **1a**→ **3**. Thus solitary ketene-water ions do not communicate with their 1,3-hydrogen shift isomers CH_2=C(OH)$_2^{\bullet+}$ (**2**) and CH_3-C(=O)OH$^{\bullet+}$ (**3**).

Fig.3a. Optimized geometries (CBSB7 basis set) of stable configurations on the potential energy surface of the ketene-water radical cation

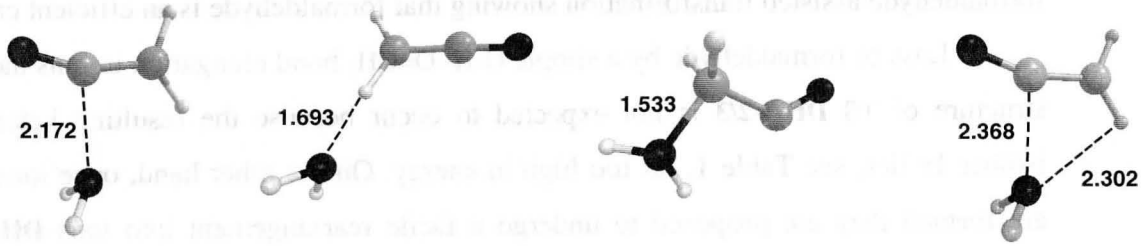

3.2. The loss of formaldehyde from low energy 1,3-dihydroxyacetone ions.

We will use the energy diagram of Fig. 2 as a guide in the discussion of our proposed mechanism for the formation of enol ions **2** from metastable 1,3-dihydroxyacetone ions. Starting from ion **DHA-1**, we see that elongation of the $HOCH_2$----C(=O) bond with the concomitant formation of a new O-H bond may lead to the

hydrogen-bridged radical cation **DHA-2** via a low energy barrier. Ion **DHA-2** then rearranges, via a barrier which is calculated to lie at 113 kcal mol^{-1}, into a ter-body complex, ion **DHA-3**. The height of this barrier is very close to the enthalpy calculated for the dissociation level **1a** + CH_2=O, 112 kcal mol^{-1}, and this supports – see Introduction – our alternative interpretation of the AE measurements of Postma et al.[9], namely that the experimental AE actually corresponds to a barrier, i.e. TS **DHA-2/ 3**.

Once ions **DHA-3** have been formed, they may undergo a barrierless rearrangement involving the migration of the OH_2•••O=CH_2 moiety to the carbon atom of the carbonyl group of the ketene part to form HBRC **DHA-4**. A rotation of the OH_2•••O=CH_2 moiety yields its more stable conformer **DHA-5,** via a TS lying only 2 kcal mol^{-1} above **DHA-4**. A formal 1,3-H shift assisted by the CH_2=O molecule in **DHA-5**, the proton-transport catalysis step, then yields **DHA-6**, the desired precursor ion for the generation of **2** + CH_2=O. The TS connecting **DHA-5** and **DHA-6** lies at 85 kcal mol^{-1}, well below the energy requirement for dissociation into **2** + CH_2=O, at 95 kcal mol^{-1}.

It was stated in the Introduction that since formaldehyde fulfils the PA criterion, the transformation should be smooth, i.e. the barrier for proton-transport catalysis should be low. Indeed, as can be seen from Fig. 2 and Table 1, the barrier for the isomerization is reduced from 29 kcal mol^{-1} for the solitary ions to a mere 0.6 kcal mol^{-1} for the formaldehyde assisted transformation showing that formaldehyde is an efficient catalyst.

Loss of formaldehyde by a simple O-H--O=CH_2 bond elongation in ions having the structure of TS **DHA-2/3** is not expected to occur because the resulting ketene-water isomer **1c** lies, see Table 1, far too high in energy. On the other hand, once ions **DHA-3** are formed they are proposed to undergo a facile rearrangement into ions **DHA-4** and these could dissociate by direct bond cleavage into **1a** + CH_2=O. This reaction, however, is not observed for the dissociation of the metastable **DHA** ions – these exclusively yield **2** + CH_2=O – and we propose that the following kinetic argument provides a rationale.

For simplicity, we assume that a model involving only three isomers suffices. These are **DHA-1**, **DHA-3** and **DHA-6**, where **DHA-3** may dissociate into **1a** + CH_2=O, whereas **DHA-6** may yield **2** + CH_2=O. In this model the barrier between **DHA-3** and

Fig.3b. Selected optimized geometries (CBSB7 basis set) for stable intermediates and transition states involved in the formaldehyde elimination from ionized 1,3-dihydroxyacetone (**DHA-1**).

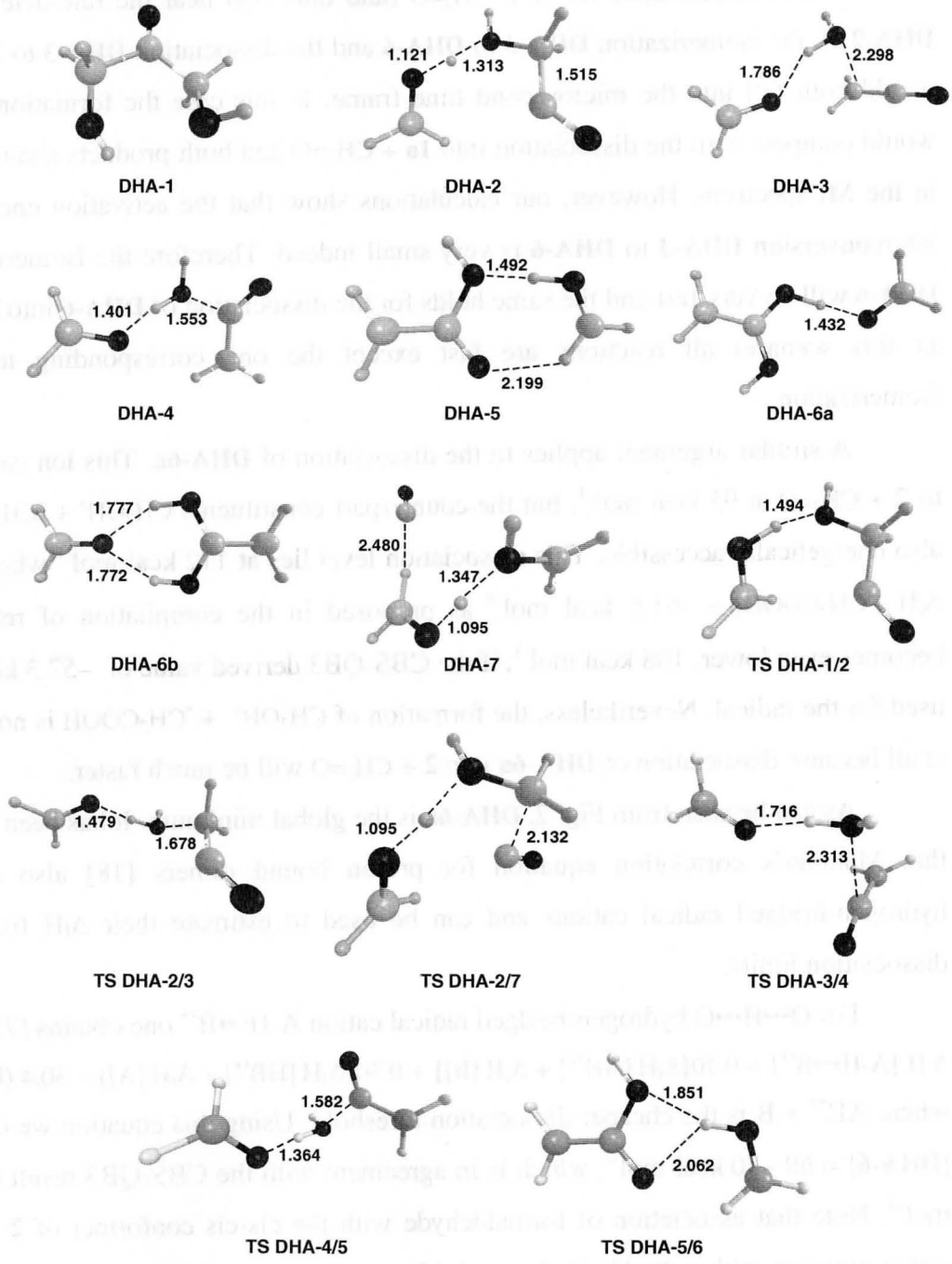

DHA-6 is essential for the product yields: if the corresponding TS (TS **DHA-3/4**) would lie near the dissociation limit for **1a** + CH_2=O (and thus also near the rate-determining TS **DHA-2/3**), the isomerization **DHA-3** to **DHA-6** and the dissociation **DHA-**3 to **1a** + CH_2=O would both fall into the microsecond time frame. In this case the formation of **DHA-6** would compete with the dissociation into **1a** + CH_2=O and both products should be found in the MI spectrum. However, our calculations show that the activation energy for the interconversion **DHA-3** to **DHA-6** is very small indeed. Therefore the isomerization into **DHA-6** will be very fast and the same holds for the dissociation of **DHA-6** into **2** + CH_2=O. In this scenario all reactions are fast except the one corresponding to the first isomerization.

A similar argument applies to the dissociation of **DHA-6a**. This ion can fragment to **2** + CH_2=O at 95 kcal mol^{-1}, but the counterpart constituents CH_2OH^+ + $^{\bullet}CH_2COOH$ are also energetically accessible. This dissociation level lies at 112 kcal mol^{-1} when one uses Δ_fH [$^{\bullet}CH_2COOH$] = -61.6 kcal mol^{-1} as proposed in the compilation of ref. 10a ; it becomes even lower, 108 kcal mol^{-1}, if the CBS-QB3 derived value of –57.3 kcal mol^{-1} is used for the radical. Nevertheless, the formation of CH_2OH^+ + $^{\bullet}CH_2COOH$ is not observed at all because dissociation of **DHA-6a** into **2** + CH_2=O will be much faster.

As can be seen from Fig. 2, **DHA-6a** is the global minimum. It has been shown [7] that Mautner's correlation equation for proton bound dimers [18] also applies to hydrogen-bridged radical cations and can be used to estimate their Δ_fH from known dissociation limits.

For O•••H•••O hydrogen-bridged radical cation A-H•••$B^{\bullet+}$ one obtains [7] :

Δ_fH [A-H•••$B^{\bullet+}$] = 0.70{Δ_fH [$AH^{\bullet+}$] + Δ_fH [B]} + 0.30{Δ_fH [$HB^{\bullet+}$] + Δ_fH [A]} – 30.4 (kcal mol^{-1}),

where $AH^{\bullet+}$ + B is the cheaper dissociation threshold. Using this equation we obtain Δ_fH [**DHA-6**] = 69 –70 kcal mol^{-1}, which is in agreement with the CBS-QB3 result of 72 kcal mol^{-1}. Note that association of formaldehyde with the cis-cis conformer of **2** leads to a stable complex with a double hydrogen bridge, see structure **DHA-6b** in Figure 3, whose enthalpy lies at 71 kcal mol^{-1}.

Finally we note that ion **DHA-2** could in principle rearrange into **DHA-7**, the precursor ion for the formation of HBRC **4** and CO. The heat of formation of the decarbonylation products **4** + CO actually lies lower in energy than that of **1a** + CH_2=O but the TS connecting **DHA-2** and **DHA-7** lies at 116 kcal mol^{-1}, 3 kcal mol^{-1} higher in energy than TS **DHA-2/3**. Thus the fact that the decarbonylation reaction has a significant reverse activation energy may explain why this process is not detected in the MI spectrum of 1,3-dihydroxyacetone.

4. Conclusions

Tandem mass spectrometry based collision experiments reveal that low energy 1,3-dihydroxyacetone ions (**DHA-1**) dissociate by loss of formaldehyde to produce the ionized enol of acetic acid, i.e. $HOCH_2C(=O)CH_2OH^{\bullet+} \rightarrow CH_2=C(OH)_2^{\bullet+} + CH_2=O$. The mechanism of this seemingly unintelligible reaction has been elucidated with the help of the CBS-QB3 model chemistry. Key intermediate in this dissociation is the ketene-water ion associated via a hydrogen bridge with a formaldehyde molecule, $^{\bullet}CH_2$-C(=O)-O^+(H)-H •••O=CH_2 (**DHA-4/5** in Fig. 2). This ion can undergo an almost barrier-free proton-transport catalysis to produce $CH_2=C(OH)_2^{\bullet+}$ associated with formaldehyde (the global minimum) which then dissociates.

Formation of **DHA-4**, see Fig. 2, is also mechanistically intriguing. After hydrogen bridging of the two hydroxyl groups and concomitant C-C cleavage in **DHA-1**, HBRC **DHA-2** is formed. Next the hydrogen of the H-bridge moves towards the O(H) group and the entire H-O-H•••O=CH_2 moiety can shift from the ketene methylene carbon atom to its carbonyl carbon atom to produce **DHA-4**. This rearrangement constitutes the rate-determining step; hence all subsequent reactions will be fast precluding the formation of higher energy products such as the ketene-water ion-dipole complex itself. The calculated energy of the rate-determining transition state, 113.0 kcal mol^{-1}, is in excellent agreement with that (112.5 ± 1.0 kcal mol^{-1}) derived from the experimental appearance energy.

References

[1] D.K. Böhme, H. Schwarz, Angew. Chem. Int. Ed. 44 (2005) 2.

[2] D.K. Böhme, Int. J. Mass. Spectrom. Ion Process. 115 (1992) 95.

[3] C.Y. Wong, P.J.A. Ruttink, P.C. Burgers, J.K.Terlouw, Chem. Phys. Lett, 387, (2004) 204.

[4] J.W. Gauld, L. Radom, J. Am. Chem. Soc., 119 (1997) 9831.

[5] C.Y. Wong, P.J.A. Ruttink, P.C. Burgers, J.K.Terlouw, Chem. Phys. Lett, 390, (2004) 176.

[6] For selected recent references see : (a) G. van der Rest, P. Mourgues, H.E. Audier, Int. J. Mass Spectrom., 231 (2004) 83; (b) X. Wang, J.L.. Holmes, Can. J. Chem., (2005), in press ; (c) M.A. Trikoupis, P.J.A. Ruttink, P.C. Burgers, J.K. Terlouw, Eur. J. Mass Spectrom., 10 (2004) 801.

[7] P.C. Burgers and J.K. Terlouw in: Encyclopedia of Mass Spectrometry, vol. 4 (N.M.M. Nibbering, ed.), Elsevier, Amsterdam, 2005, 173.

[8] G. Orlova, V. Blagojevic, D.K. Bohme, J. Phys. Chem. A. (in preparation).

[9] R. Postma, P.J.A. Ruttink, J.K. Terlouw, J.L. Holmes, J. Chem. Soc., Chem Commun. 9 (1986) 683.

[10] (a) Yu-Ran Luo. Handbook of dissociation energies in organic compounds. CRC Press, Boca Raton. 2003 ; (b) E.P.L. Hunter and S.G. Lias. J. Phys. Chem. Ref. Data 27, 413 (1998) ; (c) S.G. Lias, J.E. Bartmess, J.F. Liebman, J.L. Holmes, R.O. Levin, and W.G. Maillard. J. Phys. Chem. Ref. Data, Suppl.1, 17 (1988).

[11] J.L. Holmes, J.K. Terlouw, Org. Mass Spectrom, 15 (1980) 383.

[12] (a) J.W. Ochterski, G.A. Petersson, and J.A. Montgomery, Jr. J. Chem. Phys. 104, (1996) 2598. (b) J.A. Montgomery, Jr, M.J. Frisch, J.W. Ochterski, and G.A. Petersson. J. Chem. Phys. 112, (2000) 6532.

[13] R. Lee, P.J.A. Ruttink, P.C. Burgers, J.K. Terlouw. Can. J. Chem. (2005) in press.

[14] H.F. van Garderen, P.J.A. Ruttink, P.C. Burgers, G.A. McGibbon, and J.K. Terlouw. Int. J. Mass Spectrom. Ion Proc. 121, (1992) 159.

[15] L.M. Fell, J.T. Francis, J.L. Holmes, J.K. Terlouw, Int. J. Mass Spectrom. Ion. Process. 165/166 (1997) 179.

[16] Gaussian 03, Revision C.02, M. J. Frisch, G. W. Trucks, H. B. Schlegel, G. E. Scuseria, M. A. Robb, J. R. Cheeseman, J. A. Montgomery, Jr., T. Vreven, K. N. Kudin, J. C. Burant, J. M. Millam, S. S. Iyengar, J. Tomasi, V. Barone, B. Mennucci, M. Cossi, G. Scalmani, N. Rega, G. A. Petersson, H. Nakatsuji, M. Hada, M. Ehara, K. Toyota, R. Fukuda, J. Hasegawa, M. Ishida, T. Nakajima, Y. Honda, O. Kitao, H. Nakai, M. Klene, X. Li, J. E. Knox, H. P. Hratchian, J. B. Cross, V. Bakken, C. Adamo, J. Jaramillo, R. Gomperts, R. E. Stratmann, O. Yazyev, A. J. Austin, R. Cammi, C. Pomelli, J. W. Ochterski, P. Y. Ayala, K. Morokuma, G. A. Voth, P. Salvador, J. J. Dannenberg, V. G. Zakrzewski, S. Dapprich, A. D. Daniels, M. C. Strain, O. Farkas, D. K. Malick, A. D. Rabuck, K. Raghavachari, J. B. Foresman, J. V. Ortiz, Q. Cui, A. G. Baboul, S. Clifford, J. Cioslowski, B. B. Stefanov, G. Liu, A. Liashenko, P. Piskorz, I. Komaromi, R. L. Martin, D. J. Fox, T. Keith, M. A. Al-Laham, C. Y. Peng, A. Nanayakkara, M. Challacombe, P. M. W. Gill, B. Johnson, W. Chen, M. W. Wong, C. Gonzalez, and J. A. Pople, Gaussian, Inc., Wallingford CT, 2004.

[17] GAMESS-UK is a package of ab initio programs written by M.F. Guest, J.H. van Lenthe, J. Kendrick, K. Schoffel, and P. Sherwood, with contributions from R.D. Amos, R.J. Buenker, H.J.J. van Dam, M. Dupuis, N.C. Handy, I.H. Hillier, P.J. Knowles, V. Bonacic-Koutecky, W. von Niessen, R.J. Harrison, A.P. Rendell, V.R. Saunders, A.J. Stone, D.J. Tozer, and A.H. de Vries. The package is derived from the original GAMESS code due to M. Dupuis, D. Spangler, and J. Wendolowski, NRCC Software Catalogue 1, Vol. 1, Program No. QG01 (GAMESS) (1980).

[18] M. Meot-Ner (Mautner), J. Am. Chem. Soc. 106 (1984) 1257 and references cited therein.

Chapter 2b

Does proton transport catalysis play a role in the decarboxylation of ionized pyruvic acid ?

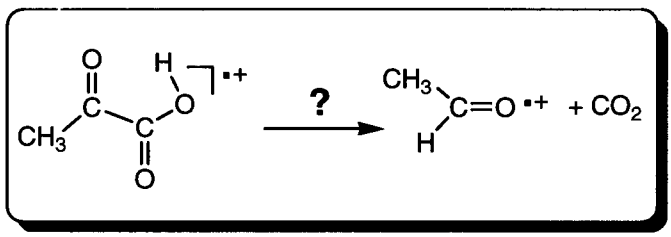

Abstract

Mass spectrometric studies have shown that metastable pyruvic acid radical cations, $CH_3C(=O)COOH^{\bullet+}$ (**1**), undergo decarboxylation into $C_2H_4O^{\bullet+}$ ions in competition with the formation of $CH_3C{\equiv}O^+ + COOH^{\bullet}$ by direct bond cleavage. Recent work on metastable glyoxilic acid radical cations, $HC(=O)COOH^{\bullet+}$, revealed that the CO_2 molecule formed in its decarboxylation catalyses the isomerization of the incipient oxycarbene ion $HCOH^{\bullet+}$ into its more stable $CH_2{=}O^{\bullet+}$ isomer. This raises the question whether the decarboxylation of **1** also involves proton-transport catalysis by CO_2. This may be the case, but only to a minor extent. Our collision experiments agree with an earlier report that oxycarbene ions $CH_3COH^{\bullet+}$ are formed but they also indicate that the (slightly) more stable isomer $CH_3C(H){=}O^{\bullet+}$ may be co-generated. A mechanistic analysis using the CBS-QB3 model chemistry provides a rationale. Ions **1** can rearrange into the (more stable) hydrogen-bridged radical cations $[CH_3CO\text{-}H{\bullet\bullet\bullet}O{=}C{=}O]^{\bullet+}$ (**2a**). However, the barriers for this reaction *and* that of a subsequent CO_2 assisted isomerization of **2a** into $[CH_3C(=O)\text{-}H{\bullet\bullet\bullet}O{=}C{=}O]^{\bullet+}$ (**2b**) lie 6-7 kcal mol^{-1} *above* the dissociation level of $CH_3COH^{\bullet+} + CO_2$. Thus ions **2a** are not prone to rearrange by proton-transport catalysis but they rather dissociate into $CH_3COH^{\bullet+} + CO_2$.

1. Introduction

For the $HCOH^{\bullet+}/CH_2{=}O^{\bullet+}$ system of ions, interconversion does not take place at all with the solitary ions because the barrier is much higher than the lowest energy direct bond cleavage reaction. However, in a recent study from our group [1], it was shown that proton-transport catalysis by CO and CO_2 does lead to the isomerization of $HCOH^{\bullet+}$ into its (slightly) more stable 1,2-H shift isomer $CH_2{=}O^{\bullet+}$. Collision experiments show that $CH_2{=}O^{\bullet+}$ is cleanly generated in the decarbonylation of low-energy (metastable) glyoxal ions $O{=}CH\text{-}CH{=}O^{\bullet+}$. Likewise, glyoxilic acid ions, $HC(=O)COOH^{\bullet+}$, decarboxylate into $CH_2{=}O^{\bullet+}$, albeit in admixture with some $HCOH^{\bullet+}$. A mechanistic analysis using the CBS-QB3 model chemistry indicates that the above ions first rearrange into hydrogen-bridged radical cations, $[HCO\text{-}H{\bullet\bullet\bullet}C{=}O]^{\bullet+}$ and $[HCO\text{-}H{\bullet\bullet\bullet}O{=}C{=}O]^{\bullet+}$, respectively. As mentioned above, solitary ions $HCOH^{\bullet+}$ do not isomerize but the CO or CO_2 molecule in the above complexes catalyses this transformation prior to dissociation. Carbon monoxide is the better catalyst because its proton affinity is closer to Radom's criterion for efficient proton-transport catalysis as discussed in Chapter 2a.

These results prompted us to re-examine the dissociation chemistry of ionized pyruvic acid, $CH_3C(=O)COOH^{\bullet+}$ (**1**), which also undergoes a spontaneous decarboxylation in the metastable time-frame [2]. If the reaction is catalysed by CO_2 – as in ionized glyoxilic acid – the m/z 44 $[C_2H_4O]^{\bullet+}$ product ion would be $CH_3C(H){=}O^{\bullet+}$ rather than its higher energy isomer $CH_3COH^{\bullet+}$ [3,4] as proposed in ref. 2. As with the $HCOH^{\bullet+}/CH_2{=}O^{\bullet+}$ system of ions, solitary ions $CH_3COH^{\bullet+}$ and $CH_3C(H){=}O^{\bullet+}$ cannot interconvert because the barrier is much higher than the lowest energy direct bond cleavage reaction [3].

As pointed out in ref. 2, a study reported in 1983 by Terlouw et al., it had earlier been concluded that the decarboxylation of ionized pyruvic acid yielded $[C_2H_4O]^{\bullet+}$ ions having the vinyl alcohol structure $CH_2{=}C(H)OH^{\bullet+}$. This was because the broad metastable peak for $H^{\bullet}$ loss from the (source generated) ion was the same as that for ions known to possess the structure $CH_2{=}C(H)OH^{\bullet+}$, the most stable isomer of the family of $[C_2H_4O]^{\bullet+}$ isomers [3]. The study of ref. 2. further noted that ab initio calculations by Bouma et al.

[5] – these results have been confirmed by the higher level calculations published in 1998 by Bertrand and Bouchoux [3] – indicate that CH_2=C(H)$OH^{\bullet+}$ ions isomerize to $CH_3COH^{\bullet+}$ as the reacting configuration leading to the formation of $CH_3C{=}O^+$. Thus the metastable peak for loss of $H^\bullet$, instead of being solely characteristic of CH_2=C(H)$OH^{\bullet+}$ ions, is indicative of either these and/or $CH_3COH^{\bullet+}$.

In this context we note that the calculations of ref. 3 indicate that loss of $H^\bullet$ from $CH_3COH^{\bullet+}$ is associated with a large reverse activation energy [3]. This provides a rationale why loss of $H^\bullet$ from CH_2=C(H)$OH^{\bullet+}$ and $CH_3COH^{\bullet+}$ is associated with a broad metastable peak whose $T_{0.5}$ value – the kinetic energy release as obtained from the width at half height of the peak [6] – is c. 500 meV [7]. In contrast, loss of $H^\bullet$ from the isomer $CH_3C(H){=}O^{\bullet+}$ has a only a small reverse activation energy [3] and the $T_{0.5}$ value is 43 meV [7].

Distinguishing the CH_2=C(H)$OH^{\bullet+}$ / $CH_3COH^{\bullet+}$ pair of isomers therefore, it was argued [2], must rest upon examination of ions of *low* internal energy content, preferably those generated via *metastable* dissociation of their precursors. Using a magnetic deflection mass spectrometer of BE geometry it was then shown that the collision induced (CID) mass spectrum of the $[C_2H_4O]^{\bullet+}$ product ions generated from metastable pyruvic acid ions dissociating in the first field region is characteristic of ions $CH_3COH^{\bullet+}$ and *not* of reference ions of structure CH_2=C(H)$OH^{\bullet+}$.

From appearance energy (AE) measurements on both the metastable and the source generated ions it was further proposed [2] that $\Delta_fH^\circ_{298}$ $[CH_3COH]^{\bullet+}$ = 206.7 ± 5 kcal mol^{-1} [2,8a]. The rather large uncertainty in the proposed value stems from the uncertainty in the AE of the metastable peak (10.7 ± 0.2 eV) and the fact that for the source generated ions - AE ≥ 10.4 eV (energy selected electrons) - only a lower limit could be assessed because of $^{13}CCH_3O^+$ contributions (AE m/z 43 (CH_3CO^+) = 10.28 ± 0.05 eV (energy selected electrons) [8e]). However, it has been argued that the experimentally derived enthalpy of the oxycarbene ion is too high and that the result derived from theoretical calculations using the Gaussian 2 (G2) method, 199.5 kcal mol^{-1}, is closer to reality [3,4]. We will evaluate this proposal in Section 3 but we first note that

in the decarboxylation study of ref. 2 the (co)generation of ionized acetaldehyde, $CH_3C(H)=O^{\bullet+}$, whose well-established $\Delta_fH^o_{298}$ value of 196.2 kcal mol^{-1} [4,8a/b] lies in between that of $CH_3COH^{\bullet+}$ and $CH_2=C(H)OH^{\bullet+}$, has not been explicitly considered.

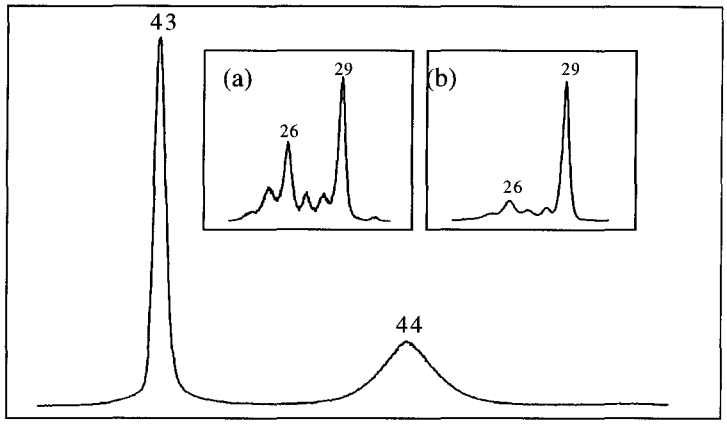

Fig. 1 Metastable ion spectrum of ionized pyruvic acid. Inset (a) partial 3ffr CID spectrum of $CH_3COH^{\bullet+}$ and inset (b) partial 3ffr CID reference spectrum of $CH_3C(H)=O^{\bullet+}$ from ionized acetaldehyde.

Figure 1 shows the metastable ion (MI) spectrum of ionized pyruvic acid obtained under conditions of good energy resolution. The spectrum displays two peaks : a peak at m/z 43 corresponding with the formation of $CH_3C=O^+$ by loss of $COOH^{\bullet}$ and a peak at m/z 44 corresponding with the decarboxylation. The width of the very narrow m/z 43 peak is that of the main beam of ions so that only an upper limit for the kinetic energy release can be derived : $T_{0.5} \leq 0.5$ meV. Such a small energy release is indicative for dissociation via ion-dipole complexes. The peak at m/z 44 is of simple Gaussian shape [6] and the associated $T_{0.5}$ value is 15 meV. We further note that the intensity of the m/z 43 peak increases strongly when a collision gas is introduced whereas this has hardly any effect on the m/z 44 peak intensity. The CID mass spectrum of these m/z 44 ions was recorded in the 3ffr and the structure characteristic part of the spectrum is shown in inset (a) of Fig. 1. The intensity distribution of the peaks in this spectrum is very close to that reported in ref. 2 and indeed characteristically different from that of vinyl alcohol type ions $CH_2=C(H)OH^{\bullet+}$. On the other hand, see inset (b) of Fig.1, the m/z 24-30 region of the CID mass spectrum of acetaldehyde reference ions $CH_3C(H)=O^{\bullet+}$ is not so different from that of ions of putative structure $CH_3COH^{\bullet+}$ that the possibility can be dismissed that the

spectrum of inset (a) represents ions $CH_3COH^{\bullet+}$ in admixture with some $CH_3C(H)=O^{\bullet+}$. Unfortunately, a reference CID mass spectrum of the isomerically pure oxycarbene ion is not available : the dissociative ionization of pyruvic acid is the only reported source of this ion.

The experimental results presented in Fig. 2 lend support to the proposal that the m/z 44 ions generated by the decarboxylation of *metastable* pyruvic acid ions are not pure ions $CH_3COH^{\bullet+}$ but rather $CH_3COH^{\bullet+}$ in admixture with $CH_3C(H)=O^{\bullet+}$. Fig. 2a displays the m/z 43 peak obtained by the collision induced dissociation of *source* generated m/z 44 ions from ionized pyruvic acid. The spectrum was obtained in the third field free region using the maximum energy resolution available with the second electrostatic analyser (10 V for 4 keV ions). It is seen that the m/z 43 CID peak is much broader than that of the main beam of ions indicating that the collision induced loss of $H^{\bullet}$ is associated with a large kinetic energy release. The peak has a simple non-composite shape [6] and the large $T_{0.5}$ value derived from its width at half height, 730 meV, leaves little doubt that we are dealing with $CH_3COH^{\bullet+}$ and not with a $CH_3COH^{\bullet+}/CH_3C(H)=O^{\bullet+}$ mixture of ions. (As pointed out above, $T_{0.5}$ = 500 meV for loss of $H^{\bullet}$ from source generated ions that decompose *spontaneously* ; the larger kinetic energy release observed in the CID experiments simply results from "collisional broadening" caused by the larger internal energy content of the dissociating ions.)

In contrast, the peak at m/z 43 displayed in Fig. 2b, which refers to the collision induced $H^{\bullet}$ loss from the *metastably* generated m/z 44 ions, is considerably less broad and the associated $T_{0.5}$ value is only 200 meV. We tentatively suggest that this peak is a composite consisting of a broad component that corresponds with loss of $H^{\bullet}$ from ions $CH_3COH^{\bullet+}$ and a narrow component that stems from loss of $H^{\bullet}$ from ions $CH_3C(H)=O^{\bullet+}$. A more detailed analysis is required to substantiate this claim. This would involve analysis of the peak shape for the collision induced loss of $H^{\bullet}$ from ionized acetaldehyde and that for loss of $D^{\bullet}$ from the m/z 45 $[C_2H_3DO]^{\bullet+}$ ions generated by the decarboxylation of metastable ions $CH_3C(=O)COOD^{\bullet+}$.

Thus, the experiments show that metastable pyruvic acid ions competitively dissociate into $CH_3C{=}O^+ + COOH^{\bullet}$ and $C_2H_4O^{\bullet+} + CO_2$. The decarboxylation reaction yields oxycarbene ions $CH_3COH^{\bullet+}$ but some $CH_3C(H){=}O^{\bullet+}$ may also be co-generated, possibly by proton-transport catalysis. Section 3 provides a mechanistic analysis of these intriguing reactions using computational results obtained from the CBS-QB3 model chemistry and related theoretical approaches.

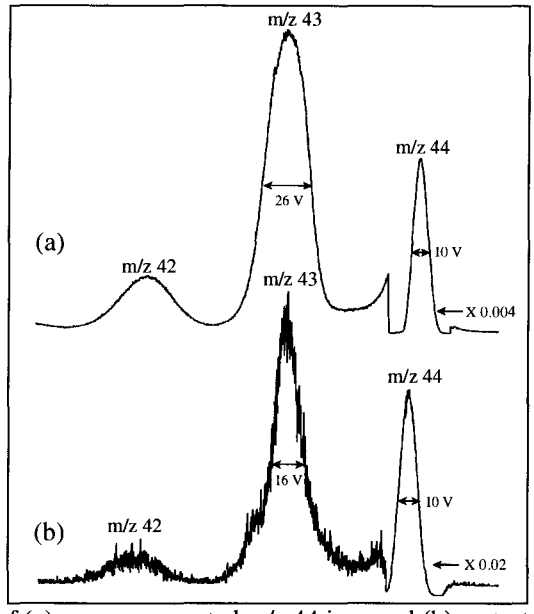

Fig. 2 Partial CID spectrum of (a) source generated m/z 44 ions and (b) metastably generated 44 ions from ionized pyruvic acid.

2. Experimental and theoretical methods

All mass spectrometric experiments were performed with the VG Analytical ZAB-R mass spectrometer. Details of the geometry of this three-sector (BEE) instrument have been reported elsewhere [7]. Typical operating conditions were 70 eV ionizing electron energy and 8 or 10 kV accelerating voltage. The pyruvic acid sample (Aldrich, research grade) was introduced via an all quartz direct insertion probe whose sample reservoir was cooled with an ice water mixture. The spontaneous and collision induced dissociations of the mass selected pyruvic acid ions were monitored in the second field free region (2ffr) by recording their metastable ion (MI) and collision induced dissociation (CID) mass spectra. These spectra (Fig. 1a/b) were obtained at a fairly high

energy resolution by setting the half-height width of the main beam of 8000 eV ions at 4V. The kinetic energy releases were estimated form the width at half-height of the appropriate metastable peak, by means of the standard one-line equation after applying the usual correction for the width at half-height of the main beam [8]. The partial CID mass spectrum of inset (a) in Fig. 1, which refers to the m/z 44 product ions generated from 10 keV metastable pyruvic acid ions in the 2ffr, was obtained in the 3ffr. Since these product ions have 5 keV of translational energy, the reference spectrum of source generated acetaldehyde ions in inset (b) was obtained at an accelerating voltage of 5 kV. To facilitate comparison with the spectra reported in ref. 2, in these experiments helium rather than oxygen was used as the collision gas.

The calculations were performed with the CBS-QB3 [10a] model chemistry using Gaussian 98, Rev A.11.3 [11] and Gaussian 2003, C.02 [12]. For selected species the Gaussian 3 (G3) model [13] and the higher level (computationally much more demanding) CBS-QCI/APNO method [10b] were also used. The resulting enthalpies of formation (298 K) for minima, transition states and dissociation levels for the pyruvic acid system are presented in Table 1 while the potential energy diagram derived from the CBS-QB3 calculations is presented in Figure 3. Spin contaminations were within an acceptable range. The optimized structures of the principal species are displayed in Fig. 4.

3. Results and discussion

In the discussion of our mechanistic analysis we will use the CBS-QB3 derived potential energy diagram of Fig. 3 and the compilation of theoretical and experimental results of Table 1 as a guide.

The computations indicate that ions **1a** and **1b** represent the two most stable conformers of ionized pyruvic acid. They both have the carbonyl groups in a *trans* position and a long O=C---C=O bond : 1.91 Å and 1.77 Å respectively, see Fig. 4. These long-bonded species should be viewed as one-electron bonded species [14] rather than ion-dipole type complexes. However, HO-C=O$^{\bullet}$ has a large dipole moment (3.0 – 3.7 D,

from the model chemistries of this study) and conversion of ions **1a/b** with (acetyl)ion-(COOH$^{\bullet}$)dipole complexes is expected to take place en route to their dissociation into $CH_3C{=}O^+ + COOH^{\bullet}$.

For neutral pyruvic acid, calculations were performed on two conformers which both have (except for two of the methylic hydrogens) almost planar geometries with the carbonyl groups in the *trans* position. The one of lowest energy has the hydroxylic H bridging with the keto-carbonyl in a geometry closely similar to that derived from microwave experiments [15]. The geometry of this neutral conformer, **1a**(N), corresponds to that of ion **1a** apart from the O=C-C=O bond which has the expected typical value of 1.55 Å. This implies that upon vertical ionization, the incipient ions **1a** have a considerably shorther O=C-C=O bond length and also a higher energy than the long-bonded species **1a**. In line with this, the vertical ionization energy of pyruvic acid, 10.42 eV, - as determined in the photoelectron spectroscopy study of McGlynn and Meekes [8g] - is considerably higher than its (estimated) adiabatic value, 9.9 eV [8c]. Our CBS-QB3 (and also G3) calculations, see Table 1, yield a gratifyingly close adiabatic ionization energy of 10.0 eV for the pyruvic acid conformer **1a**(N).

The energies of ionized pyruvic acid's conformers **1a** and **1b** are very close but clearly only **1a** can serve as the reacting configuration for the decarboxylation. In contrast, both conformers may dissociate by direct bond cleavage into $CH_3C{=}O^+ + COOH^{\bullet}$. Considering that the associated kinetic energy release is very small (see above), this reaction undoubtedly takes place at the thermochemical threshold. As seen in Table 1, all levels of theory and experiment agree that this threshold lies at 111 – 113 kcal mol^{-1}. The measured AE for this reaction, AE (m/z 43) = 10.28 ± 0.05 eV [8e], leads to 110 kcal mol^{-1} as the apparent heat of formation of the reaction products at 298 K if one uses the relationship $AE_{298\ expmt}$ (m/z 43) = $\Delta_fH^o_{298}$ $[CH_3C{=}O]^+$ + $\Delta_fH^o_{298}$ $[COOH]^{\bullet}$ - $\Delta_fH^o_{298}$ [pyruvic acid] with $\Delta_fH^o_{298}$ [acid] = -127.0 kcal mol^{-1}. The latter value is an empirical estimate that does not account for the stabilization provided by hydroxylic H bridging which theory predicts to be c. 2.5 kcal mol^{-1}, see the results of Table 1. Applying this correction term *lowers* $\Delta_fH^o_{298}$ [pyruvic acid] to -129.5 kcal mol^{-1} and brings down the

apparent heat of formation of the reaction products at 298 K to the *unrealistic* value of 107 kcal mol^{-1}. However, another correction term may have to be considered. This is the so-called Traeger-McLoughlin correction term $\Delta H_{cor} = \Delta H_{298}$ (reaction products) – 1.48, whose basis is discussed in detail in Chapter 4 and ref. 16. This correction term raises the apparent heat of formation of the reaction products at 298 K by typically 5 ± 2 kcal mol^{-1} [17]. For the present system the ΔH_{298} component (representing heat capacity terms, obtained from the CBS-QB3 calculations) is 3.9 kcal mol^{-1} so that ΔH_{cor} becomes 2.4 kcal mol^{-1}. Thus, if both corrections are applied the apparent heat of formation of the reaction products at 298 K remains at 110 kcal mol^{-1}, close to the thermochemical threshold derived from theory and experiment.

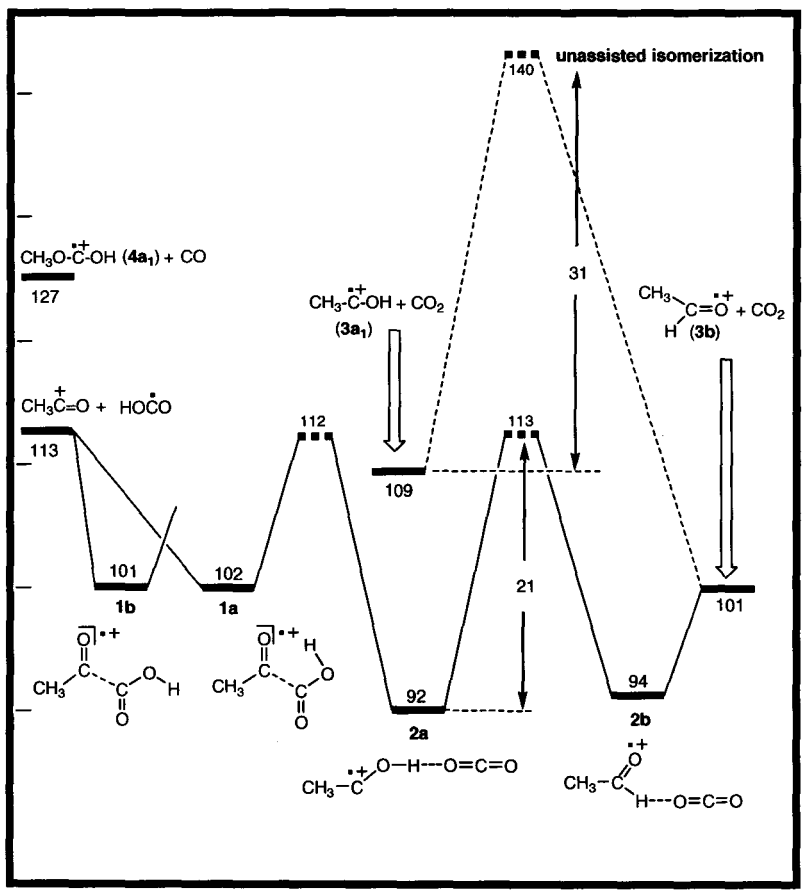

Fig. 3 Energy level diagram derived from CBS-QB3 calculations describing the elimination of carbondioxide from ionized pyruvic acid radical cations ions. The numbers refer to $\Delta_f H^0_{298}$ values in kcal mol^{-1}.

Next we consider the competing decarboxylation. Starting from ion **1a**, a simple 1,4-H shift involving transfer of the hydroxylic H atom to the carbonyl oxygen atom of the acetyl moiety, yields the distonic ion $[CH_3C(OH)COO]^{\bullet+}$, **1c.** However, for *metastable* ions, decarboxylation from **1c**, which is calculated to be a minimum on the potential energy surface, can be ruled out : $\Delta_fH^\circ_{298}$ (**1c**) = 127.0 kcal mol^{-1}, much higher than the energy level for dissociation into $CH_3C{=}O^+$ + $COOH^\bullet$. A much more economical route involves a 1,4-H transfer with a concomitant cleavage of the O=C--C=O bond. This yields ion **2a**, a hydrogen-bridged radical cation (HBRC). The transition state is calculated to lie at 112 kcal mol^{-1}, i.e. at a par with the energy requirement for dissociation into $CH_3C{=}O^+$ + $COOH^\bullet$. HBRC **2a,** $[CH_3\text{-}C\text{-}O\text{-}H{\bullet\bullet\bullet}O{=}C{=}O]^{\bullet+}$, may then dissociate by direct bond cleavage into the oxycarbene "Z" conformer $\mathbf{3a}_1$ (see Figure 4 for its geometry) and CO_2. Both the CBS-QB3 and the G3 method predict that the "Z" conformer $\mathbf{3a}_1$ is *less* stable than its "U" shaped counterpart $\mathbf{3a}_2$, by c. 4 kcal mol^{-1}. Surprisingly, the higher level CBS-QCI/APNO approach leads to exactly the opposite : it predicts $\Delta_fH^\circ_{298}$ values for $\mathbf{3a}_1$ and $\mathbf{3a}_2$ of 198.9 and 203.1 kcal mol^{-1} respectively !

This unexpected unusually large discrepancy with the results of the other model chemistries requires a detailed further analysis which we plan to perform in due course in collaboration with Prof. P.J.A. Ruttink. Since this discrepancy concerns the stability of the oxycarbene conformer ($\mathbf{3a}_1$) that connects with the precursor ion that undergoes decarboxylation (**1a**), the associated transition state (TS **1a** → **2a** at 112 kcal mol^{-1} in Fig. 3) may also be lower, by a few kcal mol^{-1}, if indeed the lower value for $\Delta_fH^\circ_{298}$ [$\mathbf{3a}_1$] predicted by the CBS-QCI/APNO method is reliable.

However, irrespective of the outcome of the above analysis – which is primarily of importance for a *kinetic* analysis of the degree of competition between the formation of $CH_3C{=}O^+$ + $COOH^\bullet$ and the decarboxylation pathway(s) – it seems likely that at higher levels of theory TS **1a** → **2a** will remain higher in energy than its dissociation products. This implies that the AE measured for this reaction with energy selected electrons, ≥ 10.4 eV, (see above, note that in these experiments ions are sampled that dissociate in the lower *milli*second timeframe) would refer to the barrier for the rearrangement rather than

the thermochemical threshold of the dissociation products. This may well be the case : the standard equation AE_{298}(m/z 44) = $\Sigma\Delta_fH^o_{298}$[dissociation products] - $\Delta_fH^o_{298}$ [pyruvic acid] with $\Delta_fH^o_{298}$ [acid] = -129.6 kcal mol^{-1} (CBS-QB3 value of Table 1) yields a minimum energy requirement of ≥ 110 kcal mol^{-1} for the dissociation. This value lies slightly above the calculated thermochemical threshold (108.7 kcal mol^{-1}) and slightly below the calculated barrier (111.6 kcal mol^{-1}). For the decarboxylation of the *metastable* ions (which dissociate in the *micro*second timeframe) the measured AE is considerably higher, 10.7 ± 0.2 eV, (see above) and the associated minimum energy requirement for dissociation now becomes 117 ± 4.5 kcal mol^{-1}. Taking the lower limit of this rather crude experiment, 112.5 kcal mol^{-1}, as the most plausible value, the calculations at all levels of theory still agree that the experiment probes the transition state energy rather than the thermochemical threshold of the dissociation products.

Returning to the energy diagram of Fig. 3, we note that HBRC **2a** could rearrange into HBRC **2b**, $[CH_3C(=O)\text{-}H\bullet\bullet\bullet O=C=O]^{\bullet+}$, via a formal 1,2-H shift and then decarboxylate to yield the acetaldehyde radical cation **3b**. The calculated barrier for this CO_2 assisted rearrangement $\mathbf{3a_1} \rightarrow \mathbf{3b}$, is c. 10 kcal mol^{-1} lower than that for the unassisted isomerization but it is still substantial, 21 kcal mol^{-1}. This is not unexpected considering that the PA of CO_2 (129 kcal mol^{-1} [8c]) lies far below that prescribed by Radom's criterion (discussed in Chapter 1) for a base that enables efficient proton-transport catalysis. For our system the PA of such a base should lie in the range 159 – 167 kcal mol^{-1} (from a standard calculation of PA($CH_3C=O^{\bullet}$) @ O and PA($CH_3C=O^{\bullet}$) @ C, using the CBS-QB3 data of Table 1).

Nevertheless, the calculated isomerization barrier **2a**→**2b** of 113 kcal mol^{-1} may just be low enough to allow, as the experiments indicate, a small fraction of ions **2a** to undergo a CO_2 assisted dissociation into ions **3b** but a detailed kinetic analysis is required to substantiate this possibility.

As an aside we note that the CBS-QB3 derived stabilization energy (SE) of HBRC **2a**, $[CH_3\text{-}C\text{-}O\text{-}H\bullet\bullet\bullet O=C=O]^{\bullet+}$, is 17.2 kcal mol^{-1} : from $\Sigma\Delta_fH^o_{298}[\mathbf{3a_1} + CO_2] - \Delta_fH^o_{298}$ [**2a**]. The SE becomes 18.9 kcal mol^{-1} if one substitutes $\Delta_fH^o_{298}[CO_2]$ (CBS-QB3) by its well-

established experimental heat of formation. As discussed in Chapter 1, the SE for O•••H•••O type HBRCs can also be derived from the empirical relationship developed by Mautner [18,14] : SE = 30.4 – 0.30(ΔPA) kcal mol^{-1}. The PA of the CO_2 component is experimentally well-established : 129.3 kcal mol^{-1} [8c]. The PA of the other component, $CH_3C{=}O^{\bullet}$ @ O, is calculated as 159.2 kcal mol^{-1} from ($\Delta_fH^o_{298}[H^+]$(expt) + $\Delta_fH^o_{298}[CH_3C{=}O^{\bullet}]$(expt) – $\Delta_fH^o_{298}[\mathbf{3a}_1]$ (CBS-QB3). Thus ΔPA = 30 kcal mol^{-1} and the "Mautner" SE becomes 21.4 kcal mol^{-1}, in only fair agreement with the CBS-QB3 derived stabilization energy.

In summary, we propose that the CBS-QB3 derived energy diagram of Figure 3 provides a solid basis for the rationalization of the dissociation chemistry of metastable pyruvic acid radical cations. However, a complete mechanistic picture requires (i) complementary experiments to substantiate our proposal that proton-transport catalysis indeed plays a (minor) role in the decarboxylation ; (ii) further analysis of the conflicting theoretical results regarding the structure and stability of the most stable oxycarbene conformer and (iii) probing the dynamics of the competing reactions featuring in the energy diagram. This would involve analysis of the system in terms of the statistical approach used in RRKM theory [19]. However, we note that a mere RRKM treatment of our system may not be adequate if, indeed, the dissociation of ionized pyruvic acid into $CH_3C{=}O^+ + COOH^{\bullet}$ involves the participation of ion-dipole complexes [20].

Table 1. Enthalpies of formation (kcal mol^{-1}) derived from CBS-QB3, Gaussian 3 (G3) and CBS-QCI/APNO (APNO) calculations pertaining to the dissociation chemistry of ionized pyruvic acid

		CBS-QB3 E_{total} (0 K)*	CBS $\Delta_fH^0_0$	CBS $\Delta_fH^0_{298}$	G3 $\Delta_fH^0_{298}$	APNO $\Delta_fH^0_{298}$	Exp. $\Delta_fH^0_{298}$	
$CH_3C(=O)COOH$	**1a**(N)	-341.94328	-126.2	-129.6	-128.3	-129.4	-127.0	a
$CH_3C(=O)COOH^{\bullet+}$	**1a**	-341.57578	104.4	101.5	103.5	-		
$CH_3C(=O)COOH^{\bullet+}$	**1b**	-341.57688	103.7	100.9	103.5	-		
$CH_3C(=O)\bullet\bullet\bullet COOH^{\bullet+}$	**ID-1**							
$CH_3C\text{-}O\text{-}H\bullet\bullet\bullet O{=}C{=}O^{\bullet+}$	**2a**	-341.59262	93.8	91.5	92.5	-		
$CH_3C(=O)\text{-}H\bullet\bullet\bullet O{=}C{=}O^{\bullet+}$	**2b**	-341.58951	95.8	93.6	94.5	-		
TS **1a**→**2a**		-341.55954	114.6	111.6	112.6	?		
TS **2a**→**2b**		-341.55781	115.7	113.0		?		
$[CH_3C(OH)COO]^{\bullet+}$	**2c**	-341.53482	130.1	127.0	-	-		
$CH_3\text{-}C\text{-}OH^{\bullet+}$	$\mathbf{3a_1}$	-153.19220	207.3	204.5	203.7	198.9		b
$CH_3\text{-}C\text{-}OH^{\bullet+}$	$\mathbf{3a_2}$	-153.19893	203.1	200.3	199.6	203.1		
$CH_3C(=O)H^{\bullet+}$	**3b**	-153.20492	199.4	196.9	197.1	196.0	196.3	c
$CH_2{=}CH\text{-}OH^{\bullet+}$	**3c**	-153.22518	186.6	183.9	183.5	-	183.5	d
TS $\mathbf{3a_1}$→**3b**		-153.14322	238.1	235.7	235.5	-		
$CH_3\text{-}C\text{-}OH^{\bullet+}$ ($\mathbf{3a_1}$) + CO_2				**108.7**	**108.4**	**104.4**	(112.7)	e
$CH_3C(=O)H^{\bullet+}$ (**3b**) + CO_2				**101.1**	**101.8**	**101.5**	102.2	
CO_2		-188.37210	-95.7	-95.8	-95.3	-94.5	-94.1	c
$CH_3\text{-}C{=}O^+ + HO\text{-}C{=}O^{\bullet}$				**112.9**	**113.3**	**112.0**	**110.7**	
$CH_3\text{-}C{=}O^+$		-152.68586	159.8	158.1	157.8	156.9	156.7	f
$HO\text{-}C{=}O^{\bullet}$ (2A', trans conf.)		-188.87249	-44.5	- 45.2	-44.5	-44.9	-46.0	g
$CH_3\text{-}C{=}O^{\bullet}$		-152.94202	-1.0	- 2.5		-	- 2.4	h
$CH_3O\text{-}C\text{-}OH^{\bullet+}$ ($\mathbf{4a_1}$) + CO				126.9	127.9	-	131.6	
$CH_3O\text{-}C\text{-}OH^{\bullet+}$ (W)	$\mathbf{4a_1}$	-228.35408	157.0	153.7	154.6	-	158.0	i
$CH_3O\text{-}C\text{-}OH^{\bullet+}$ (U)	$\mathbf{4a_2}$	-228.35173	158.5	155.1		-		
CO		-113.18196	-27.6	-26.8	-26.7	-26.4	-26.4	c

* E_{total} (0 K) in Hartree.

(a) Expt. value from ref 8e, an estimate based upon Benson additivity terms; the older estimate of ref. 2 uses -131 kcal mol^{-1}; the calculated value refers to the lowest energy conformer which has the hydroxylic H bridging with the keto-carbonyl. The non H-bridged conformer yielded -127.0 kcal mol^{-1}; (b) Refs. 3 and 4 propose a value of 199.5 kcal mol^{-1} based upon G2 type calculations, our G2 value is 202.1 kcal mol^{-1}, see text for further discussion; (c) Expt. value from ref. 8a/b ; (d) Expt. value from ref. 3, the computed values refer to the most stable anti conformer; (e) Expt. value from ref. 2, having an uncertaintly of ± 5 kcal mol^{-1}, see text for further discussion ; (f) Expt. value from ref. 8f, the compilation of ref. 8d reports 156 kcal mol^{-1}; (g) Expt. value from ref. 8e, the compilation of ref. 8d proposes -46.5 ± 0.7 kcal mol^{-1} for the trans isomer and an (unrealistic) value of -52.5 kcal mol^{-1} for the cis isomer. Its CBS-QB3 value is – 43.2 kcal mol^{-1} ; (h) ref. 8d ; (i) Expt. value from ref. 2, the G2 type calculations of ref. 4 yield 153.0 kcal mol^{-1} (conformer not specified).

Fig. 3. Selected optimized geometries for stable intermediates and transition states involved in the carbon dioxide elimination from ionized pyruvic acid (**1a**).

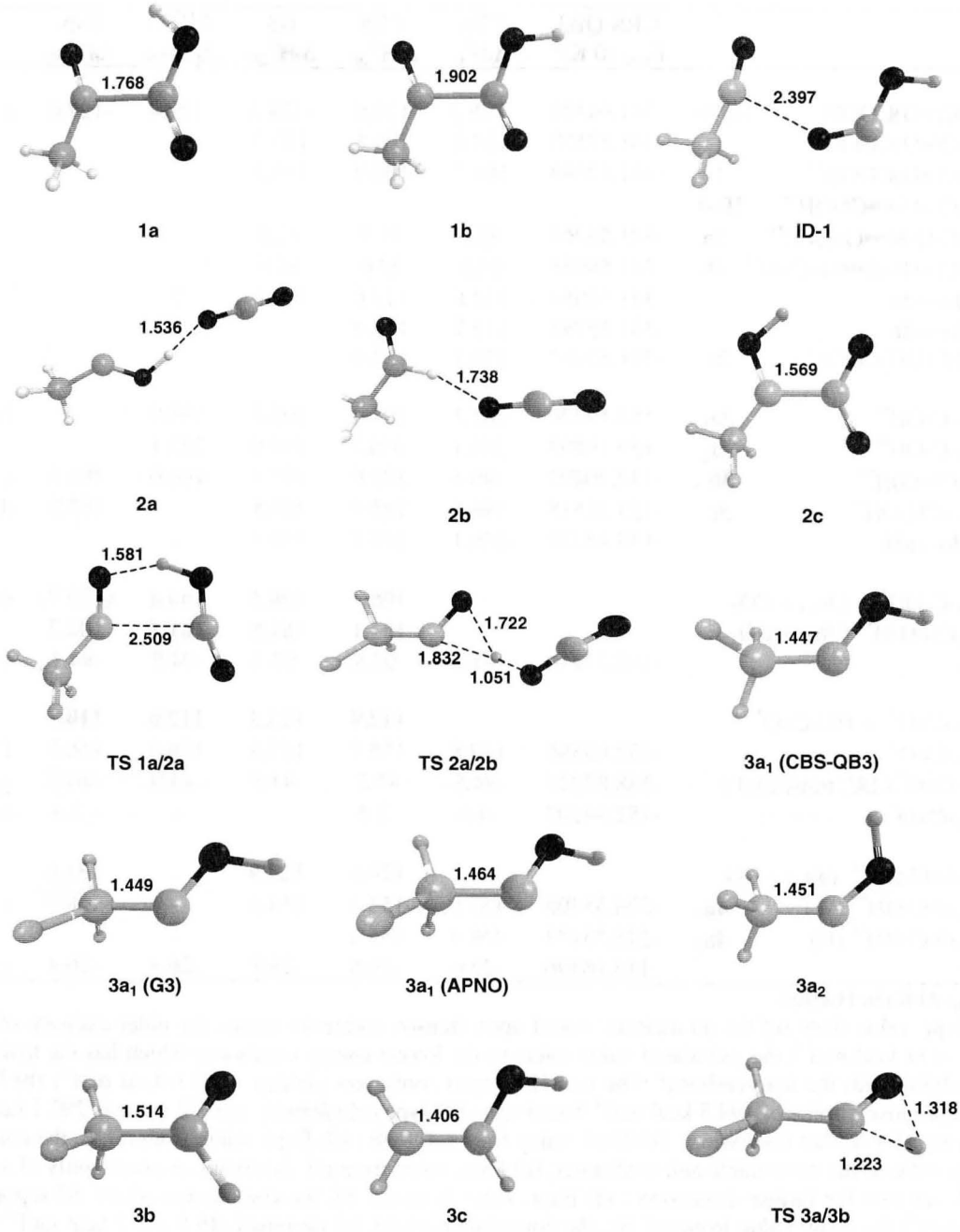

References

[1] C.Y. Wong, P.J.A Ruttink, P.C. Burgers, J.K. Terlouw, Chem. Phys. Lett. 387 (2004) 204.

[2] J.K. Terlouw, J. Wezenberg, P.C. Burgers, J.L. Holmes, J. Chem. Soc. Chem. Commun. 1121 (1983).

[3] W. Bertrand, G. Bouchoux, Rapid Commun. Mass Spectrom. 12 (1998) 1697.

[4] R. Flammang, M.T. Nguyen, G. Bouchoux, P. Gerbaux, Int. J. Mass Spectrom. 202 (2000) A8.

[5] W.J. Bouma, J.K. MacLeod, L. Radom. J. Am. Chem. Soc. 101 91979) 5540.

[6] J.L. Holmes, J.K. Terlouw, Org. Mass Spectrom. 15 (1980) 383.

[7] J.L. Holmes, J.K. Terlouw, Can. J. Chem. 53 (1975) 2076.

[8] (a) S.G. Lias, J.E. Bartmess, J.F. Liebman, J.L. Holmes, R.O. Levin, W.G. Maillard. J. Phys. Chem. Ref. Data, Suppl.1, **17** (1988) ; (b) NIST Chemistry WebBook, September 2005, National Institute of Standards and Technology, Gaithersburg MD, 20899 (http://webbook.nist.gov) ; (c) E.P.L. Hunter, S.G. Lias. J. Phys. Chem. Ref. Data **27,** 413 (1998) ; (d) Yu-Ran Luo. Handbook of dissociation energies in organic compounds. CRC Press, Boca Raton. 2003 ; (e) J.L. Holmes, F.P. Lossing and P.M. Mayer, J. Am. Chem. Soc. 113 (1991) 9723 ; (f) J.C. Traeger, B.M. Kompe. In *Energetics of Organic Free Radicals.* J.A.M. Simoes, A. Greenberg,, J.F. Liebman Eds. Blackie Academic & Professional, New York, 1996. Chapter 3 ; (g) S.P. McGlynn, J.L. Meeks, J. Electron Spectroscopy and related Phenomena, 6 (1975) 269; (h) N. Cohen and S.W. Benson. Chem. Rev. 93 (1993) 2419.

[9] H.F. van Garderen,, P.J.A. Ruttink, P.C. Burgers, G.A. McGibbon, J.K. Terlouw, Int. J. Mass Spectrom. Ion Processes 121 (1992) 159.

[10] (a) J.A. Montgomery Jr., M.J. Frisch, J.W. Ochterski, G.A. Petersson, J. Chem. Phys. 110 (1999) 2822; ibid. 112 (2000) 6532 ; (c) J.W. Ochterski, G.A. Petersson, J.A. Montgomery Jr., J. Chem. Phys. 104 (1996) 2598 (CBS-APNO reference).

[11] M.J. Frisch et.al., Gaussian 98, Revision A.11, Gaussian Inc., Pittsburg, PA, 1998

[12] M.J. Frisch et.al., Gaussian 03, Revision C.02, Gaussian Inc., Wallingford, CT, 2004

[13] L.A. Curtiss, K. Raghavachari, P.C. Redfern, V. Rassolov, J.A. Pople, J. Chem. Phys. 109 (1998) 7764.

[14] P.C. Burgers and J.K. Terlouw. *In* Encyclopedia of mass spectrometry. Vol. 4. *Edited by* N.M.M. Nibbering. Elsevier, Amsterdam. 2005. p. 173.

[15] K.-M. Marstokk, H.Mollendal, J.Mol. Struc., 20 (1974) 257.

[16] R. Lee, P.C. Burgers, P.J.A. Ruttink, J.K. Terlouw, Can. J. Chem. (2005), in press.

[17] J.C. Traeger. *In* Encyclopedia of mass spectrometry. Vol. 4. *Edited by* N.M.M. Nibbering. Elsevier, Amsterdam. 2005. p. 19.

[18] M.Meot-Ner, J.Am.Chem.Soc.106 (1984) 1257.

[19] T. Baer and W.L. Hase. Unimolecular reaction dynamics. Oxford University Press, New York. 1996. Chapter 7, p. 270-277.

[20] T. Baer and J.A. Booze. *In* Advances in classical trajectory methods. Vol. 2. *Edited by* W.L. Hase. JAI Press Inc., Hampton Hill England. 1994. p. 31-33.

Chapter 3

The characterization of isomeric CH_3O-P=$S^{\bullet+}$ and CH_3S-P=$O^{\bullet+}$ ions and the mechanism of their spontaneous water loss

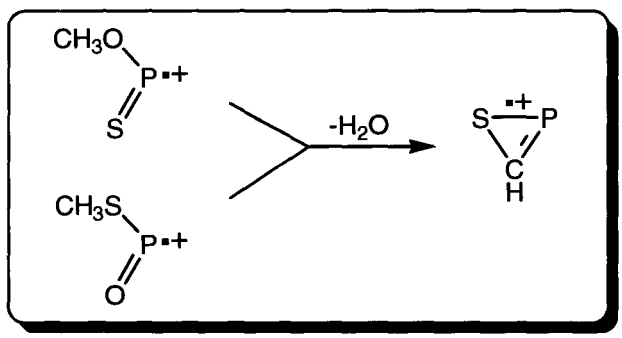

This Chapter describes the characterization of isomeric ions CH_3O-P=$S^{\bullet+}$ (**1a**) and CH_3S-P=$O^{\bullet+}$ (**1b**). A previous study on low energy CH_3O-P=$O^{\bullet+}$ ions reports that this ion undergoes a decarbonylation reaction as the predominate process to generate m/z 50 ions, HP-$OH_2^{\bullet+}$. However, the sulphur analogues appear to have their own unique chemistry. Low energy ions **1a** and **1b** spontaneously lose water to yield m/z 74 cyclic product ion [-S-CH=]$P^{\bullet+}$. Using the CBS-QB3, model chemistry a mechanism is proposed for the water loss from ions **1a** and **1b**. Dehydration of **1b** formally involves two H-shifts and a ring closure, while water elimination from **1a** involves a skeletal rearrangement. Our calculations also show that these two isomers communicate via a common intermediate, the distonic ion CH_2S-P-$OH^{\bullet+}$ (**1c**), prior to the loss of water.

1. Introduction

The study of organophosphorus compounds in the gas phase is an active research topic in the chemistry field mainly because of their integral role in the chemistry of pesticides and insecticides. Recently there has been a great deal of research focused on the mechanisms for decomposition of organophosphorus compounds upon ionization in the gas-phase [1-3].

Recent studies dealing with the dissociation of organophosphorus ions in the gas-phase have used tandem mass spectrometry in conjunction with computational chemistry to probe the associated ion structures and reaction mechanisms [2-4]. In this approach, a collision induced dissociation (CID) experiment, in which a mass-selected ion is collisionally energized to induce dissociation, often provides conclusive information about the structure (atom connectivity) of the ion of interest. The technique of neutralization reionization mass spectrometry (NR) [5] may provide useful complementary information, particularly where it concerns the isomeric purity of the ions [2]. This technique is also eminently suited to probing the structure and stability of elusive neutral species in the gas-phase [2]

Heydorn et al. previously reported the identity of the isobaric ions, $CH_3O\text{-}P{=}O^{\bullet+}$ and $CH_3O\text{-}P\text{-}NH_2^+$ (m/z 78), from the insecticide acephate [2]. It was found that the m/z 78 ions of acephate consist of the $CH_3O\text{-}P{=}O^{\bullet+}$ and $CH_2O\text{-}P\text{-}OH^{\bullet+}$ isomers in admixture with the isobaric ion $CH_3O\text{-}P\text{-}NH_2^+$. As a result the CID spectrum of the m/z 78 ions from acephate is not pure, and neither is the NR spectrum. Consequently the "survivor" ion signal is not indicative of the stability of the $CH_3O\text{-}P{=}O$ neutral as originally proposed by Srinivas and co-workers [3]. This is further supported by the computations that Heydorn and co-workers performed [2] : these indicate that the $CH_3O\text{-}P\text{-}NH_2^+$ ion may indeed have a stable neutral counterpart. Moreover, the "survivor" CID spectrum was found to be different from that of pure $CH_3O\text{-}P{=}O^{\bullet+}$ ions. The stability of the $CH_3O\text{-}P{=}O$ neutral was, however, ascertained by performing a collision-induced dissociative ionization (CIDI) experiment on an ion, $C_6H_5\text{-}P(=O)(H)OCH_3^{\bullet+}$, which loses $CH_3O\text{-}P{=}O$ neutrals. The resulting CID spectrum of the m/z 78 ions generated in the CIDI experiment of the above

precursor agrees with that of independently generated $CH_3O\text{-}P{=}O^{\bullet+}$ ions, thus attesting to the stability of $CH_3O\text{-}P{=}O$ as a neutral species. A follow-up study on the mechanism of the remarkable decarbonylation of the low energy (metastable) $CH_3O\text{-}P{=}O^{\bullet+}$ ions [5], established that there are a great many stable isomers of the $CH_3O\text{-}P{=}O^{\bullet+}$ ion.

Based on these observations we decided to explore the sulphur analogs of $CH_3O\text{-}P{=}O^{\bullet+}$, namely $CH_3O\text{-}P{=}S^{\bullet+}$ (**1a**) and $CH_3S\text{-}P{=}O^{\bullet+}$ (**1b**) ions, using computational chemistry and tandem mass spectrometric techniques. Some aspects of the dissociation chemistry of the $CH_3S\text{-}P{=}O^{\bullet+}$ ion and its neutral counterpart have recently been reported by Vivekananda et al. [3]. In their study they report that $CH_3S\text{-}P{=}O^{\bullet+}$ ions have a stable neutral counterpart, with a heat of formation of -60.1 kcal mol^{-1}. The presence of the sulfur atom in this system appears to have introduced its own chemistry. Metastable ions $CH_3O\text{-}P{=}S^{\bullet+}$ (**1a**) and $CH_3S\text{-}P{=}O^{\bullet+}$ (**1b**) spontaneously eliminate water and do not decarbonylate.

2. Experimental

The experiments were performed with the VG Analytical ZAB-R mass spectrometer of BEE geometry (B, magnet; E, electric sector). Metastable ion (MI) mass spectra were recorded in the second field free region (2ffr); collision-induced dissociation (CID) mass spectra were recorded in the 2 and 3ffr using oxygen as collision gas (Transmittance, T = 70%). The CID mass spectra of the 2ffr metastable peaks were obtained in the 3ffr using O_2 as collision gas. CID spectra of reference ions having a translational energy close to that of the product ions resulting from (MI or CID) dissociations in the 2ffr, were also obtained in the 3ffr. Neutralization-reionization mass spectra were recorded using N,N-dimethylaniline as the reducing agent and oxygen gas for reionization [5]. All spectra were recorded using a PC-based data system developed by Mommers Technologies Inc. (Ottawa).

Samples of *O*-methyl phosphorodichloridothioate, $CH_3O\text{-}P(=S)Cl_2$ (**I**), *S*-methyl phosphorodichloridothioate, $CH_3S\text{-}P(=O)Cl_2$ (**II**) and methamidophos,

$CH_3O(CH_3S)P(=O)NH_2$, were prepared as outlined by J.A. Lubkowitz and co-workers [6]. The reagents used for these syntheses were commercially available (Sigma-Aldrich) and of research grade. Dimethyl chlorothiophosphate, $(CH_3O)_2P(=S)Cl$ was of research grade from Sigma-Aldrich and used without further purification.

Structures and energies of the $CH_3S\text{-}P{=}O^{\bullet+}$ and $CH_3O\text{-}P{=}S^{\bullet+}$ ions and neutrals pertinent to this study, connecting transition states and dissociation products were probed by the standard CBS-QB3 model chemistry [7]. The calculations were performed using Gaussian 98 Revision A11.3 [8]. The calculated energies are presented in Table 1a/b and the potential energy diagrams of Figures 3 and 4. Frequency calculations gave the correct number of negative eigenvalues for all minima and transition states. Spin contamination was within the acceptable range. Figure 5 displays the optimized geometries for the principal species

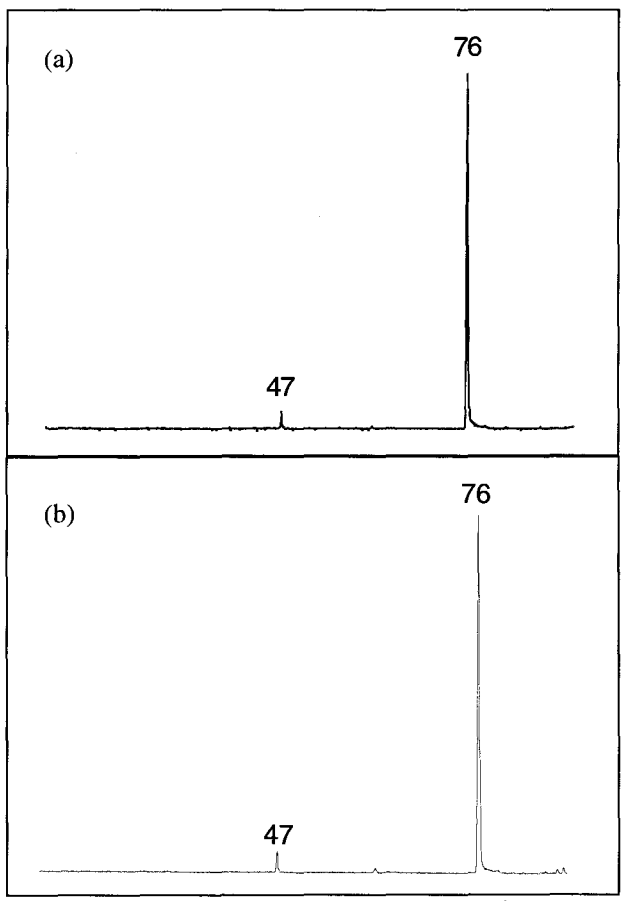

Fig. 1. Metastable ion spectrum of (a) $CH_3O\text{-}P{=}S^{\bullet+}$ and (b) $CH_3S\text{-}P{=}O^{\bullet+}$.

3. Results and Discussion

*3.1 Characterization of the ions CH_3O-P=$S^{\bullet+}$, **1a**, and CH_3S-P=$O^{\bullet+}$, **1b**, and their neutral counterparts*

Ion **1a**, CH_3O-P=$S^{\bullet+}$, was generated from two independent precursor ions : (i) from ionized O-methyl phosphorodichloridothiolate, $CH_3OP(=S)Cl_2$, **I**, by two consecutive $Cl^{\bullet}$ losses and (ii) by loss of $Cl^{\bullet}$ and $CH_3O^{\bullet}$ from ionized dimethyl chloro-thiophosphate, $(CH_3O)_2P(=S)Cl$. The CID spectra of the m/z 94 ions generated by the two routes were closely similar. The CID spectrum of **1a** (see Fig. 2a) displays a characteristic base peak at m/z 63, PS^+, the result of a direct bond cleavage. Other intense signals are present at m/z 31 (CH_2OH^+), m/z 47 (loss of $PO^{\bullet}$), m/z 62 ($CH_3OP^{\bullet+}$), m/z 64 (loss of H_2C=O), m/z 76 (loss of H_2O), and m/z 79 ($S=P=O^+$). The presence of a peak at m/z 62, which is a direct bond cleavage reaction resulting from the loss of a S atom from **1a**, serves as evidence that ions **1a** maintain their structure connectivity.

As in the case of **1a**, ions **1b**, CH_3S-P=$O^{\bullet+}$, were generated by two different routes : (i) by two consecutive $Cl^{\bullet}$ losses from ionized S-methyl phosphorodichloridothiolate, $CH_3SP(=O)Cl_2$, **II**, and (ii) from the collision induced dissociation of the m/z 125 $CH_3SP(=O)CH_3^+$ ions generated from ionized acephate. The closely similar CID mass spectra of the resulting m/z 94 ions are, see Fig. 2b, characteristically different from the CID mass spectrum of **1a**. The CID spectrum of **1b** ions shows a base peak at m/z 47 (CH_2SH^+), followed by peaks at m/z 63 (PS^+) and m/z 76 ((-HC-S-)$P^{\bullet+}$).

In the CID spectrum of **1b**, the base peak at m/z 47 corresponds to CH_2SH^+ ions. To generate the CH_2SH^+ cation directly from ion **1b**, an energetically costly 1,2-H shift is required, which is unlikely. Alternatively, ion **1b** may undergo a 1,4-H shift to form its more stable distonic ion counterpart, **1c**, CH_2S-P-$OH^{\bullet+}$. The calculations, see Fig.3 and Table 1, indicate that the formation of the distonic ion is reasonable since the barrier for the 1,4-H shift lies only 2 kcal mol^{-1} above **1b.** This ion can then rearrange via a 1,3-H shift to form the ion-dipole complex,**1e**, $[CH_2SH\bullet\bullet\bullet PO]^{\bullet+}$, the immediate precursor ion for the generation of $CH_2SH^+ + PO^{\bullet}$.

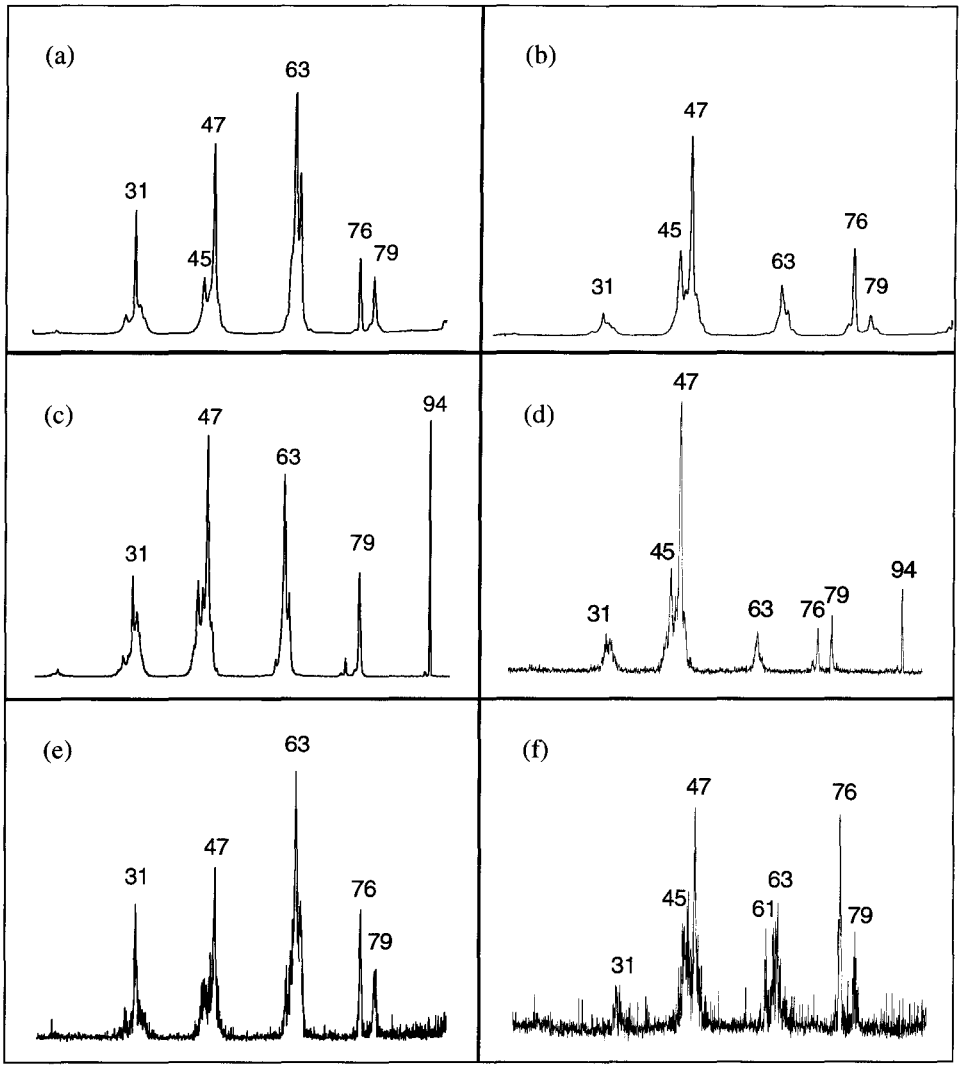

Fig. 2. Spectra of m/z ions 94 **1a** and **1b** (top) CID, (middle) NRMS, (bottom) Survivour

The CID spectra indicate that ions **1a** maintain their structural integrity, while **1b** ions preferentially isomerize into their distonic counterpart, ions **1c**, $CH_2S\text{-}P\text{-}OH^{\bullet+}$. The computational results agree with the experimentally observed behaviour of ions **1a** and **1b**.

The MI spectrum of ion **1a** shows one prominent reaction, the elimination of H_2O to yield m/z 74 ions, and only a minor peak at m/z 47, see Fig. 1a. The kinetic energy releases of both these reactions are small, 26.1 meV and 6.5 meV, for m/z 74 and 47, respectively and are not indicative of any significant reverse activation energy.

The m/z 74 product ion of the water loss was identified to be the cyclic ion, P[-C(H)-S-]$^{\bullet+}$. Three stable CHSP$^{\bullet+}$ structures were calculated, of the three the cyclic ion P[-C(H)-S-]$^{\bullet+}$ was calculated to be the most stable CHSP$^{\bullet+}$ isomer lying at 247.7 kcal mol^{-1}, see Table 1b. Remarkably, the MI spectrum of ion **1b** is virtually identical to the MI spectrum of **1a**, see Fig. 1b. The kinetic energy releases of both these reactions are small, similar to **1a**, 29.2 meV and 3.3 meV, for m/z 74 and 47, respectively.

The m/z 74 product ion was found to be the same cyclic ion, P[-C(H)-S-]$^{\bullet+}$. The mechanism of the water loss and the communication of ions **1a** and **1b** were probed by theory, uncovering a complex system of isomers. The details of the mechanism of communication between ions **1a** and **1b** and their water loss will be discussed in Section 3.2 and 3.3, respectively.

To characterize neutral **1a** and **1b** molecules, experiments involving neutralization-reionization mass spectrometry (NRMS) [5] were conducted. In the NRMS experiments the beam of mass selected m/z 94 ions was neutralized by charge-exchange with N,N-dimethylaniline. The subsequent beam of neutral molecules was then re-ionized by collision with O_2 gas. The NR spectrum of neutral **1a**, see Fig. 2c, displays a sizable peak at m/z 94, expected to correspond to re-ionized CH_3O-P=S molecules. This is indeed the case as demonstrated by the CID spectrum of the m/z 94 survivor ions shown in Fig. 2e. A comparison of the survivor CID spectrum of Fig. 2e with the CID spectrum of Fig. 2a leaves little doubt that the re-ionized m/z 94 ions correspond to CH_3O-P=S$^{\bullet+}$. The heat of formation of **1a** was calculated to be - 45 kcal mol^{-1}, see Table 1, in agreement with the NR results.

The NR spectrum of **1b** shows a fairly strong peak at m/z 94, see Fig. 2d, Comparison of the survivor CID spectrum of **1b** to its 3ffr CID spectrum, see Fig. 2b, it can be concluded that these ions are of different structure. The CID spectrum of the survivor CH_3SP=O$^{\bullet+}$ ions has a fairly intense peak at m/z 76 of almost equal intensity to the base peak at m/z 47 but the 3ffr CID of source generated **1b** ions show the peak at m/z 76 is nearly half the intensity of the base peak. This result implies the neutral counterpart

of ion **1b** is not stable on the μs time scale and may undergo a facile isomerization into its distonic counterpart upon ionization.

3.2 Communication between ions 1a and 1b

The CID spectra of ions **1a** and **1b** indicate that the isomeric ions do not easily communicate. However, their respective MI spectra do show that the two ions may lose water via a sufficiently low interconversion barrier. In both cases, the MI spectrum displays an intense base peak at m/z 76 (loss of H_2O) and a minor peak at m/z 47, see Fig.1. The loss of water from these two isomers suggests that ions **1a** and **1b** communicate via a common intermediate.

A 1,3-CH_3 shift would be an obvious route of communication between ions **1a** and **1b** but this appears to be a very energy demanding process, requiring 54 kcal mol^{-1}, see Fig. 3 and Table 1. Thus, there must be an alternative pathway connecting these two isomers. In order for these two ions to communicate, the pathway must lie below the energy for the formation of CH_2SH^+ + $PO^•$, as indicated in the energy diagram of Fig. 3.

We will use the energy diagram of Fig. 3 as a guide in the discussion of the proposed mechanism for the communication of **1a** and **1b**. Starting from ion **1a**, a 1,4-H shift may lead to the formation of its distonic ion **1d**, via a TS calculated to lie at 187 kcal mol^{-1}. Elongation of the O-P bond and the concomitant formation of an O-H bond may lead to the hydrogen-bridged radical cation, **1f**, via a TS lying at 194 kcal mol^{-1}. A rotation of the CH_2OH moiety of HBRC **1f** yields a slightly more stable ion, **1g**, via a barrier of 9 kcal mol^{-1}. Ion **1g** can then rearrange into ion **1h** by breaking the S--O bond and forming a C-S bond. Once ions **1h** have been formed, a formal 1-3-CH_2 shift will lead to the stable distonic ion, **1c.** The transition state at 200 kcal mol^{-1} connecting ions **1h** and **1c** is quite high in energy but it lies is still below the dissociation level of CH_2SH^+ + $PO^•$. Ion **1b** can undergo a 1,4-H shift to form its distonic counterpart **1c**, via a TS lying only 2 kcal mol^{-1} above **1b**. Ion **1c** is the common intermediate shared by ions **1a** and **1b** prior to

their water elimination and it will be shown in the next section that the water elimination proceeds via ion **1c**.

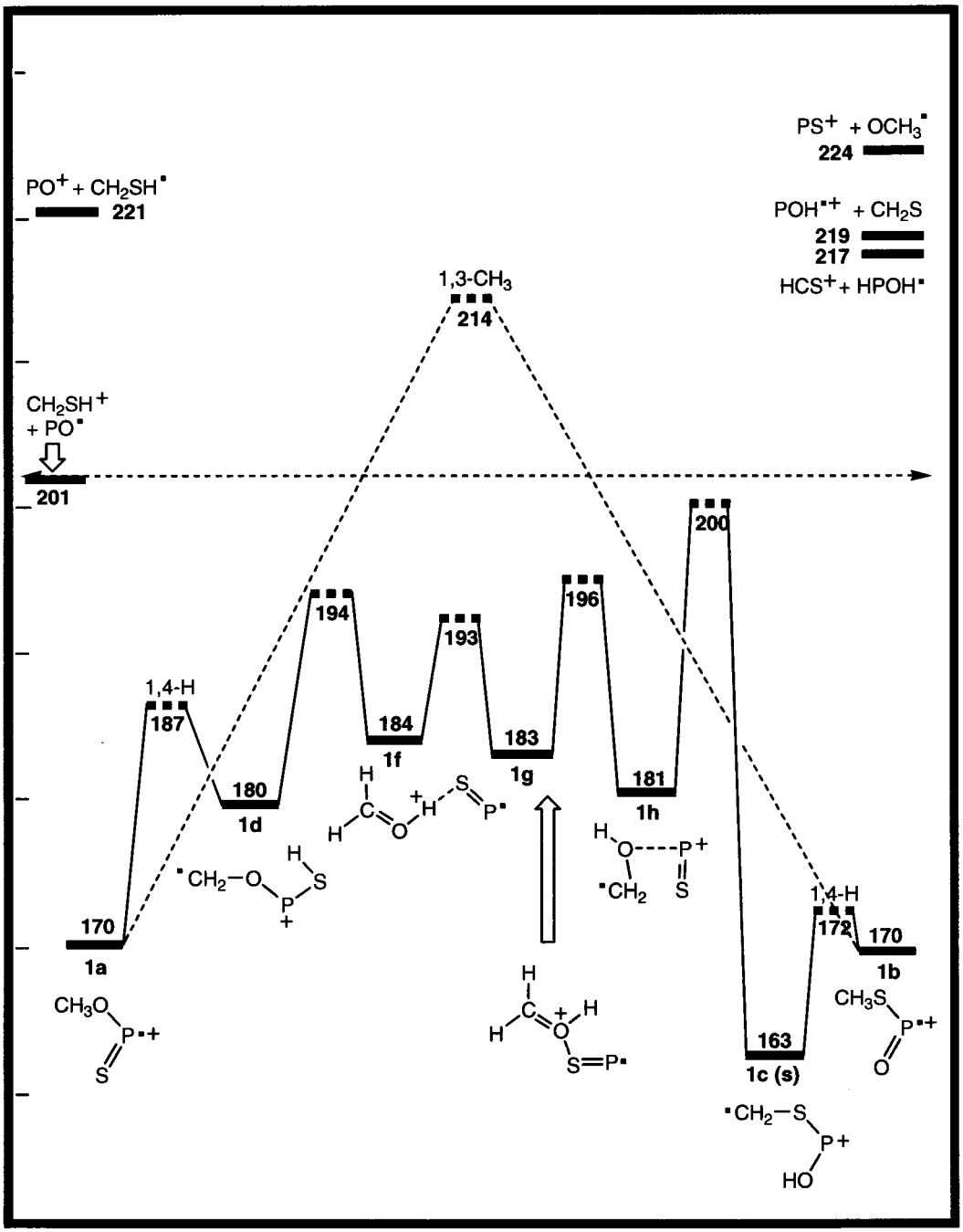

Fig. 3 Energy level diagram derived from CBS-QB3 calculations describing the communication between metastable $CH_3O\text{-}P{=}S^{\bullet+}$ (**1a**) and $CH_3S\text{-}P{=}O^{\bullet+}$ (**1b**) ions. The numbers refer to $\Delta_f H^0_{298}$ values in kcal mol^{-1}.

3.3 Spontaneous water loss from ions 1a and 1b

In the previous section it was shown that ions **1a** and **1b** can communicate via a common intermediate **1c**, and we will describe the water elimination beginning with ion **1c**. The energy diagram of Fig. 4 will act as a guide to describe the water loss. Starting from ion **1c**, a bond formation between C and P may lead to the formation of the cyclic ion **1j**, via a fairly high barrier of 20 kcal mol^{-1}. A formal 1,3-H shift in ion **1j** then yields the ion-dipole complex **1k**, $H_2O\bullet\bullet\bullet P[\text{-}C(H)\text{-}S\text{-}]^{\bullet+}$, the direct precursor ion for the formation of $P[\text{-}C(H)\text{-}S\text{-}]^{\bullet+} + H_2O$. The barrier **1j** → **1k** lies at 202 kcal mol^{-1}, close to the level for the dissociation products $CH_2SH^+ + PO^\bullet$.

Finally we note that the TS connecting **1j** and **1k** can compete with a 1,3-H shift from **1c** to yield the ion-dipole complex **1e**, which serves as the direct precursor to the generation of $CH_2SH^+ + PO^\bullet$ at 201 kcal mol^{-1}. The barrier for TS **1c** → **1e** lies at the same level as TS **1j** → **1k**. Although the energy barrier of both competing 1,3-H shifts lie at the thermochemical threshold, the water elimination is the predominant reaction with a minor loss of $PO^\bullet$, see Fig. 1a/b. This result can be rationalized by comparing the energy levels of the dissociation products. Ions **1c** with enough energy will preferentially dissociate into $[\text{-}S\text{-}P\text{-}CH_2\text{-}]^{\bullet+} + H_2O$ because the energy difference between the 1,3-H shift transition states and their respective dissociation products is greater for TS **1c** →**1j** → **1k** than **1c** → **1e**, as a result the loss of $PO^\bullet$ competes poorly with the water elimination reaction.

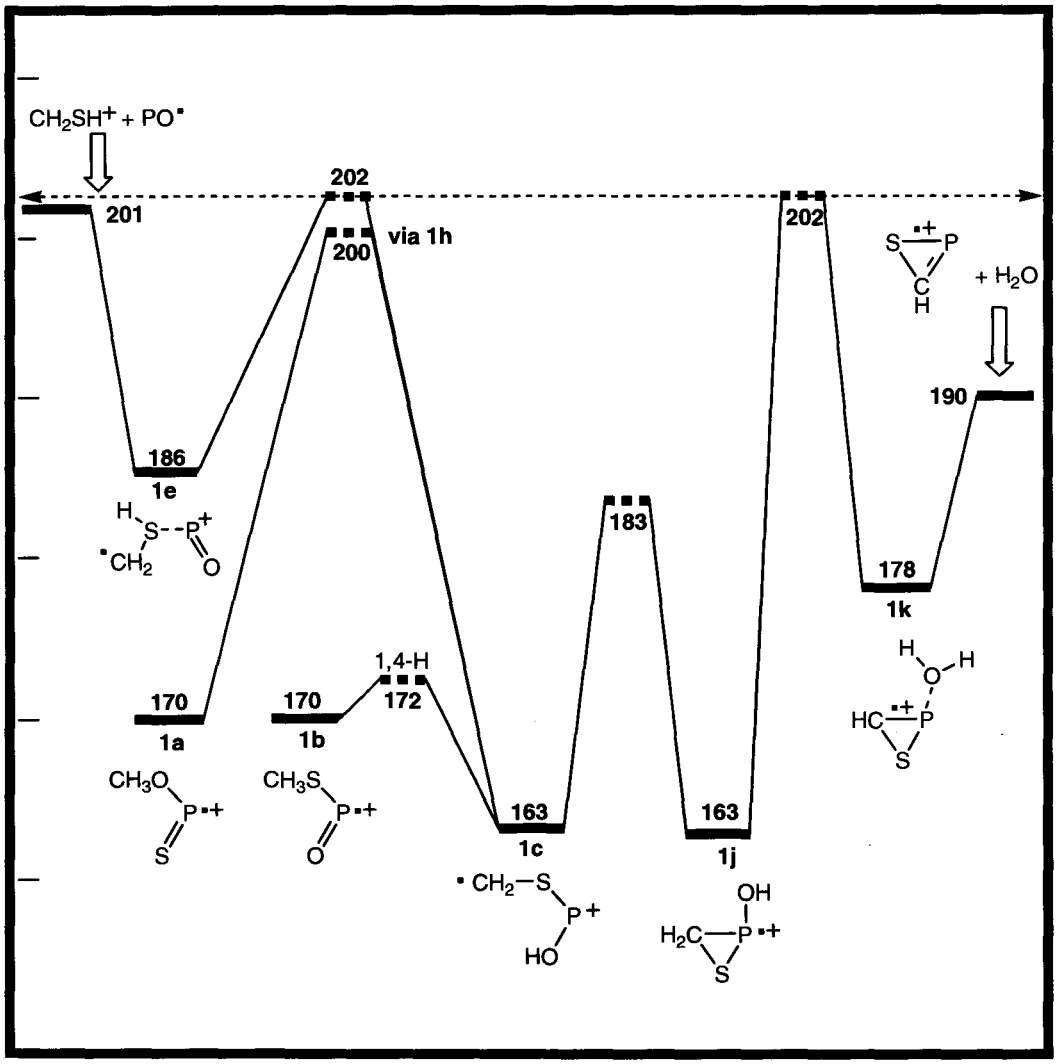

Fig. 4 Energy-level diagram derived from CBS-QB3 calculations describing the water elimination from metastable $CH_3O\text{-}P{=}S^{\bullet+}$ (**1a**) and $CH_3S\text{-}P{=}O^{\bullet+}$ (**1b**) ions. The numbers refer to $\Delta_f H^0_{298}$ values in kcal mol^{-1}.

Conclusion

The structure, stability and isomerization behaviour of isomeric ions **1a,** $CH_3O\text{-}P{=}S^{\bullet+}$, and **1b,** $CH_3S\text{-}P{=}O^{\bullet+}$, was probed using the CBS-QB3 model chemistry. From neutralization-reionization experiments on ions **1a** and **1b**, it follows that ion **1a** has a stable neutral counterpart, as predicted by theory. The NR experiments of **1b** do not show it has a stable neutral counterpart in the gas-phase. The communication between low energy **1a** and **1b** ions and their mechanism of the water was established by theory. The details of the mechanism of water elimination process revealed that ions **1a** and **1b**

communicate via ion **1c**, $CH_2S\text{-}P\text{-}OH^{\bullet+}$, prior to H_2O loss. The water elimination proceeds via ion **1c**, which can isomerize into **1k**, the direct precursor ion to yield $[\text{-}S\text{-}P\text{-}CH_2\text{-}]^{\bullet+}$ and water.

References

[1] L.N. Heydorn, Y. Ling, D. de Oliveria, J.M.L. Martin, C. Lifshitz, J.K. Terlouw, Zeit. Physik. Chemie 215 (2001) 141.

[2] L.N. Heydorn, C.Y Wong, R. Srinivas, J.K. Terlouw, Int. J. Mass Spectom. 225 (2003) 11

[3] S. Vivekananda, R Srinivas, Int. J. Mass Spectrom. Ion Proc. 171 (1997) 79.

[4] L.N. Heydorn, P.C Burgers, P.J.A. Ruttink, J.K. Terlouw. Chem. Phys. Let. 368 (2003) 584.

[5] For selected recent reviews see: (a) G. Schalley, G. Hornung, D. Schroder and H. Schwarz, Chem. Soc. Rev 27 (1998) 91; (b) N. Goldberg and H. Schwarz, Acc. Chem. Res. (1994) 43.

[6] J.A. Lubkowitz, A.P. Revilla, J. Baruel, J. Agr. Food Chem. 22 (1974) 151.

[7] (a) J.W. Ochterski, G.A. Petersson, and J.A. Montgomery, Jr. J. Chem. Phys. 104 (1996) 2598. (b) J.A. Montgomery, Jr, M.J. Frisch, J.W. Ochterski, and G.A. Petersson. J. Chem. Phys. 112 (2000) 6532.

[8] M.J. Frisch, et al. Gaussian 98, Reversion A.9 Gaussian Inc., Pittsburgh, PA,1998.

Appendix to Chapter 3

Fig.5. The CBS-QB3 optimized geometries for $CH_3O\text{-}P{=}S^{\bullet+}$ **1a**, $CH_3S\text{-}P{=}O^{\bullet+}$ **1b** ions and selected transition states.

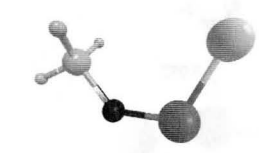

1a (s)

1a (a)

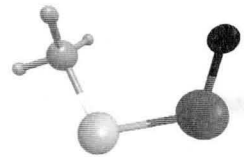

1b (s)

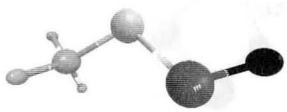

1b (a)

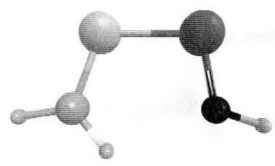

1c (s)

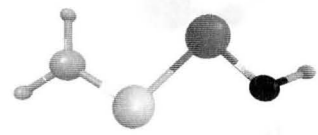

1c (a)

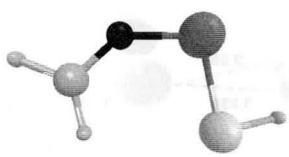

1d (s)

1d (a)

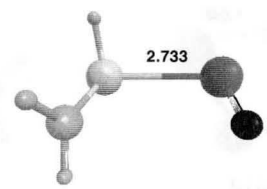

1e

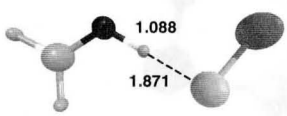

1f

1g

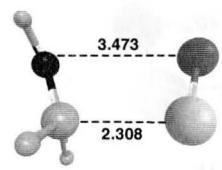

1h

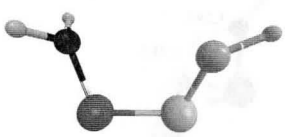

1i

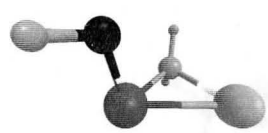

1j

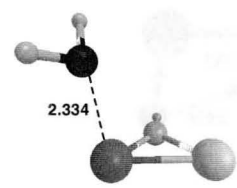

1k

Fig. 5. *cont*

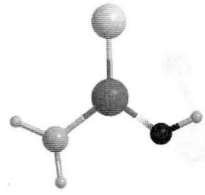

1l

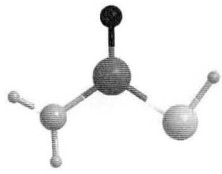

1m

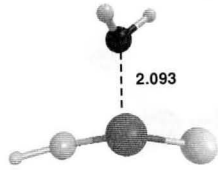

1n

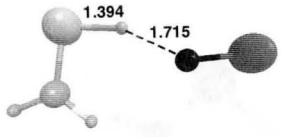

1o

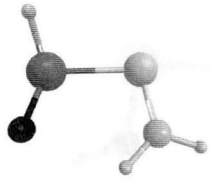

1p

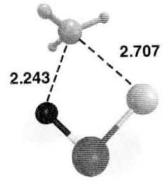

TS 1a/1b

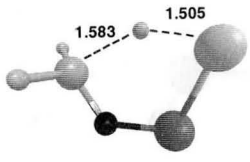

TS 1a/1d

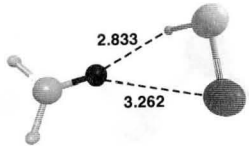

TS 1d/1f

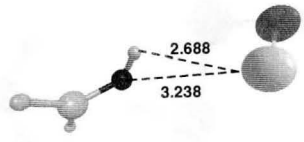

TS 1f/1g

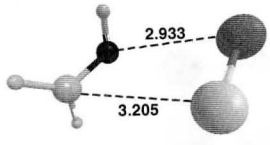

TS 1g/1h

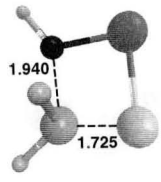

TS 1h/1c

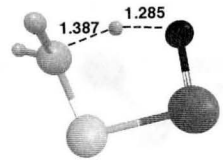

TS 1b/1c

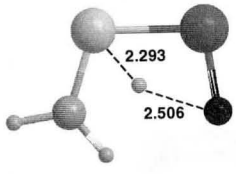

TS 1c/1e

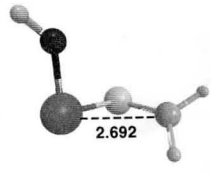

TS 1c/1j

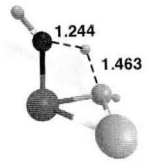

TS 1j/1k

Table 1a. Enthalpies of formation derived from CBS-QB3 calculations of stable isomers and connecting transition states involved in the water loss from $CH_3O\text{-}P{=}S^{\bullet+}$, **1a**, and $CH_3S\text{-}P{=}O^{\bullet+}$, **1b**.

Ionic Species		CBS-QB3 [0 K] E(total)	ZPE	$\Delta_f H^0_0$	$\Delta_f H^0_{298}$
$CH_3O\text{-}P{=}S^{\bullet+}$ (syn)	**1a** (s)	-853.30864	27.17	172.5	170.0
$CH_3O\text{-}P{=}S^{\bullet+}$ (anti)	**1a** (a)	-853.30729	27.04	173.4	170.9
$CH_3S\text{-}P{=}O^{\bullet+}$ (syn)	**1b** (s)	-853.30486	25.99	174.9	170.0
$CH_3S\text{-}P{=}O^{\bullet+}$ (anti)	**1b** (a)	-853.30762	26.12	173.2	171.9
$CH_2S\text{-}P\text{-}OH^{\bullet+}$	**1c**	-853.31756	25.27	166.9	164.5
$CH_2S\text{-}P\text{-}OH^{\bullet+}$ (syn)	**1c** (s)	-853.32009	25.58	165.3	162.7
$CH_2O\text{-}P\text{-}SH^{\bullet+}$	**1d**	-853.29330	24.23	182.2	179.8
$CH_2O\text{-}P\text{-}SH^{\bullet+}$ (syn)	**1d** (s)	-853.29422	24.18	181.6	179.1
$CH_2S(H)\text{-}P{=}O^{\bullet+}$	**1e**	-853.28471	23.60	187.5	185.5
$CH_2O{\bullet\bullet\bullet}H{\bullet\bullet\bullet}SP^{\bullet+}$	**1f**	-853.28718	23.79	186.0	184.0
$CH_2O(H){\bullet\bullet\bullet}S{=}P^{\bullet+}$	**1g**	-853.28806	23.80	185.4	182.8
$CH_2O(H)\text{-}P{=}S^{\bullet+}$	**1h**	-853.29136	27.40	183.4	181.0
$H_2O{\bullet\bullet\bullet}PSCH^{\bullet+}$	**1i**	-853.20012	24.43	240.6	238.7
$[\text{-}CH_2\text{-}S\text{-}]P\text{-}OH^{\bullet+}$	**1j**	-853.31894	26.16	166.1	163.2
$H_2O{\bullet\bullet\bullet}P[\text{-}C(H)\text{-}S\text{-}]^{\bullet+}$	**1k**	-853.29734	25.10	179.6	177.8
$CH_2{=}P(OH)\text{-}S^{\bullet+}$	**1l**	-853.32482	25.72	162.4	159.7
$CH_2{=}P(SH)\text{-}O^{\bullet+}$	**1m**	-853.30090	24.01	177.4	174.8
$H_2O{\bullet\bullet\bullet}S(P)CH^{\bullet+}$	**1n**	-853.22040	21.84	227.9	226.3
$CH_2S{\bullet\bullet\bullet}H{\bullet\bullet\bullet\bullet}OP^{\bullet+}$	**1o**	-853.28709	23.85	186.0	184.1
$CH_2SP(H)O^{\bullet+}$	**1p**	-853.28729	24.29	185.9	183.3
$CH_2O(H)\text{-}P{=}S^{\bullet+}$	**1q**	-853.25860	25.90	204.3	202.5
$CH_3O\text{-}P{=}S$		-853.65061	27.37	-42.1	-44.7
$CH_3S\text{-}P{=}O$		-853.65973	26.61	-47.8	-50.3
TS **1a** (s) → **1b** (s)		-853.23930	20.87	216.0	213.5
TS **1a** (s) → **1d** (s)		-853.28036	22.92	190.3	187.2
TS **1d** (s) → **1f**		-853.26937	27.61	197.2	194.4
TS **1f** (s) → **1g** (s)		-853.26506	26.09	196.9	192.6
TS **1g** (s) → **1h** (s)		-853.26537	26.31	199.7	195.7
TS **1h** (s) → **1c** (s)		-853.25956	25.64	203.3	200.3
TS **1b** (s) → **1c**		-853.30457	25.89	175.1	172.3
TS **1c** → **1e**		-853.25817	23.89	204.4	201.1
TS **1c** → **1j**		-853.28694	25.02	186.1	183.4
TS **1j** → **1k**		-853.25656	22.91	205.2	202.1

Table 1b. Relative energies, E_{rel} (kcal/mol), of dissociation reactions of ion **1c**$^{\bullet+}$ derived from CBS-QB3 calculations.

Ions	E_{Total} [0K]	ZPVE	ΔH°_f [0K]	ΔH°_f [298K]
$S{=}P{=}O^{+}$	-813.46753	3.28	196.7	197.3
$CH_3^{\bullet}$	-39.74479	18.37	36.6	35.5
$HP{=}C{=}S^{\bullet+}$	-776.93310	8.09	253.9	254.9
HP=C=S	-777.25248	8.40	53.5	53.7
$HSCP^{\bullet+}$	-776.91774	8.55	263.5	263.0
$HCPS^{\bullet+}$	-776.85785	8.43	301.1	300.7
$[\text{-CH-S-}]P^{\bullet+}$	-776.94154	10.19	248.6	247.7
H_2O	-76.33746	13.24	-57.5	-58.2
$CH_3S\text{-}P^{\bullet+}$	-778.15015	24.05	220.8	218.6
O	-74.98764	0.00	59.0	59.4
$PSH^{\bullet+}$	-738.90533	5.53	236.0	235.2
$CH_2{=}O$	-114.34413	16.45	-26.4	-27.3
PS^{+}	-738.35031	1.21	219.0	218.8
$OCH_3^{\bullet}$	-114.87434	22.78	6.5	4.7
$CH_3O\text{-}P^{\bullet+}$	-455.52165	25.72	188.2	185.5
S	-397.65737	0.00	93.8	94.2
$HPCO^{\bullet+}$	-454.3302	9.53	205.3	204.7
H_2S	-398.93491	9.32	-5.5	-6.2
$POH^{\bullet+}$	-416.29431	7.70	192.5	191.6
$CH_2{=}S$	-436.93816	15.33	27.8	26.9
CH_2SH^{+}	-437.22771	21.75	211.4	209.5
SCH_3^{+}	-437.15072	18.70	259.7	257.5
$PO^{\bullet}$	-416.03233	1.77	-8.4	-8.6
PO^{+}	-416.27365	2.05	184.7	184.5
$CH_2SH^{\bullet}$	-437.50390	19.18	38.1	36.5
$CH_2{=}S^{\bullet+}$	-436.59456	14.67	243.4	242.5
POH	-416.57873	8.01	14.1	13.2
$H\text{-}C{\equiv}S^{+}$	-436.01617	7.82	241.1	241.2
$HPOH^{\bullet}$	-417.21888	12.99	-22.4	-24.0
$S{=}P{=}O^{\bullet}$	-813.77711	2.39	2.4	1.6
CH_3^{+}	-39.38466	19.17	262.2	261.3

*E_{total} in Hartrees, all other values in kcal/mol, including the ZPVE scaled by 0.99.

Chapter 4

The water elimination from the ethyl acetate radical cation : Answers from theory to a longstanding mechanistic problem

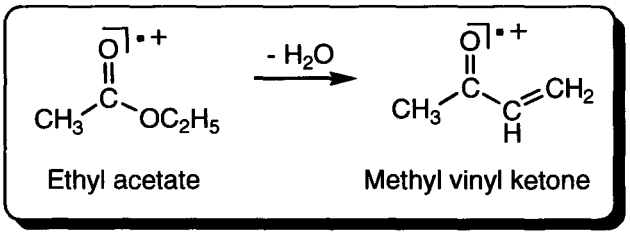

Abstract

Previous experimental studies of the water elimination from ionized ethyl acetate (**EA-1**) and its enol, CH_2=C(OH)$OC_2H_5^{\bullet+}$ (**EA-2**) provide no mechanistic proposals but note that the reaction is complex because all hydrogen atoms and both oxygen atoms participate. Loss of H_2O is the predominant process observed for the metastable ions, yielding ionized methyl vinyl ketone, $CH_3C(=O)CH=CH_2^{\bullet+}$ (**MVK**), as the product ion. Metastable keto-alcohol ions $CH_3C(=O)CH_2CH_2OH^{\bullet+}$ (**HB-1**) also abundantly lose H_2O, yielding **MVK** at the thermochemical threshold. Using the CBS-QB3 model chemistry and complementary RRKM calculations, we have examined plausible mechanisms for the water elimination from metastable ions **EA-1/2** and **HB-1**. Our calculations support the proposal that (i) ions **HB-1** dissociate into **MVK** at the thermochemical threshold via a 1,4-H shift and a consecutive [1,2]-hydroxycarbene shift and (ii) ions **EA-1/2** undergo a three-step isomerization reaction into **HB-1**, which serves as the precursor for the ensuing water elimination. It is further shown that synergy between theory and experiment leads to a complex yet transparent mechanistic picture of ionized ethyl acetate's isomerization and dissociation behaviour which accounts for the labelling results.

Introduction

Since the inception of electron ionization (EI) mass spectrometry as a powerful method for the structure analysis of organic molecules in the mid 1950's, the gas-phase ion chemistry of ethyl acetate has been studied extensively. Two dissociations of the ethyl acetate radical cation, $CH_3C(=O)OCH_2CH_3^{\bullet+}$ (**EA-1**), have received particular attention : **EA-1** $\rightarrow C_2H_5O_2^+ + C_2H_3^\bullet$ and **EA-1** $\rightarrow C_4H_6O^{\bullet+} + H_2O$. Peaks at m/z 61 and 70 resulting from these rearrangement reactions prominently feature in the ester's conventional EI mass spectrum, as shown in Fig. 1a.

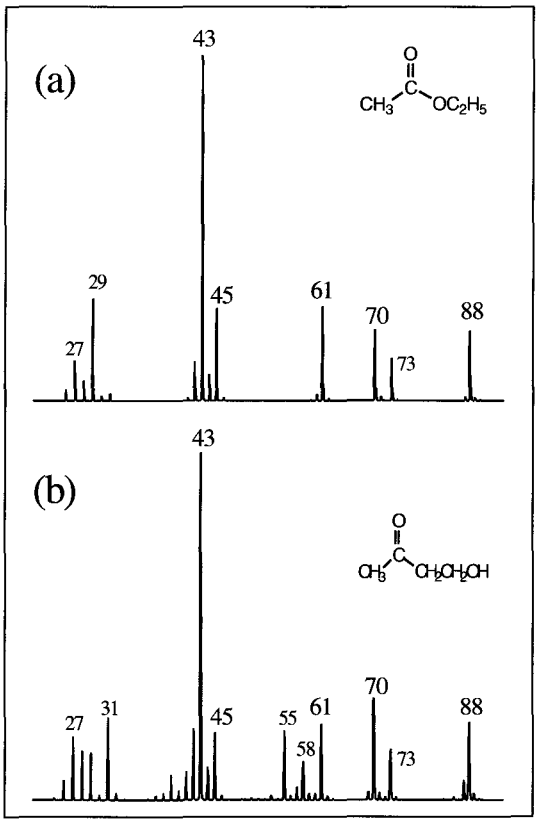

Fig.1 70 eV EI mass spectra of ethyl acetate (item a) and its 4-hydroxy-2-butanone isomer (item b).

In 1962, Godbole and Kebarle [1] using deuterium labeling found that the acetyl methyl group remained intact during the formation of $C_2H_5O_2^+$, while hydrogen atoms were randomly transferred from the ethyl group. In 1977, Benoit, Harrison and Lossing

[2] concluded that the m/z 61 product ion is carbonyl protonated acetic acid, $CH_3C(OH)_2^+$, rather than its higher energy isomer $CH_3C(=O)OH_2^+$ [3] and that the keto ester ion **EA-1** may isomerize to its more stable [4] enol form $CH_2=C(OH)OCH_2CH_3^{\bullet+}$ (**EA-2**) prior to dissociation. Dissociation into $CH_3C(OH)_2^+$ has become a textbook example of a "McLafferty + 1" rearrangement [5]. The first step of the proposed mechanism [5] leads to the distonic ion $[CH_3C(OH)OCH_2CH_2]^{\bullet+}$ (**EA-3**) via a 1,5-H shift in **EA-1**. A consecutive 1,3-H shift from the terminal CH_2 group to the ether O atom in **EA-3** then initiates the $C_2H_3^\bullet$ loss. We will examine this proposal in more detail in Section 1.3 of the Results and Discussion.

The elimination of H_2O into ions $C_4H_6O^{\bullet+}$ (m/z 70) has been studied in much greater detail [6-8] than the $C_2H_3^\bullet$ loss, but its mechanism is still shrouded in mystery. Loss of water represents the unimolecular reaction of lowest energy requirement for ionized ethyl acetate [7,8]. In line with this, it is the predominant process observed for metastable [9] ions **EA-1** dissociating in the μs time-frame : loss of $C_2H_3^\bullet$ competes unfavourably as its metastable peak is only 0.02 as intense as that for the H_2O loss process [7].

The reaction was first studied by Yeo [6] in 1970. He studied both metastable ions and ions dissociating in the source and found that deuteriums on the ethyl group more readily end up in the neutral water fragment than do the deuteriums on the acetyl group. The degree of hydrogen exchange becomes greater as the lifetime of the precursor ion increases, that is when the internal energy content of the ion becomes lower. Yeo proposed that the intra- and inter-alkyl H-H exchange reactions take place from the *unrearranged* keto ion **EA-1** and that the actual mechanism for H_2O loss involves ring closure of **EA-1** into the 2-hydroxy-2-methyloxetane ion, as depicted in Scheme 1.

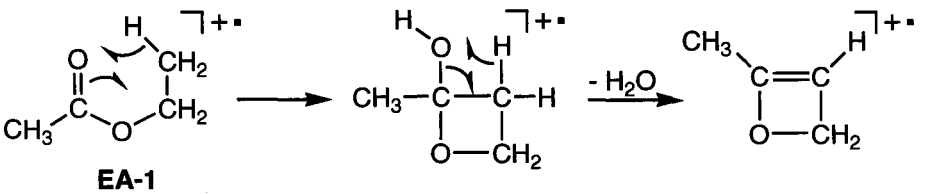

Scheme 1

The cyclic ion would then undergo H_2O elimination yielding ionized 2-methyloxetene, the four-membered ring-closed form of ionized methyl vinyl ketone, $CH_3C(=O)CH=CH_2^{\bullet+}$ (**MVK**). Yeo formulated this proposal some twenty years before the role of distonic ions as stable key intermediates was fully established [10]. A more plausible formulation of the cyclization step in his mechanism would involve formation of the distonic ion **EA-3** as the first step (as in the mechanism for $C_2H_3^{\bullet}$ loss discussed above), followed by cyclization. We further note that Yeo's proposal remains speculative because there is no experimental evidence for the proposed product ion structure.

In 1981, Holmes et al. [7] investigated the H_2O loss from **EA-1** and its independently generated enol **EA-2**, employing most of the presently available methodology for the detailed study of unimolecular ionic dissociations [11]. These included metastable ion (MI) and collision induced dissociation (CID) mass spectra, appearance energy (AE) measurements using electron ionization (EI), thermochemical data [12] and analysis of D- and ^{18}O-labelled isotopologues. Shortly thereafter, Baer and co-workers [8] used photoionization (PI) to study the energetics of the five primary dissociations of **EA-1**; in addition, they studied the rate of the H_2O elimination using photoion-photoelectron coincidence (PIPECO) experiments in conjunction with RRKM/QET calculations.

Although these two papers contain a wealth of experimental observations on ethyl acetate's gas-phase ion chemistry, they do not provide a clear mechanistic picture of the H_2O loss. The most important results and conclusions pertaining to the H_2O elimination are the following :

(i) Holmes et al. [7] found that metastable enol ions **EA-2** also abundantly lose H_2O and deduce from their D- and ^{18}O-labelling experiments that the reaction probably occurs via the reacting configuration(s) of the less stable keto tautomer **EA-1**. The isomers have different CID spectra - see Fig. 2a/b of this study - but this does not imply that keto ions cannot partially tautomerize : the CID spectrum of **EA-1** is not necessarily that of a *single* ionic species.

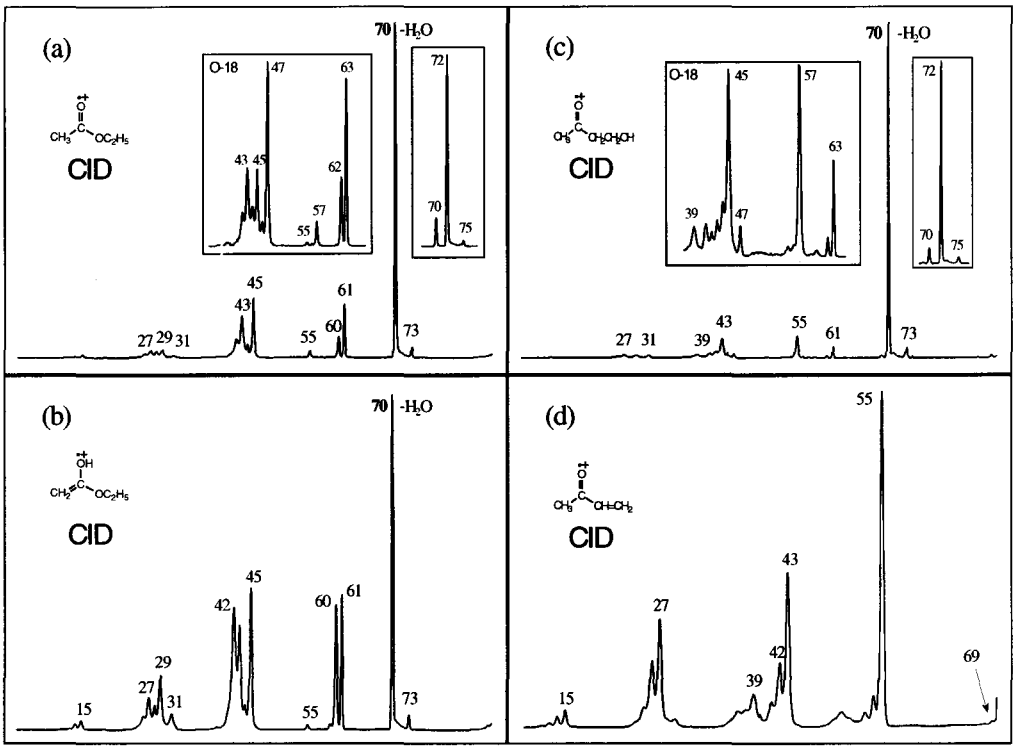

Fig. 2 CID mass spectra of the radical cations of ethyl acetate, its enol and the 4-hydroxy-2-butanone isomer (**HB-1**), items (a), (b) and (c) respectively. Partial spectra of $CH_3C(=O)^{18}OC_2H_5$ and $CH_3C(=O^{18})CH_2CH_2OH$ are shown in the insets of (a) and (c) respectively. Item (d) represents the CID mass spectrum of the m/z 70 product ion generated by the loss of water from *metastable* ion **HB-1**.

(ii) Analysis of ^{18}O labelled ions [7] showed that for ion source decompositions and all metastable ion observation times the keto and enol O atoms in both **EA-1** and **EA-2** are similarly preferentially lost : ion source 65%, metastable ions 70 – 90%. It is likely that this process has a lower energy requirement than the H_2O loss which involves the ester O atom. This is because (*i*) the associated kinetic energy release [9] is lower than that for the ester O atom and (*ii*) the degree of exchange becomes increasingly less important at longer ion lifetimes, which is just the opposite of the H atom exchange results [6,7]. These data indicate that there is a significant barrier to O atom migration, whereas the H atoms have no significant barrier for exchange but do so at a slow rate because of circuitous (high entropy) pathways (7,8).

(iii) From their analysis of the CID spectra of various $C_4H_6O^{\bullet+}$ isomers (13), Holmes et al. (7) conclude that $CH_3C(=O)CH=CH_2^{\bullet+}$ (**MVK**) is generated by H_2O loss from

either metastable ions **EA-1** and **EA-2** or those fragmenting in the ion source. They further note that the CID results do not exclude that a *minor* fraction of the ions would be CH_2=C(OH)CH=$CH_2^{\bullet+}$, the enol of **MVK** which is 13 kcal mol^{-1} lower in energy than **MVK** (11a). They entertained this possibility because their AE measurements on **EA-1** yielded an apparent $\Delta_fH^0_{298}$ = 190 kcal mol^{-1} for the $C_4H_6O^{\bullet+}$ ion which lies below the proposed value for **MVK**, 195 kcal mol^{-1} [13a].

(iv) Baer and co-workers [8] note that this enthalpy difference is on the border line of being significant. They conclude from their experiments on **EA-1** that **MVK** ions – for which they derive $\Delta_fH^0_{298}$ = 194 kcal mol^{-1} - are also generated at threshold. They further conclude that **EA-1** isomerizes to a more stable structure prior to dissociating, possibly the enol ion **EA-2**.

In the summary of their paper Baer and co-workers state : " we know the energy of the isomerized molecular ion, but not its structure; we suspect that the transition state is cyclic; and we believe that the product ion is **MVK**. With all this information it should be possible to derive a mechanism and determine the structure of the molecular ion. However, as was already pointed out by Holmes et al. the loss of H_2O is a very complicated reaction". Yeo's mechanistic proposal of Scheme 1 is mentioned in these studies but not discussed.

At the time the above studies were published, the use of ab initio MO calculations as a complementary tool in studying structures and reactions of gas-phase organic ions was only in its infancy. However, theory steadily progressed and in 1989 a review of structures and reactions of gas-phase ions [10b] stated that the computational results of Heinrich et al. on ionized methyl acetate [14] offer some hope that the chemistry of ionized ethyl acetate may some day be understood. A hydrogen-bridged radical cation [15], CH_3-CH=O•••H•••OCH=$CH_2^{\bullet+}$, was suggested to play a key role in the water elimination from **EA-1**. It was also stressed that ab initio calculations are required to solve this problem but that, considering the size of the system and the number of possible intermediates, this would be a formidable task.

Fortunately, the following decade witnessed a development in methodology and computing power short of a revolution, enabling computational chemistry to become a key player in the field of gas-phase ion chemistry [11]. The G-3 variant of the Gaussian methods of Pople and co-workers [16] and the CBS-QB3 variant of the complete basis set methods of Petersson and co-workers [17] provide absolute enthalpies of chemical accuracy for medium sized ions and neutrals. This makes both model chemistries attractive for a study of ethyl acetate's gas-phase ion chemistry. During the past five years we have successfully used the CBS-QB3 method in mechanistic studies of organophosporus ester ions [18] and proton-transport catalysis in various organic radical cations [19]. We therefore decided to use this CBS variant, which uses density functional geometries and frequencies in the calculations, as the primary computational tool in probing the elusive mechanism for the H_2O elimination from metastable ions **EA-1** and **EA-2**.

It will be shown that synergy between theory and experiment leads to a complex yet transparent mechanistic proposal for the H_2O elimination into **MVK** which satisfies the energetic constraints imposed by experiment and accounts for the labelling results.

Experimental and theoretical methods

The experiments were performed with the VG Analytical ZAB-R mass spectrometer of BEE geometry (B, magnet; E, electric sector) [29]. Metastable ion (MI) mass spectra were recorded in the second field free region (2ffr); collision-induced dissociation (CID) mass spectra were recorded in the 2 and 3ffr using oxygen as collision gas (Transmittance, T = 70%). The CID mass spectra of the 2ffr metastable peaks were obtained in the 3ffr using O_2 as collision gas. For these experiments the maximum available accelerating voltage, 10 kV, was used. CID spectra of reference ions having a translational energy close to that of the product ions resulting from (MI or CID) dissociations in the 2ffr, were also obtained in the 3ffr. All spectra were recorded using a PC-based data system developed by Mommers Technologies Inc. (Ottawa).

Ethyl acetate, methyl vinyl ketone, and 4-hydroxy-2-butanone were of research grade (Aldrich) and used without further purification. The ^{18}O-labelled ester

$CH_3C(=O)^{18}OCH_2CH_3$ was synthesized on a microscale by esterification of acetic acid with $C_2H_5{}^{18}OH$ (MSD Canada) ; samples of $CH_3C(=O^{18})OCH_2CH_3$ and $CH_3C(=O^{18})CH_2CH_2OH$ were prepared by exchange of the carbonyl oxygen of the unlabelled precursors with $H_2{}^{18}O$ (Prochem 90 atom %) under slightly acidic conditions.

The calculations were performed with the CBS-QB3 model chemistry [17] using Gaussian 2003, Rev C.02 [30] and (for selected transition state searches) GAMESS-UK [31]. In this model chemistry the geometries of minima and connecting transition states are obtained from B3LYP density functional theory in combination with the 6-311G(2d,d,p) basis set (also denoted as the CBSB7 basis set). The resulting total energies and enthalpies of formation for minima and connecting transition states (TS) in the ethyl acetate (EA), acetoin (AC) and 4-hydroxy-2-butanone (HB) systems of ions are presented in Table 1a/b. Computational and experimental enthalpies for various dissociation products are presented in Table 2. We have also used the G3 model chemistry [16b] to calculate the enthalpies of the species of Table 2 : agreement with the results of the CBS-QB3 method (and experiment) was quite satisfactory, within ± 1-2 kcal mol^{-1}.

Spin contaminations were within an acceptable range. The correct identity of transition states was verified (where not trivially evident) by means of Intrinsic Reaction Coordinate (IRC) calculations using the algorithm implemented in Gaussian 2003.

For several facile isomerization reactions, including **EA-1a** → **EA-3a** in Fig. 3, the CBS-QB3 energy of the TS is calculated to be slightly lower than that of the least stable of the connecting isomers. This may happen since transition states are more sensitive to correlation effects than minima and the ZPE also tends to favour transition states.

However, the TS connecting **HB-1b** and **HB-2a**, see Fig. 3 and Table 1b, is calculated to lie much lower in energy : 4.5 kcal mol^{-1} below that of **HB-1b**. Here, the discrepancy between the B3LYP/CBSB7 energies and the final CBS-QB3 results is probably due to the fact that the B3LYP and the MP2 parts of the CBS-QB3 calculation disagree about the geometry of the transition state. We have compared the contributions to the CBS-QB3 energy for **HB-1b** and two transition states relating to this isomer. It was found that for **HB-1b** and TS **HB-1a** → **1b** the various contributions are nearly the same

but this is not case for TS **HB-1b → 2a**. Here, the ΔE(MP2) contribution is much larger and the effect is enhanced in the ΔE(CBS) component, which is based on the MP2 energies. In contrast, the ΔE(MP4) contribution for this TS is smaller. This analysis suggests that for this transition state the MP2 method is not reliable enough to give satisfactory results.

Figure 5 displays the optimized geometries for the principal species. The complete set of computational results is available from the authors upon request.

RRKM theory [23] was used to calculate microcanonical rate constants. The harmonic frequencies and rotational constants were taken from the B3LYP/CBSB7 part of the CBS-QB3 calculations. The internal energies were calculated from the CBS-QB3 heats of formation at 0 K.

The extended RRKM model used is that described by Baer and Hase [23]. Here several reaction steps are combined to get an overall rate constant. As will be discussed in a separate publication (in preparation) this procedure also makes it possible to compare the yields of various dissociation products.

We have also complied data comparing CBS-QB3, G3B3, and G3 calculated energies on selected ions and transition states as seen in Table 4. The energies calculated by G3B3 were all systematically lower than their CBS-QB3 counterparts by 4 kcal mol^{-1}. The discrepancy can be attributed to the basis set used in the geometry optimization step of the model chemistries. Both model chemistries use B3LYP DFT method to optimize the geometry but CBS-QB3 employs a much larger basis set, 6-311G(2d,d,p), whereas, G3B3 uses a smaller basis set, 6-31G(d). The smaller basis set can account for the slight energy difference since the geometry optimization using G3B3 is not has refined as CBS-QB3.

Results and discussion

1.1. Experimental and theoretical preliminaries

In our computational quest of plausible mechanisms for the H_2O elimination from **EA-1** and **EA-2** we focussed on the behaviour of the *metastable* ions. For such ions the experiments [7,8] stipulate that none of the stable intermediates or connecting transition

states of a viable calculated mechanism should lie significantly higher in energy than the thermochemical threshold for the formation of **MVK** + H_2O. The experimental and calculated enthalpies for this threshold are close : 137 ± 3 and 139 kcal mol^{-1} respectively, see Table 2. The experimental value suffers from a rather large uncertainty because the heat of formation of neutral methyl vinyl ketone has not been measured with great precision. The computed enthalpies of the stable structures (minima) presented in Tables 1 and 2 of this study are expected to be reliable to 2 kcal mol^{-1} [17,18a] ; for the uncertainty in computed barrier heights we affix ± 4 kcal mol^{-1} as a conservative estimate [18a].

As mentioned in the Introduction, Holmes et al. [7] in their detailed experimental study do not propose a mechanism for the water loss from **EA-1/2**. However, they do make the intriguing suggestion that the isomeric 4-hydroxy-2-butanone ion, $CH_3C(=O)CH_2CH_2OH^{\bullet+}$, **HB-1**, is a participating structure in the complex behaviour of the keto and enol ions of ethyl acetate. This suggestion is based upon their observations that metastable ions **HB-1** readily lose H_2O, with a small kinetic energy release, and that the source generated ions **HB-1**, see Figure 1b, also generate m/z 61 ions $CH_3C(OH)_2^+$. The CID mass spectrum of **HB-1**, see Fig. 2c, also displays a m/z 61 peak, supporting the idea that **EA-1/2** and **HB-1** can (inter)convert via a fairly low energy route. There is no mechanistic proposal for the loss of H_2O from **HB-1** but, as will be discussed in Section 1.2, there is little doubt that the product ion generated is **MVK** and that the reaction occurs at the thermochemical threshold.

We decided to further explore the idea that ions **EA-1/2** can access the potential energy surface (PES) that describes the water elimination from **HB-1**. Ions **EA-1** may well undergo a facile isomerization into distonic ions **EA-3** or **EA-4** as depicted in Scheme 2. Ion **EA-3** could in principle connect to the PES of **HB-1** via a well-documented skeletal rearrangement, the [1,3]-hydroxycarbene shift [10b]. In this rearrangement the CH_3-C-OH moiety of **EA-3** migrates, via a cyclic transition state, to the radical position, yielding $[CH_3C(OH)CH_2CH_2O]^{\bullet+}$, a 1,5-hydrogen-shift isomer of **HB-1**. Our computational results for this reaction sequence are presented in the energy-level diagram of Fig. 4a which will

be discussed in detail in Section 1.4. Here we note that the barrier for the hydroxycarbene shift is too high to account for the loss of water at the thermochemical threshold.

Table 1. Enthalpies of formation derived from CBS-QB3 calculations of stable isomers and connecting transition states involved in the water loss from the ethyl acetate (EA) radical cation.

Ionic species (a)	B3LYP/ CBSB7 E(total)	CBS-QB3 [0 K] E(total)	ZPE	$\Delta_f H^0_0$	$\Delta_f H^0_{298}$
EA-1a (Fig. 3a/4a)	-307.43701	-306.83417	71.2	132.4	126.5
EA-1b (Fig. 4b)	-307.43573	-306.83503	71.4	131.9	126.3
EA-2a (Fig. 5)	-307.46197	-306.86357	72.8	114.0	108.0
EA-2b (Fig. 4a)	-307.45361	-306.85647	72.6	118.3	112.4
EA-2c (Fig. 4a)	-307.45268	-306.85569	72.7	118.9	113.0
EA-3a (Fig. 3a/4a)	-307.45414	-306.85760	71.7	117.7	112.2
EA-3b (Fig. 3a/4a)	-307.45000	-306.85448	72.6	119.7	113.9
EA-3c (Fig. 4a)	-307.45252	-306.85565	71.8	118.9	113.3
EA-4a (Fig. 4b)	-307.45513	-306.85827	71.4	117.3	111.7
EA-4b (Fig. 4b)	-307.46221	-306.86186	71.4	115.1	109.5
EA-4c (Fig. 4b)	-307.45945	-306.85995	71.4	116.3	110.7
EA-5 (Fig. 4a)	-307.42616	-306.82834	70.1	136.1	131.1
EA-6a (Fig. 4a)	-307.41941	-306.82415	69.3	138.6	133.6
EA-6b (Fig. 5)	-307.41997	-306.82469	68.2	138.4	133.6
TS EA-1a → 3b	-307.43426	-306.83666	69.4	130.9	124.5
TS EA-3a → 3b	-307.39355	-306.83688	70.2	130.7	125.1
TS EA-3a → 5	-307.42543	-306.82502	69.7	138.1	132.8
TS EA-5 → HB-1b	-307.41738	-306.82077	69.8	140.8	135.3
TS EA-3b → 6a	-307.41335	-306.81679	66.0	143.2	138.1
TS EA-6a → 6a (b)	-307.41768	-306.82381	68.8	138.2	133.6
TS EA-3a → 3c	-307.43466	-306.83390	70.7	132.5	126.9
TS EA-3c → 2b	-307.42637	-306.83177	70.1	133.8	127.1
TS EA-3a → HB-5b	-307.39355	-306.79996	71.9	153.9	147.3
TS EA-1b → 4a	-307.42702	-306.83023	68.9	134.9	128.8
TS EA-4a → 4b	-307.44507	-306.84473	70.2	125.8	120.0
TS EA-4b → 4c	-307.43112	-306.83260	70.1	133.4	127.4
TS EA-4c → 2c	-307.41198	-306.81925	69.4	141.8	135.4
TS EA-4c → AC-2a	-307.39971	-306.80465	70.8	151.0	144.8
TS AC-2a → AC-1a	-307.41178	-306.81565	68.9	144.1	137.9
AC-1a (Fig. 4b)	-307.44905	-306.84929	71.2	122.9	117.6
AC-1b (Fig. 5)	-307.45270	-306.85452	71.4	119.7	114.2
AC-2a (Fig. 4b)	-307.42693	-306.82804	71.8	136.3	130.3
TS AC-1b → HB-3c	-307.40616	-306.81321	68.6	145.5	139.3

(a) E(total) in Hartrees, all other components, including the ZPE scaled by 0.99, in kcal mol^{-1}. (b) the transition state for the O-equilibration, see Figure 3a.

Table 2. Energetic data for dissociation reactions of the radical cations of ethylacetate and 4-hydroxy-2-butanone derived from CBS-QB3 calculations and experimental observations (a).

	CBS-QB3 **E(total)** [0K]	CBS $\Delta_fH^0_0$	CBS $\Delta_fH^0_{298}$		Exp. $\Delta_fH^0_{298}$	**Ref**
$CH_3C(=O)OCH_2CH_3^{\bullet+}$ (EA-1b)	-306.83503	131.9	126.3		125 ± 1	8
$CH_3C(=O)OCH_2CH_3$	-307.20745	-101.8	-107.7		-106.1	12a
$CH_3C(=O)CH=CH_2^{\bullet+} + H_2O$			**139.2**	(b)	**137± 3**	(c)
$CH_3C(=O)CH=CH_2$	-230.83494	-22.3	-26.2	(b)	-27.4	12b
$CH_3C(=O)CH=CH_2^{\bullet+}$	-230.47885	201.1	197.4	(b)	195	(c)
$CH_2=C(OH)CH=CH_2^{\bullet+}$	-230.49955	188.2	184.1		182	13a
2-methyloxetene ion (Scheme 1)	-230.47852	201.3	197.2			
$CH_3C\text{-}O\text{-}CH=CH_2^{\bullet+}$	-230.44607	221.6	218.1			
$CH_3C{=}O^+ + CH_3CH_2O^\bullet$			**154.5**		**155**	
$CH_3C{=}O^+ + CH_2CH_2OH^\bullet$			**151.9**		**150**	
$CH_3C(H)OH^+ + CH_3C{=}O^\bullet$			**139.7**		**140**	
$CH_3C{=}O^+$	-152.68582	159.8	158.0		157	(d)
$CH_3C(H)OH^+$	-153.87250	145.7	142.2		142.4	(e)
$CH_2CH_2OH^\bullet$	-154.10928	-2.9	-6.1	(f)	-7	12d
$CH_3CH_2O^\bullet$	-154.10513	-0.3	-3.5	(g)	-3.6	12d
$CH_3C{=}O^\bullet$	-152.94202	-1.0	-2.5		-2.4	12d
$CH_3C(OH)_2^+ + CH_2{=}CH^\bullet$			**146.4**		**147**	
$CH_2{=}C(OH)_2^{\bullet+} + CH_2{=}CH_2$			**135.0**		**132.5**	
$CH_3COOH + CH_2{=}CH_2^{\bullet+}$			**152.2**		**152.5**	
$CH_3C(OH)_2^+$	-229.06154	78.3	74.7	(h)	75	(i)
$CH_2{=}C(OH)_2^{\bullet+}$	-228.40494	40.0	121.8	(j)	120	12a
CH_3COOH	-228.76536	-101.2	-104.3		-103.3	12a
$CH_2{=}CH^\bullet$	-77.74299	72.7	71.7		71.6	12d
$CH_2{=}CH_2^{\bullet+}$	-78.02908	258.4	256.5		254.8	12a
$CH_2{=}CH_2$	-78.41664	15.3	13.2		12.5	12a
$CH_3C(OH){=}CH_2^{\bullet+} + CH_2{=}O$			**135.7**		**137.4**	
$CH_3C(OH){=}CH_2^{\bullet+}$	-192.47686	167.0	163.0		163.4	(k)
$CH_2{=}O$	-114.34411	-26.4	-27.3		-26.0	12a

(a) $E_{(total)}$ in Hartrees, all other components, including the ZPE scaled by 0.99, are in kcal mol^{-1}.
(b) refers to the *anti* conformer; the ionic and neutral *syn* conformers are 0.5 kcal mol^{-1} higher in energy; (c) ionic $\Delta_fH^0_{298}$ based upon IE_a = 9.65 ± 0.02 eV and Δ_fH^0 neutral ketone = -27.4 ± 2.6 kcal mol^{-1} as quoted in ref. 12b; (d) derived from PA ketene = 197.3 kcal mol^{-1} [12b] and $\Delta_fH^0_{298}$ ketene = -11.4 ± 0.6 kcal mol^{-1} [12a]; (e) from PA acetaldehyde = 183.7 kcal mol^{-1} [12c] and Δ_fH^0 aldehyde = -39.6 ± 0.1 kcal mol^{-1} [12a]; (f) refers to the "U" shaped conformer, the "S" conformer is 0.6 kcal mol^{-1} higher in energy; (g) 2A′ state; (h) value of the lowest energy *syn/anti* (position hydroxylic H's relative to CH_3 group) conformer; [i] from PA acetic acid = 187.3 kcal mol^{-1} [12c] and $\Delta_fH^0_{298}$ acid = -103.3 ± 0.1 kcal mol^{-1} [12a]; (j) lowest energy conformer; (k) upper limit : see ref. 21d for details.

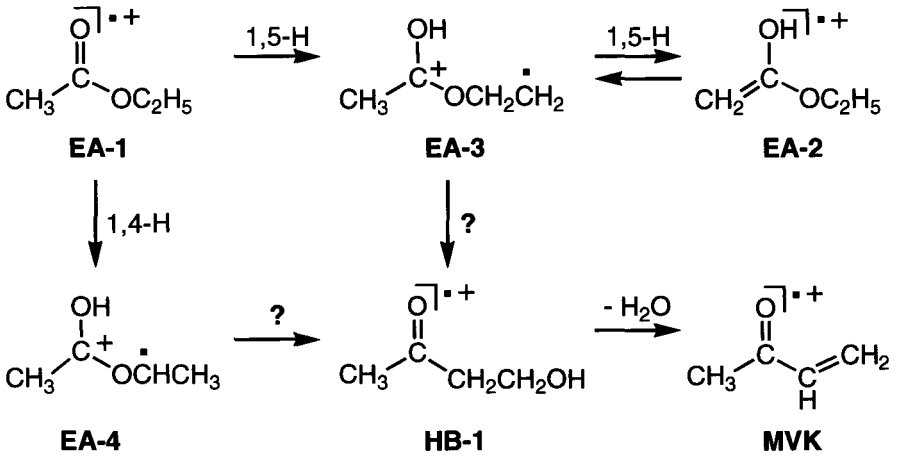

Scheme 2

In the same vein, ion **EA-4** could undergo a [1,2]-hydroxycarbene shift [10b], leading to $[CH_3C(OH)C(H)(CH_3)O]^{\bullet+}$, a 1,5-hydrogen-shift isomer of $CH_3C(=O)CH(OH)CH_3^{\bullet+}$, ionized acetoin. This reaction does not play a role in the water elimination either, since (i) the isomerization barrier is not sufficiently low and (ii) low energy acetoin ions do not lose H_2O but rather dissociate into $CH_3C(H)OH^+ + CH_3C{=}O^{\bullet}$, via a remarkable hidden rearrangement [20]. However, as will be discussed in Section 1.5 in conjunction with the energy diagram of Fig. 4b, this rearrangement sheds light on another intriguing aspect of ethyl acetate's ion chemistry (8). This concerns the formation of the prominent m/z 45 $C_2H_5O^+$ ions in the CID mass spectra of **EA-1/2** shown in Fig. 2a/b.

Despite these negative answers from theory, we further pursued the idea that the water loss from **EA-1/2** occurs via the PES of **HB-1** and considered the distonic ion **EA-3** to be the most likely intermediate for the conversion. This indeed proved to be the case : as shown in the calculated energy diagram of Fig. 3a, **EA-3** can rearrange into **HB-1** via a two-step low energy route. This finding and its implication on the interpretation of the labelling results will be discussed in Section **1.3**. However, we will first deal with our

mechanistic proposal for the water elimination from **HB-1,** which, as we shall see, involves a [1,2]-hydroxycarbene shift [10b] as the key step of the reaction.

1.2. The water elimination from ionized 4-hydroxy-2-butanone (HB-1)

Before we discuss our mechanistic proposal for the water loss from **HB-1** we will first briefly review the experimental observations. The spectrum of metastable ions **HB-1** displays a single narrow peak at m/z 70, indicating that loss of H_2O represents the reaction of lowest energy requirement. The kinetic energy release derived from the m/z 70 peak at half-height, $T_{0.5}$, is only 7 meV [7] indicating that the water elimination may well occur at the thermochemical threshold. The CID mass spectrum of the resulting $C_4H_6O^{\bullet+}$ product ion, generated from *metastable* ions **HB-1**, is shown in Fig. 2d. Comparison of this spectrum with that of $CH_3C(=O)CH=CH_2^{\bullet+}$ (**MVK**) and other isomeric $C_4H_6O^{\bullet+}$ ions [7,13] leaves little doubt that **MVK** is the product ion generated from **HB-1.** We note in particular that the peak at m/z 69 (loss of $H^{\bullet}$) in the spectrum of Fig. 2d is barely visible (< 1% of the base peak at m/z 55). Since loss of $H^{\bullet}$ represents [7,13a] a major collision induced dissociation of the enol ion of **MVK**, $CH_2=C(OH)CH=CH_2^{\bullet+}$, it is unlikely that this more stable isomer (see Table 2) is co-generated from **HB-1** to any significant extent.

Our CID mass spectrum of the $C_4H_6O^{\bullet+}$ ion generated from *metastable* ethyl acetate ions is identical with that of Fig. 2d. This reinforces the conclusion of the PI study of Baer et al. [8] that the water elimination from **EA-1** yields **MVK** at the thermochemical threshold. Their derived $\Delta_fH^{\circ}_{298}$ value of 194 ± 2 kcal mol^{-1} is close to its experimental estimate of 195 ± 3 kcal mol^{-1}, see Table 2. On the other hand, see Introduction, Holmes et al. [7] invoked the co-generation of the enol ion because the $\Delta_fH^{\circ}_{298}$ ($C_4H_6O^{\bullet+}$) they derived from their AE (EI) measurements, 190 kcal mol^{-1}, lies 5 kcal mol^{-1} below the experimental estimate for **MVK**. We note that the AE values from the PI and EI studies are virtually the same, 10.31 ± 0.1 eV, and that the discrepancy between the derived $\Delta_fH^{\circ}_{298}$ values arises from differences in the thermochemical treatment of the appearance energies [8].

The ambiguities in defining appearance energies and their conversion into $\Delta_f H^\circ_{298}$ values of the reaction products has been a matter of considerable debate [21]. Here we note that applying the Traeger-McLoughlin correction term [21a], $\Delta H_{cor} = \Delta H_{298}$ (**MVK** + H_2O) – 1.48 kcal mol^{-1}, raises the $\Delta_f H^\circ_{298}$ ($C_4H_6O^{\bullet+}$) value derived by Holmes et al. by 5.3 kcal mol^{-1} to 195 kcal mol^{-1} (using the ΔH_{298} values available from the CBS-QB3 calculations). Note that ΔH_{cor} is negative and this negative number is subtracted from the measured AE, thereby raising the derived $\Delta_f H^\circ_{298}$. This correction holds rigorously if all the available internal energy of the precursor ion is used for dissociation, that is, the products are formed at 0 K. The actual thermal content of the products is not known and hence the correction term only provides an upper limit to the derived enthalpy.

Interestingly, the same situation obtains for the water loss from **HB-1**. The available AE, 9.78 eV [22], leads to a $\Delta_f H^\circ_{298}$ ($C_4H_6O^{\bullet+}$) value of only 190.3 kcal mol^{-1}* ; when the above correction term is applied, the number increases to 195.6 kcal mol^{-1} and becomes compatible with the formation of **MVK**.

The above observations lead us to conclude that the water elimination from both **HB-1** and **EA-1** yields **MVK** at the thermochemical threshold. Further, the MI spectrum of the ^{18}O labelled isotopologue $CH_3C(=O^{18})CH_2CH_2OH^{\bullet+}$ reveals that the H_2O molecule lost from metastable ions **HB-1** largely (~ 95%) consists of the hydroxyl ^{16}O atom. The inset of the CID mass spectrum of Fig. 2c shows that this is also true for stable ions undergoing collision induced dissociation, although it should be noted that the larger part (~ 70 %) of the dominating peak for water loss in the CID spectrum is of metastable origin. This also applies to the m/z 70 peak in the CID mass spectrum of **EA-1** but now the water loss, see inset of Fig. 2a, largely (~ 90 %) involves the keto ^{16}O atom. For both isomers the kinetic energy release ($T_{0.5}$ value) associated with the major loss of $H_2{}^{16}O$ from the labelled isotopomers is significantly lower than that of the minor $H_2{}^{18}O$ loss : 8.6 vs 13.0 meV for **EA-1** [7] and 5.5 vs 11.5 meV for **HB-1** (this work). This observation

* #1 Using $\Delta_f H^\circ_{298}$ (4-hydroxy-2-butanone) = - 93 kcal mol^{-1}, from Benson additivity (12e) estimate ; our CBS-QB3 value is - 93.4 kcal mol^{-1}.

suggests that the $H_2{}^{18}O$ loss from **EA-1** and **HB-1** involves an oxygen equilibration reaction whose energy requirement is somewhat higher than the atom specific water loss. As we shall see, the mechanistic proposal of Fig. 3 provides a rationale for these labelling results.

Our mechanistic proposal for water loss from metastable ions **HB-1** is presented in the bottom part of the energy diagram of Fig. 3. Starting from the lowest energy conformer **HB-1a**, a facile rotation of the CH_2OH moiety yields conformer **HB-1b** which forms the connection with the PES of ethyl acetate in the top part of the energy diagram. Ion **HB-1b** then rearranges into the very stable distonic ion **HB-2a** via a 1,4-H shift. The TS for this shift is undoubtedly not high but the calculated value is clearly too low; this point is further discussed in the Theoretical Methods section.

Ion **HB-2a** may undergo a facile rotation of its HCOH moiety to yield the slightly more stable conformer **HB-2b**, which has a planar structure. However, its HCOH and CH_3COH moieties can slightly move out of the plane - with a negligible energy requirement, see Table 1b - to form **HB-2c** which, see also Fig. 5, can be viewed as a one-electron long bonded species. Contraction of its one-electron bond was expected to initiate the isomerization of **HB-2c** into **HB-3a**, see Fig. 3b, via a [1,2]-hydroxycarbene shift [10b]. However, **HB-3a** does not appear to be a minimum on the PES : all attempts to optimize its geometry yielded its conformer **HB-3b**, in which the hydroxyl groups are bridged, in such a way that an ensuing loss of water into **MVK** can easily be envisaged. We were able to locate the transition state connecting **HB-2c** and **HB-3b** and it appears to lie at only 124 kcal mol^{-1}, well below the threshold for the water elimination. **HB-3b** does not directly lose water but rather it isomerizes (TS at 138 kcal mol^{-1}) into an ion-dipole type complex between **MVK** and H_2O, **HB-4**, which then dissociates into its components at the thermochemical threshold.

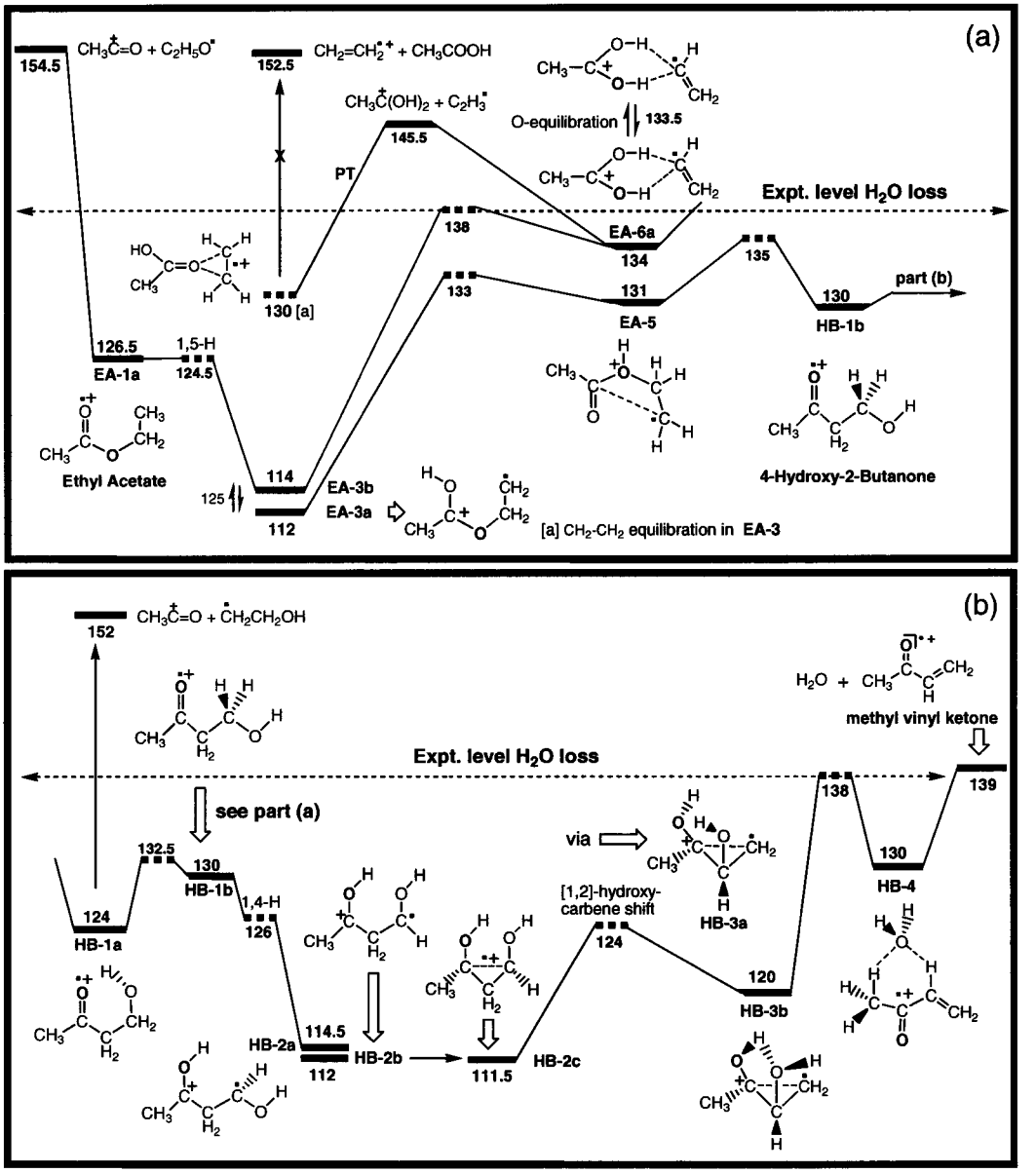

Fig. 3 Energy-level diagram derived from CBS-QB3 calculations describing the water elimination from metastable ethyl acetate ions (**EA-1**). The top part (a) describes the isomerization of **EA-1** into ionized 4-hydroxy-2-butanone (**HB-1**); the bottom part (b) presents the mechanism by which ions **HB-1** lose H_2O. The numbers refer to $\Delta_f H^0_{298}$ values in kcal mol^{-1}.

We note that other conformers of **HB-2b** may also undergo a [1,2]-hydroxycarbene shift, as illustrated in Scheme 3 for **HB-2a**. However, the stable **HB-3** conformers then generated cannot immediately lose water but must first isomerize via rotation(s) into **HB-**

3b. We have examined several of these pathways but they all appear to have a slightly higher energy requirement than the direct route **HB-2b** → **HB-3b** depicted in Fig. 3b.

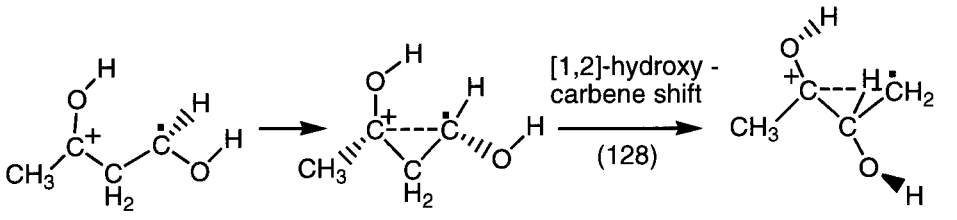

HB-2a (114.5) **HB-2d** (112.5) **HB-3c** (127)

Scheme 3

Three points deserve further comment :

(i) The minor loss of $H_2{}^{18}O$ from $CH_3C(=O^{18})CH_2CH_2OH^{\bullet+}$ could be ascribed to a partial equilibration of **HB-3b** with its 1,2-H shift isomer $CH_3C(OH)=C(OH)CH_3^{\bullet+}$ (**HB-6**) : the associated TS (see Table 1b) lies at 139 kcal mol^{-1}, i.e. at the threshold for the water elimination.

(ii) The H_2O molecule in **HB-4** is not expected to promote enolization of the ketone moiety by proton-transport catalysis [19]. This is because the proton affinity (PA) of water (164 kcal mol^{-1}) is much lower than the (calculated) topical PAs at $^{\bullet}CH_2$ and C=O in the deprotonated ketone $^{\bullet}CH_2C(=O)CH=CH_2$, 187 and 200 kcal mol^{-1} respectively.

(iii) A McLafferty type rearrangement in **HB-1** would yield enol ions $CH_3C(OH)=CH_2^{\bullet+}$ at m/z 58 by loss of $CH_2=O$. As seen from Table 2, the minimum energy requirement for this reaction is only 136 kcal mol^{-1}, i.e. lower than that for the loss of water. However, our calculations indicate that the formaldehyde loss involves a reverse barrier of 4 kcal mol^{-1}, see Fig. 4 and Table 1b, which makes the energy requirements for the losses of formaldehyde and water comparable. Yet, neither the MI nor the CID spectrum, see Fig. 2c, of **HB-1** displays a signal at m/z 58 !

Standard RRKM calculations for the formaldehyde loss from **HB-5a** and the water loss from **HB-3b** indicate that the internal energy needed for the formaldehyde loss in the metastable time frame is lower than that for the water loss. However, this model is

misleading because it does not take into account that both isomers communicate with the much more stable isomers **HB-2a** – **HB-2c** via low barriers, see Fig. 3. This leads to a rapid interconversion of the various isomeric ions involved in the competing losses of formaldehyde and water.

The extended RRKM model as described by Baer et al. [23] (see also theoretical methods Section) does account for the competition between the two dissociation channels. Calculations based on this model revealed that equilibration via the low lying distonic ions **HB-2a** – **HB-2c** leads to a much lower yield (by a factor of 140) of the m/z 58 product ion formed by loss of formaldehyde compared to the yield of m/z 70 **MVK** ions formed by loss of water. As a result, loss of formaldehyde from **HB-1** cannot effectively compete with its water loss.

1.3. The water elimination from ionized ethyl acetate (EA-1)

As discussed in the previous section, 4-hydroxy-2-butanone ions **HB-1** lose water via the mechanism presented in the bottom part of the energy diagram of Fig. 3. The top part of this diagram, Fig. 3a, shows that ionized ethyl acetate can undergo a three-step isomerization reaction into **HB-1**, which may then serve as the precursor for its subsequent water elimination. The first step involves the conversion of **EA-1** into its stable distonic isomer **EA-3** via a facile 1,5-H shift. This reaction involves ionized ethyl acetate's conformer **HB-1a** and it yields the distonic ion's conformer **EA-3b**. Rotation of its hydroxyl group via a low lying transition state converts **EA-3b** into **EA-3a**. Next, the O-CH_2 bond in **EA-3a** stretches and breaks while the methylene group moves to the hydroxyl O atom to make a new bond, yielding distonic ion **EA-5**. Ion **EA-5**, akin to the well-documented (24) distonic $C_2H_6O^{\bullet+}$ isomer H_2O^+-CH_2-$CH_2^{\bullet}$, lies in a shallow potential well and requires only 4 kcal mol^{-1} to further rearrange into ionized 4-hydroxy-2-butanone's conformer **HB-1b**. This rearrangement can be viewed as a 1,3-acetyl shift.

This three-step isomerization route of **EA-1** into **HB-1** takes place at energies below that required for the water loss and it thus satisfies the energetic constraints imposed by experiment. It further converts the ^{18}O labelled **EA-1** isotopologue

$CH_3C(=O)^{18}OC_2H_5^{\bullet+}$ into the **HB-1** isotopologue $CH_3C(=O^{18})CH_2CH_2OH^{\bullet+}$ which, see Fig. 3b, is expected to specifically lose $H_2{}^{16}O$. This, too, is in agreement with the experimental observations albeit that a small fraction of high energy metastable ions (~5%) appears to lose $H_2{}^{18}O$. The loss of $H_2{}^{18}O$ from both labelled isotopologues probably results from a weakly competing oxygen equilibration reaction rather than a different dissociation pathway. Two equilibration mechanisms are feasible : (i) the equilibration of **HB-3b** with its 1,2-H shift isomer **HB-6** mentioned in the previous Section and (ii) the route **EA-3b** → **EA-6a** depicted in Fig. 3a. The transition state energies for the two processes are very close but the first route is kinetically less attractive because the equilibration **HB-3** ↔ **HB-6** is associated with a very large activation energy (44 kcal mol^{-1} relative to **HB-6**) and a tight transition state. This makes it unlikely that this equilibration can effectively compete with the dissociation **HB-3** → **HB-4** → **MVK** + H_2O, even at elevated energies. The dynamic picture is more favourable for the second route which converts **EA-3b** by elongation of its O-CH_2 bond into the hydrogen-bridged radical cation **EA-6a**. As depicted in Fig. 3a, **EA-6a** can undergo a facile exchange of its vinyl moiety via a low-lying transition state which makes its oxygen atoms equivalent.

We further note that elongation of the O-CH_2 bond in other conformers of **EA-3** leads to various **EA-6** conformers – including **EA-6b** whose structure is shown in Fig. 5 – which are similar in energy and may dissociate into $CH_3C(OH)_2^+$ + $C_2H_3^{\bullet}$ at elevated energies. Elongation of the O-CH_2 bond in **EA-3** can also lead to ion-dipole complexes of ionized ethylene and acetic acid. Such species can be formed from **EA-3** at fairly low internal energies, as seen in Fig. 3a where the symmetrical ion-dipole structure at 130 kcal mol^{-1} represents the transition state for switching the acetic acid dipole molecule between the methylene moieties of ionized ethylene, see Section 1.5. This switching reaction makes the C and H atoms of the ethyl group in **EA-1** equivalent and accounts in part for the H-D exchange reactions of D-labelled isotopologues of **EA-1** as will be discussed in Section 1.5. At elevated energies the ion-dipole complexes do not dissociate into $C_2H_4^{\bullet+}$ + CH_3COOH. Instead, proton transfer (PT) occurs from the ionized ethylene

moiety to the acetic acid dipole which allows the energetically more favourable dissociation into $CH_3C(OH)_2^+ + C_2H_3^\bullet$ to take place.

In this context we note that the PI study by Baer and co-workers [8] reports an AE of 10.67 ± 0.08 eV for the dissociation of **EA-1** into $CH_3C(OH)_2^+$ (m/z 61) + $C_2H_3^\bullet$. From the experimental enthalpies of Table 2 and using ΔH_{cor} = 4.7 kcal mol^{-1}, we derive a thermochemical AE of 10.75 eV. These results indicate that this dissociation takes place virtually at the thermochemical threshold, i.e. it has no reverse activation barrier. As discussed above, loss of $C_2H_3^\bullet$ from **EA-1**, see Fig. 3a, may be envisaged to occur from the hydrogen-bridged ion **EA-6** or by proton transfer from ethylene-acetic acid ion-dipole complexes, rather than by a formal 1,3-H shift as mentioned in the Introduction.

1.4. The [1,3]-hydroxycarbene shift in the distonic ion $[CH_3C(OH)OCH_2CH_2]^{\bullet+}$ (EA-3)

The energy-level diagram of Fig. 4a describes the communication of ionized ethyl acetate with its enol (**EA-2**) which will be addressed in the next Section. It also shows the energetics associated with a [1,3]-hydroxycarbene shift in distonic ion **EA-3**. This isomerization leads to **HB-1** via its 1,5-hydrogen-shift isomer **HB-5** and it could in principle provide an alternative pathway for the loss of water. The energy requirement for this rearrangement precludes this possibility : Fig. 4a shows that TS **EA-3** → **HB-5** lies some 10 kcal mol^{-1} above the threshold for the dissociation of the incipient **HB-5** ions into $CH_3C(OH)=CH_2^{\bullet+}$ (m/z 58) + $CH_2=O$ by direct bond cleavage. The fact that this dissociation is not observed in either the MI, the CID or the conventional mass spectrum of **EA-1** implies that the [1,3]-hydroxycarbene shift does not even occur. This is not surprising considering the discussion of the previous Section where it was shown that ions **EA-3** are able to undergo several isomerization and dissociation reactions at energies well below that required for the [1,3]-hydroxycarbene shift.

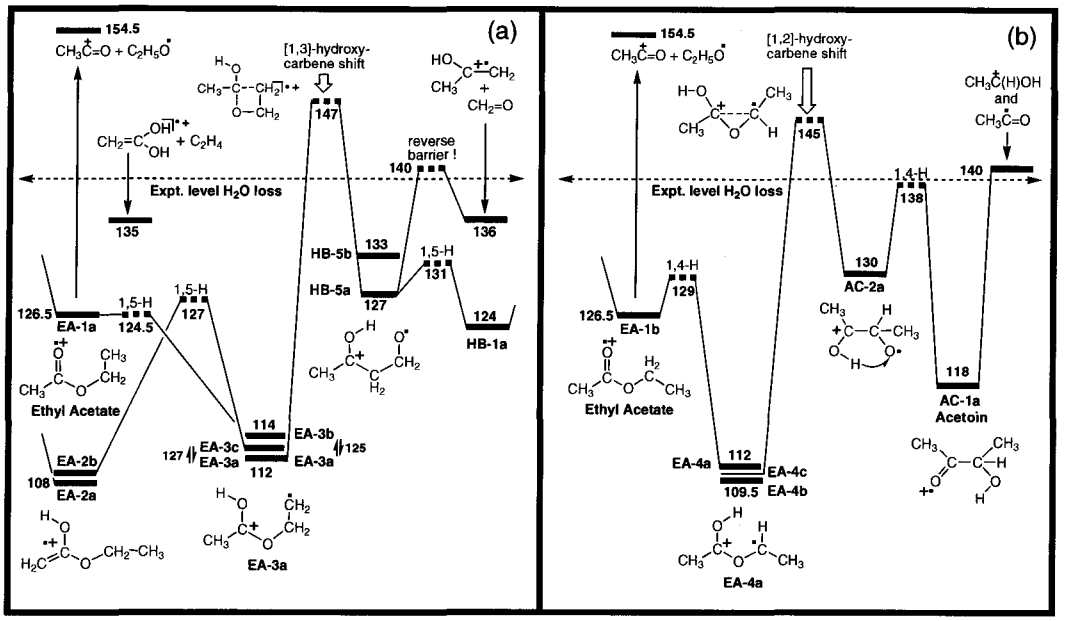

Fig. 4 Energy-level diagrams derived from CBS-QB3 calculations for the isomerization of ionized ethyl acetate (**EA-1**) into the distonic ions **EA-3** (part a) and **EA-4** (part b) and the subsequent [1,3]- and [1,2]-hydroxycarbene shift. The numbers refer to $\Delta_f H^0_{298}$ values in kcal mol^1.

The energy diagram of Fig. 4a also shows that Yeo's mechanism of Scheme 1 can be refuted : his proposed intermediate is not a minimum on the PES but rather corresponds to the high lying TS **EA-3b** → **HB-5b** associated with the [1,3]-hydroxycarbene shift. Interestingly, our calculations (see Table 2) indicate that the cyclic product ion structure proposed in his Scheme, ionized 2-methyloxetene, has the same heat of formation as its ring-opened isomer **MVK**.

Another simple mechanism for water loss from ionized ethyl acetate which complies with the finding that its keto oxygen atom is preferentially lost, would involve a double H transfer to its keto oxygen atom. This reaction would generate an ionized oxycarbene via the sequence **EA-1** (1,4H)→ **EA-4** (1,4H) → CH_3-C-O-CH=$CH_2^{\bullet+}$ + H_2O. Ionized oxycarbenes are well documented species in the gas-phase which may be as stable as their keto or aldehyde counterparts [25]. However, CH_3-C-O-CH=$CH_2^{\bullet+}$ appears to be much higher in energy than CH_3-C(=O)-CH=$CH_2^{\bullet+}$, by 21 kcal mol^{-1} (see Table 2) and so its formation, certainly as a product ion in the metastable time-frame, can effectively be ruled out.

The diagram of Fig. 4a also shows that the thermochemical energy requirement for the dissociation **EA-1/2** → $CH_2=C(OH)_2^{\bullet+}$ (m/z 60) + C_2H_4 is lower than that for the loss of H_2O. However, metastable ions **EA-1/2** do not lose C_2H_4 indicating that the associated dissociative rearrangement, possibly a 1,3-H shift in **EA-2**, has a high activation energy. As seen in Fig. 2a/b this dissociation becomes prominent upon collisional activation. A double collision experiment confirmed that the m/z 60 ions in the CID spectra are ions $CH_2=C(OH)_2^{\bullet+}$, not $CH_3COOH^{\bullet+}$.

1.5. Deuterium labelling experiments : the relationship between ionized ethyl acetate (EA-1) and its enol (EA-2) and identification of the rate-determining step for the loss of H_2O

In Table 3 are given selected deuterium labelling results taken from references 6 and 7. Metastable ions fragmenting in the second field free region (2ffr) of the ZAB and MS902 instruments do so at the same average rate so that the data are comparable [7]. From the results of Table 3 it can be deduced that there are two H/D equilibration reactions.

In the first reaction, which is so fast that it readily occurs for ions dissociating in the source, the H atoms of the ethyl chain become positionally equivalent, see the results for $CD_3C(=O)OCD_2CH_3$. A complete exchange of these H atoms would yield a H_2O : HDO : D_2O ratio of 33 : 67 : 00 which is close to the observed ratio of 39 : 52 : 09. Reversible rearrangement of **EA-1** into **EA-3** followed by isomerization into the ion-dipole complex $CH_3C(OH)=O\bullet\bullet\bullet C_2H_4^{\bullet+}$ as discussed in Section 1.3 accounts for this exchange reaction.

Table 3. Relative abundances for the loss of water from selected D- labelled isotopologues of ionized ethyl acetate and its enol.

Compound		H_2O : HDO : D_2O			Calculated[a]		
$CD_3C(=O)OCD_2CH_3$	source	39	52	09	11	53	36
	m* [b]	17	58	25			
$CH_3C(=O)OCD_2CD_3$	source	00	13	86	11	53	36
	m*	06	44	50			
$CD_3C(=O)OCH_2CH_3$	source	100	00	00	36	53	11
	m*	59	35	06			
$CH_2=C(OH)OCD_2CD_3$	source	02	56	44	11	53	36
	m*	07	51	42			
$CD_2=C(OH)OCH_2CH_3$	source	95	05	00	53	43	04
	m*	73	26	01			

[a]Assuming complete loss of positional identity; [b]metastable ions 2ffr ZAB or MS902

In the longer lived metastable ions, the H atoms of the acetyl group also participate in the exchange reactions, almost to the statistical limit. This can be rationalized by invoking a slow but reversible isomerization of **EA-3** into the enol ion **EA-2**. It leads to exchange of the H atoms of the acetyl group with those of the methyl H atoms of the ethyl group and together with the above fast exchange reaction, an (almost) complete equilibration of all H atoms now takes place. This would imply that metastable ethyl acetate ions consist of an (almost) equilibrated mixture of the keto, distonic and enol isomers.

Our calculations, see Fig. 4a, indicate that ions **EA-2** and **EA-3** are lower in energy than **EA-1** and that they can be produced at energies just above the formation of **EA-1**. This makes it very likely that metastable ions **EA-1** primarily exist as enol ions **EA-2** and distonic ions **EA-3**. This is in good agreement with a Fourier Transform Ion Cyclotron Resonance study of Kiminkinen et al. [26] who conclude that the long-lived (time scale > 1s) radical cation of ethyl acetate exists as its enol form in the gas-phase. Their experiments further indicate, in agreement with our calculations, that the energy barriers for isomerization of **EA-1** to the distonic ion **EA-3** and of **EA-3** to the enol ion **EA-2** must be near or below the enthalpy of formation of **EA-1** and that this radical cation is kinetically unstable.

As expected from the above scenario, the enol ion also shows fast H/D equilibration reactions of the ethyl side chain, see Table 3. Earlier work [7] has noted that enol ions dissociating in the source rearrange irreversibly to the distonic ion, i.e. $CH_2{=}C(OH)OCD_2CD_3^{\bullet+} \rightarrow CH_2DC^{+}(OH)OCD_2CD_2^{\bullet}$. As discussed in Section 1.3, the latter ion can then access the ion-dipole complex $CH_2DC(OH){=}O{\bullet\bullet\bullet}C_2D_4^{\bullet+}$ and fall back to the distonic form leading to equilibration of the OH hydrogen and the four C_2D_4 deuterium atoms. Again, in the metastable time-frame almost complete equilibration of all H and D atoms occurs.

The labelled ion $CD_3C(=O)OCH_2CH_3^{\bullet+}$ shows a H_2O/HDO loss ratio of 1.69, while the D_2O/HDO loss ratio for the inversely labelled compound $CH_3C(=O)OCD_2CD_3$ is 1.25 and so an H/D isotope effect is operative. According to the energy diagram of Fig. 3b, the final step is rate-determining. This step is a H transfer and so we propose that the isotope effect can be connected with this step.

From the data in Table 3 we can calculate that for the metastable ions loss of H_2O is 36% specific for the keto ions and 41% specific for the enol ions : the final entry in Table 3, for example, can be broken down into a 41% specific H_2O loss and random H_2O, HDO and D_2O losses of 32, 26 and 1%. This small increase in specificity may well indicate that the starting enol ions fragment at a slightly higher internal energy than the keto ions. This is corroborated by the finding that the kinetic energy release ($T_{0.5}$) for loss of water is slightly larger for the enol ion than for the keto ion [7]. The larger $T_{0.5}$ value cannot be taken as showing that a rate-determining isomerization precedes fragmentation of the enol ion, paralleling the behaviour of the acetamide system [27].

Baer and coworkers [8] note that the measured activation energy for loss of H_2O from ionized ethyl acetate (0.3 eV) is too small to allow the molecular ion to be metastable, unless it rearranges into a more stable form. By modelling their experimentally derived k vs E curve with standard RRKM calculations Baer and coworkers concluded that the rearranged form has a $\Delta_f H^{\circ}_{298}$ of 110 kcal mol^{-1}, which can be associated with **EA-2**, **EA-3** or **HB-2.** The slow rate constant is the result of the

participation of all the low energy isomers leading to a large density of states of the dissociating ions.

1.6. The [1,2]-hydroxycarbene shift in the distonic ion $[CH_3C(OH)OCHCH_3]^{\bullet+}$ (EA-4)

Using the energy diagram of Fig. 4b as a guide, we note that the distonic ion **EA-4** is readily accessible from **EA-1** via a low energy 1,4-H shift. The ion can communicate with **EA-2** via its conformer **EA-4c** but the TS for the associated 1,4-H shift (see Table 1a) is c. 8 kcal mol^{-1} higher in energy than that for the enolization of its slightly less stable distonic isomer **EA-3**, see Fig. 4a.

The energy diagram of Fig. 4b further shows that conformer **EA-4c** may serve as the immediate precursor for a [1,2]-hydroxycarbene shift which connects **EA-1** with the PES of the acetoin radical cation, $CH_3C(=O)CH(OH)CH_3^{\bullet+}$ (**AC-1**). This rearrangement, whose transition state lies c. 6 kcal mol^{-1} above the level for the water loss, does not contribute to the loss of water because low energy acetoin ions exclusively dissociate into $CH_3C(H)OH^+ + CH_3C{=}O^{\bullet}$. This reaction involves a remarkable hidden rearrangement - metastable ions $CH_3C(=O^{18})CH(OH)CH_3^{\bullet+}$ generate $CH_3C(H)^{18}OH^+$ and $CH_3C(H)^{16}OH^+$ in a 1:1 ratio – and a mechanism involving the hydrogen-bridged radical cation $CH_3C(=O^{18})\bullet\bullet H\bullet\bullet\bullet O{=}C(H)CH_3^{\bullet+}$ as the key intermediate has been proposed [20].

Metastable ions **EA-1** do not dissociate into $CH_3C(H)OH^+ + CH_3C{=}O^{\bullet}$ but the reaction becomes important upon collisional activation, as seen from the prominent m/z 45 peak in the CID mass spectrum of Fig. 2a. From the inset of Fig. 2a it is seen that this peak shifts almost completely to m/z 47 in the CID spectrum of $CH_3C(=O)^{18}OCH_2CH_3$. This observation is in line with the expectation that the energy rich acetoin ions $CH_3C(=O)CH(^{18}OH)CH_3^{\bullet+}$ resulting from the [1,2]-hydroxycarbene shift will not rearrange but immediately dissociate.

Baer and co-workers [8] have reported the experimental AE for this reaction, 10.70 ± 0.1 eV. They note that this value is too high to account for the threshold generation of the above products and suggest that the reaction may have a significant reverse activation barrier. From the evaluated experimental enthalpies of Table 2 and

using ΔH_{cor} = 4.7 kcal mol^{-1}, we derive a thermochemical AE of 10.46 eV, implying that a reverse barrier of c. 5.5 kcal mol^{-1} may indeed be present. Our calculations support this proposal : the barrier for the [1,2]-hydroxycarbene shift, see Fig. 4b, lies 5 kcal mol^{-1} above the dissociation level $CH_3C(H)OH^+ + CH_3C{=}O^\bullet$.

As mentioned above, metastable acetoin ions do not lose water. Nevertheless, our CBS-QB3 calculations indicate that **AC-1** can communicate with **HB-3b** of Scheme 3 at the threshold for the water loss. The barrier for the isomerization of conformer **AC-1b** into **HB-3c** lies at 139 kcal mol^{-1} while TS **HB-3c → 3b** lies at 130 kcal mol^{-1} (Table 1a/b). Thus the overall energy requirement for this rearrangement of **AC-1** is very close to that of the products formed by its direct bond cleavage into $CH_3C(H)OH^+$, 140 kcal mol^{-1}, see Table 2. However, the dynamical situation for these two reactions is very different. The rearrangement has a tight transition state, whereas the dissociation, which has no reverse activation energy, corresponds to a loose transition state. A standard RRKM calculation predicts that the excess energy needed for the rearrangement to take place in the metastable time window (10 μs) exceeds 5 kcal mol^{-1}. This is caused by the large activation energy associated with the rearrangement. For the direct bond cleavage reaction we have used the model derived from the statistical adiabatic channel theory [28]. Here the excess energy needed is less than 1 kcal mol^{-1} because the acetyl radical lost has a large dipole moment (2.5 D at the B3LYP/CBSB7 level of theory). Therefore low energy acetoin ions **AC-1** prefer the direct dissociation pathway above rearrangement into **HB-3c** and the subsequent loss of water. In the same vein, the rearrangement **HB-3b** → **AC-1** → $CH_3C(H)OH^+ + CH_3C{=}O^\bullet$ does not occur, as demonstrated by the complete shift of the m/z 45 peak to m/z 47 in the CID spectrum of ^{18}O labelled **HB-1**, see the inset of Fig. 2c.

Conclusion

Our computational study, in concert with previous and present experimental work, leads to the following mechanistic proposal for the loss of water from ionized ethyl acetate in the metastable time-frame :

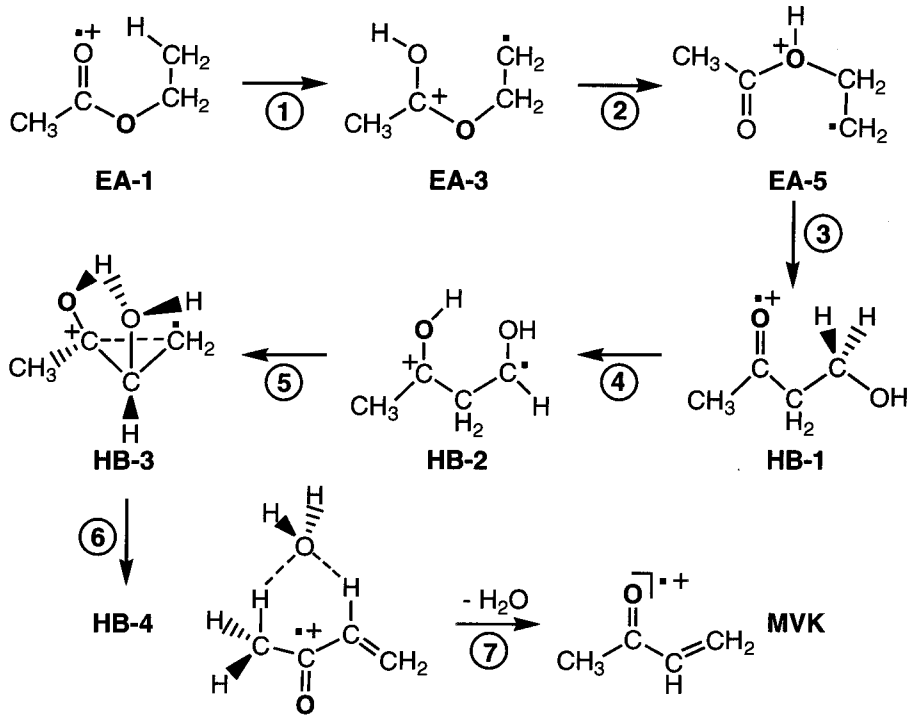

The mechanism involves seven steps. These are : (1) a 1,5-hydrogen shift in ionized ethyl acetate yielding its distonic isomer **EA-3** ; (2) an ethylene shift in **EA-3** generating another distonic ion, **EA-5** ; (3) a 1,3-acetyl shift in **EA-5** yielding a conformer of ionized 4-hydroxy-2-butanone, **HB-1** ; (4) a 1,4-hydrogen shift in **HB-1** yielding its distonic isomer **HB-2** ; (5) a 1,2-hydroxycarbene shift in **HB-2**. This step leads to **HB-3**, a one-electron long bonded species whose hydroxyl groups are bridged ; (6) a formal 1,4-hydrogen shift in which the bridging hydrogen moves to the adjacent hydroxyl group to form the water molecule of the ion-dipole complex **HB-4**. This step is rate-determining and may account for the kinetic H/D isotope effect ; and (7) dissociation into ionized methyl vinyl ketone and a water molecule.

Each step is a simple transformation in itself and all consecutive steps yield a transparent picture of the seemingly complex dissociation behaviour of ionized ethyl

acetate. Our mechanism satisfies the energetic constraints imposed by experiment and provides a rationale for the ^{18}O- and D-labelling results.

References

1. E.W. Godbole and P. Kebarle. Trans. Faraday Soc. 58, 1897 (1962).
2. F.M. Benoit, A.G. Harrison, and F.P. Lossing. Org. Mass Spectrom. 12,78 (1977).
3. C.G. de Koster, J.K. Terlouw, K. Levsen, H. Halim, and H. Schwarz. Int. J. Mass Spectrom. Ion Processes. 61, 87 (1984).
4. J.L. Holmes and F.P. Lossing. J. Am. Chem. Soc. 102, 1591 (1980).
5. F.W. McLafferty and F. Turecek. Interpretation of mass spectra. University Science Books, Mill Valley, CA 94941. 1993 (Fourth Edition). p. 81.
6. A.N.H. Yeo. J. Chem. Soc. Chem. Commun. 1154 (1970).
7. J.L. Holmes, P.C. Burgers, and J.K. Terlouw. Can. J. Chem. 59, 1805 (1981).
8. L. Fraser-Monteiro, M.L. Fraser-Monteiro, J. Butler, and T. Baer. J. Phys. Chem. 86, 752 (1982).
9. (*a*) J.L. Holmes and J.K. Terlouw. Org. Mass. Spectrom. 15, 383 (1980) ; (*b*) J.L. Holmes *In* Encyclopedia of mass spectrometry. Vol. 1. *Edited by* P.B. Armentrout. Elsevier, Amsterdam. 2004. p. 91.
10. (*a*) S. Hammerum. Mass Spectrom. Rev. 7, 123 (1988); (*b*) P.C. Burgers and J.K. Terlouw. *In* Specialist periodical reports : mass spectrometry. Vol. 10. *Edited by* M.E. Rose. The Royal Society of Chemistry, London. 1989. Chapter 2.
11. J.L. Holmes and J.K. Terlouw. *In* Encyclopedia of mass spectrometry. Vol. 4. *Edited by* N.M.M. Nibbering. Elsevier, Amsterdam. 2005. p. 287.
12. (*a*) S.G. Lias, J.E. Bartmess, J.F. Liebman, J.L. Holmes, R.O. Levin, and W.G. Maillard. J. Phys. Chem. Ref. Data, Suppl.1, 17 (1988) ; (*b*) NIST Chemistry WebBook, April 2005, National Institute of Standards and Technology, Gaithersburg MD, 20899 (http://webbook.nist.gov) ; (*c*) E.P.L. Hunter and S.G. Lias. J. Phys. Chem. Ref. Data 27, 413 (1998) ; (*d*) Yu-Ran Luo. Handbook of dissociation energies in organic compounds. CRC Press, Boca Raton. 2003 ; (*e*) N. Cohen and S.W. Benson. Chem. Rev. 93, 2419 (1993)
13. (*a*) J.K. Terlouw, W. Heerma, J.L. Holmes, and P.C. Burgers. Org. Mass. Spectrom. 15, 582 (1980) ; (b) C. Dass and M.L. Gross. Org. Mass. Spectrom. 25, 24 (1990).
14. N. Heinrich, J. Schmidt, H. Schwarz, and Y. Apeloig. J. Am. Chem. Soc. 109, 1317 (1987).
15. P.C. Burgers and J.K. Terlouw. *In* Encyclopedia of mass spectrometry. Vol. 4. *Edited by* N.M.M. Nibbering. Elsevier, Amsterdam. 2005. p. 173.
16. (*a*) L.A. Curtiss, K. Raghavachari, G.W. Trucks, and J.A. Pople. J. Chem. Phys. 98, 1293 (1993); (*b*) L.A. Curtiss, K. Raghavachari, P.C. Redfern, V. Rassolov, and J.A. Pople. J. Chem. Phys. 109, 7764 (1998) ; (*c*) A.G. Baboul, L.A. Curtiss, and P.C. Redfern. J. Chem. Phys. 110, 7650 (1999).
17. (*a*) J.W. Ochterski, G.A. Petersson, and J.A. Montgomery, Jr. J. Chem. Phys. 104, 2598 (1996). (*b*) J.A. Montgomery, Jr, M.J. Frisch, J.W. Ochterski, and G.A. Petersson. J. Chem. Phys. 112, 6532 (2000).
18. (*a*) L.N. Heydorn, Y. Ling, G. de Oliveira, J.M. Martin, C.L. Lifshitz, and J.K. Terlouw. Z. Physikalische Chemie. 215, 141 (2001) ; (*b*) L.N. Heydorn, P.C. Burgers, P.J.A. Ruttink, and J.K. Terlouw. Int. J. Mass Spectrom. Ion Processes. 228, 759 (2003).
19. C.Y. Wong, P.J.A. Ruttink, P.C. Burgers, and J.K. Terlouw. Chem. Phys. Lett. 387, 204 (2004) and references cited therein.
20. D. Suh, P.C. Burgers, and J.K. Terlouw. Int. J. Mass Spectrom. Ion Processes. 144, L1 (1995).
21. (*a*) J.C. Traeger and R.G. McLoughlin. J. Am. Chem. Soc. 103, 3647 (1981) ; (*b*) J.C. Traeger, R.G. McLoughlin, and A.J.J. Nicholson. J. Am. Chem. Soc. 104, 5318 (1982) ; (*c*) J.L. Holmes, F.P. Lossing, and P.M. Mayer. J. Am. Chem. Soc. 113, 9723 (1991) ; (*d*) F. Turecek and C.J. Cramer. J. Am. Chem. Soc. 117, 12243 (1995) ; (*e*) H. Ervasti, P.C. Burgers, and P.J.A. Ruttink. Eur. J. Mass Spectrom. 10, 791 (2004).
22. From unpublished EI results of the late Dr F.P. Lossing (J.L. Holmes, personal communication 2005).

23. (*a*) T. Baer, W.A. Brand, T.L. Bunn, and J.J. Butler. Farad. Disc. Chem. Soc. 75, 45 (1983) ; (*b*) T. Baer and W.L. Hase. Unimolecular reaction dynamics. Oxford University Press, New York. 1996.
24. (*a*) J.K. Terlouw, W. Heerma, and G. Dijkstra. Org. Mass Spectrom. 16, 326 (1981). (*b*) D.J. McAdoo and C.E. Hudson. Org. Mass Spectrom. 21, 779 (1986).
25. R. Flammang, M.T. Nguyen, G. Bouchoux, and P. Gerbaux. Int. J. Mass Spectrom. 202, A8 (2000).
26. L.K.M. Kiminkinen, L.C. Zeller and H.I. Kenttämaa. Chem. Commun. 466 (1992).
27. M.A. Trikoupis, P.J.A. Ruttink., P.C. Burgers, and J.K. Terlouw. Eur. J. Mass Spectrom. 10, 801 (2004).
28. P.J.A. Ruttink. J. Phys. Chem. 91, 703 (1987).
29. H.F. van Garderen, P.J.A. Ruttink, P.C. Burgers, G.A. McGibbon, and J.K. Terlouw. Int. J. Mass Spectrom. Ion Proc. 121, 159 (1992).
30. Gaussian 03, Revision C.02, M. J. Frisch, G. W. Trucks, H. B. Schlegel, G. E. Scuseria, M. A. Robb, J. R. Cheeseman, J. A. Montgomery, Jr., T. Vreven, K. N. Kudin, J. C. Burant, J. M. Millam, S. S. Iyengar, J. Tomasi, V. Barone, B. Mennucci, M. Cossi, G. Scalmani, N. Rega, G. A. Petersson, H. Nakatsuji, M. Hada, M. Ehara, K. Toyota, R. Fukuda, J. Hasegawa, M. Ishida, T. Nakajima, Y. Honda, O. Kitao, H. Nakai, M. Klene, X. Li, J. E. Knox, H. P. Hratchian, J. B. Cross, V. Bakken, C. Adamo, J. Jaramillo, R. Gomperts, R. E. Stratmann, O. Yazyev, A. J. Austin, R. Cammi, C. Pomelli, J. W. Ochterski, P. Y. Ayala, K. Morokuma, G. A. Voth, P. Salvador, J. J. Dannenberg, V. G. Zakrzewski, S. Dapprich, A. D. Daniels, M. C. Strain, O. Farkas, D. K. Malick, A. D. Rabuck, K. Raghavachari, J. B. Foresman, J. V. Ortiz, Q. Cui, A. G. Baboul, S. Clifford, J. Cioslowski, B. B. Stefanov, G. Liu, A. Liashenko, P. Piskorz, I. Komaromi, R. L. Martin, D. J. Fox, T. Keith, M. A. Al-Laham, C. Y. Peng, A. Nanayakkara, M. Challacombe, P. M. W. Gill, B. Johnson, W. Chen, M. W. Wong, C. Gonzalez, and J. A. Pople, Gaussian, Inc., Wallingford CT, 2004.
31. GAMESS-UK is a package of ab initio programs written by M.F. Guest, J.H. van Lenthe, J. Kendrick, K. Schoffel, and P. Sherwood, with contributions from R.D. Amos, R.J. Buenker, H.J.J. van Dam, M. Dupuis, N.C. Handy, I.H. Hillier, P.J. Knowles, V. Bonacic-Koutecky, W. von Niessen, R.J. Harrison, A.P. Rendell, V.R. Saunders, A.J. Stone, D.J. Tozer, and A.H. de Vries. The package is derived from the original GAMESS code due to M. Dupuis, D. Spangler, and J. Wendolowski, NRCC Software Catalogue 1, Vol. 1, Program No. QG01 (GAMESS) (1980).

Appendix for Chapter 4

Table 4. A comparison between energetic data derived from the CBS-QB3, G3B3 and G3 with experiment data for selected ions and neutrals in the ethyl acetate system of ions.

	CBS $\Delta_f H^0_{298}$	ZPE	G3B3 $\Delta_f H^0_{298}$	ZPE	G3 $\Delta_f H^0_{298}$	ZPE	Exp. $\Delta_f H^0_{298}$
EA-1a	126.5	71.2	122.4	69.8	126.5	70.4	125
HB-1a	124.2	72.6	120.3	71.0	cannot optimize		
HB-1b	130.3	71.5	125.9	69.8	130.7	69.9	
HB-2a	114.5	72.1	110.4	70.2	optimizes to HB-2b		
TS HB-1b/2a	125.9	70.1	121.8	68.1	cannot find this TS		
$CH_3C(=O)CH=CH_2$	-25.8	55.3	-29.8	54.1	-26.4	54.0	-27.4
$CH_3C(=O)CH=CH_2^{\bullet+}$	197.4	54.2	193.2	53.1	197.0	53.2	195
$CH_3C(H)OH^+$	142.2	45.5	140.7	41.4	142.7	41.3	142.4
$CH_2CH_2OH^{\bullet}$	-6.1	40.4	-7.9	38.9	-5.6	39.0	-7
$CH_3CH_2O^{\bullet}$	-3.5	39.8	-6.2	38.9	-3.2	39.3	-3.6
$CH_3C{\equiv}O^+$	158.0	27.6	155.4	27.0	157.8	27.0	157
$CH_3C{\equiv}O^{\bullet}$	-2.5	26.7	-4.5	26.2	-2.5	26.1	-2.4
$CH_3C(OH)_2^+$	74.3	46.0	72.0	44.8	74.9	44.8	75
CH_3COOH	-104.3	38.3	-106.3	37.4	-106.8	37.5	-103.3
$CH_2{=}CH^{\bullet}$	71.7	22.6	69.2	22.1	70.6	21.7	71.6
$CH_3C(OH){=}CH_2^{\bullet+}$	163.0	51.6	161.3	50.4	163.4	50.2	163.4
$CH_2{=}O$	-27.3	16.5	-28.3	16.2	-26.6	16.4	-26.0

Fig. 5. The CBS-QB3 optimized geometries for ionized 4-hydroxy-2-butanone, **HB-1**, and ethyl acetate, **EA-1**, isomers and selected transition states.

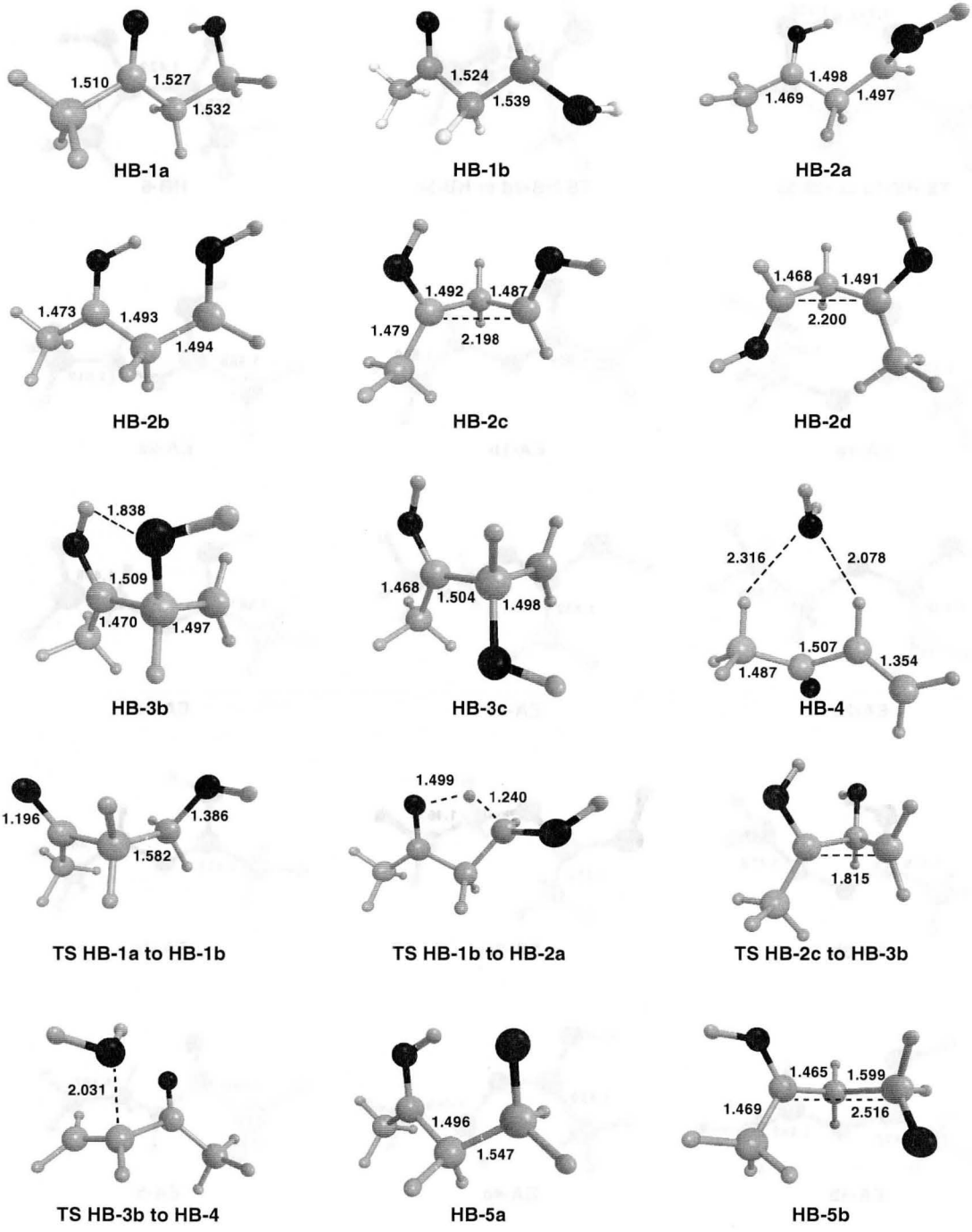

Fig. 5. ctd. (1)

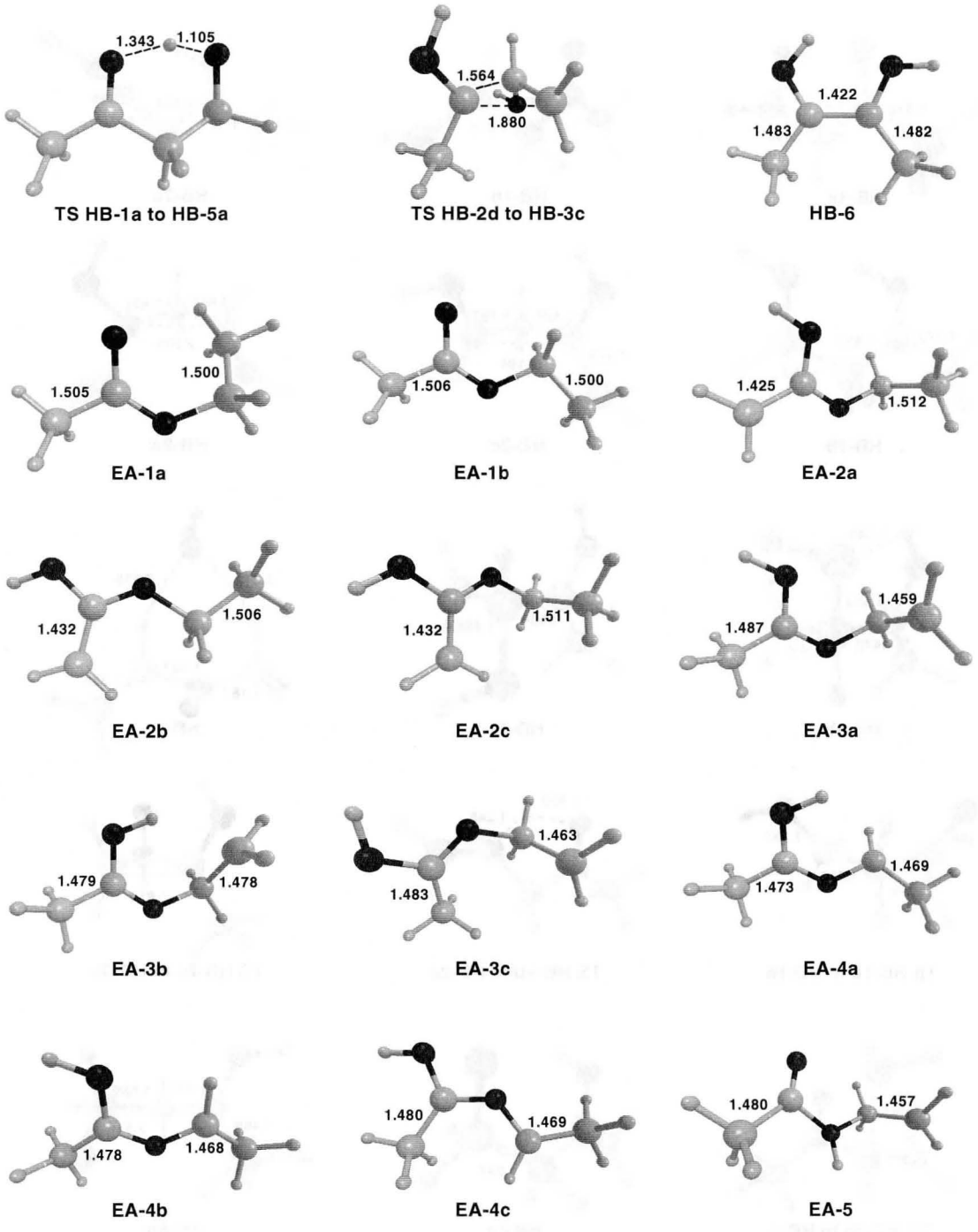
1.343
1.105
TS HB-1a to HB-5a
1.564
1.880
TS HB-2d to HB-3c
1.422
1.483
1.482
HB-6
1.505
1.500
EA-1a
1.506
1.500
EA-1b
1.425
1.512
EA-2a
1.432
1.506
EA-2b
1.432
1.511
EA-2c
1.487
1.459
EA-3a
1.479
1.478
EA-3b
1.483
1.463
EA-3c
1.473
1.469
EA-4a
1.478
1.468
EA-4b
1.480
1.469
EA-4c
1.480
1.457
EA-5

Fig. 5. ctd. (2)

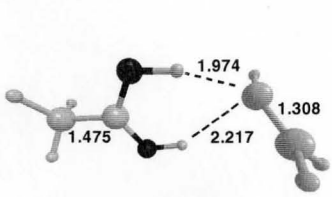

EA-6a

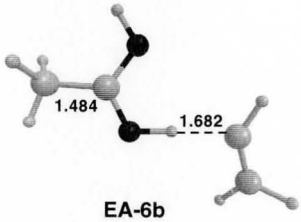

EA-6b

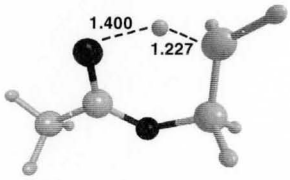

TS EA-1a to EA-3b

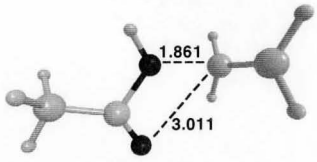

TS EA-3a to EA-5

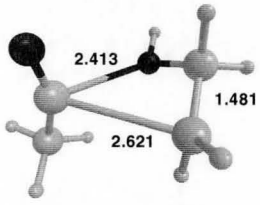

TS EA-5 to HB-1b

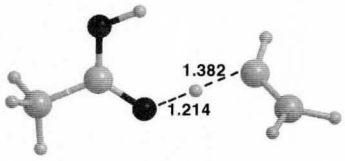

TS EA-3b to EA-6a

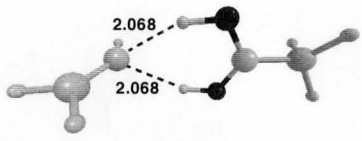

TS EA-6a to EA-6a

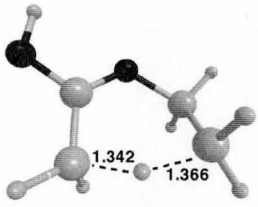

TS EA-3c to EA-2b

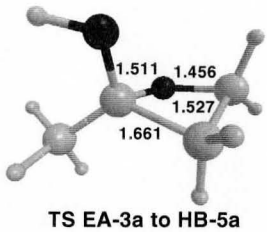

TS EA-3a to HB-5a

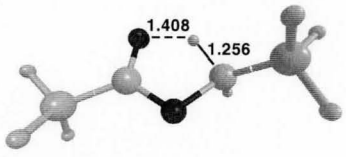

TS EA-1b to EA-4a

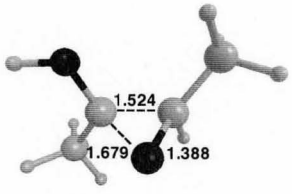

TS EA-4c to AC-2a

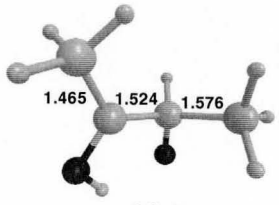

AC-2a

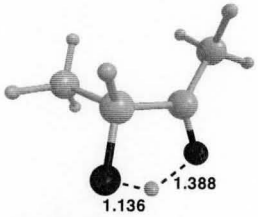

TS AC-2a to AC-1a

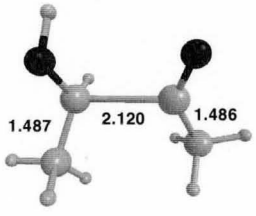

AC-1a

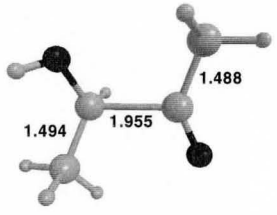

AC-1b

SUMMARY

The research presented in this thesis is focused on an integrated computational chemistry and mass spectrometric approach to solve complex dissociation mechanisms of radical cations in the gas-phase.

In Chapter 2a, it is shown that computational chemistry and tandem mass spectrometry based experiments allow for the study of proton-transport catalysis in the formaldehyde elimination of low energy 1,3-dihydroxyacetone radical cations. Theory predicts that solitary ketene-water ions, $CH_2=C(=O)OH_2^{\bullet+}$, and $CH_2=C(OH)_2^{\bullet+}$ are separated by a high energy barrier so that their unassisted interconversion does not occur. A mechanistic analysis using the CBS-QB3 model chemistry showed that metastable 1,3-dihydroxyacetone radical cations rearranged into the HBRC $[CH_2C(=O)O(H)–H\bullet\bullet\bullet OCH_2]^{\bullet+}$, where the $CH_2=O$ catalyzed the transformation of $CH_2=C(=O)OH_2^{\bullet+}$ into $CH_2=C(OH)_2^{\bullet+}$.

Chapter 2b described the dissociation of metastable pyruvic acid radical cations, $CH_3C(=O)COOH^{\bullet+}$, into m/z 44 ions, $C_2H_4O^{\bullet+}$, via decarboxylation, in competition with the formation of $CH_3C=O^+ + COOH^{\bullet}$ by direct bond cleavage. Metastable ion spectrum of ionized pyruvic acid indicated that generation of $CH_3C=O^+$ is preferred. The collision-induced dissociation experiments suggest that m/z 44 ions have structure connectivity of oxycarbene ions $CH_3COH^{\bullet+}$ but they also suggest the more stable isomer $CH_3C(H)=O^{\bullet+}$ may be co-generated. Computational results predicted that the oxycarbene ion should be equally likely to be generated as $CH_3C=O^+$ further kinetic analysis is required.

In chapter 3, the isomeric ions $CH_3O\text{-}P=S^{\bullet+}$ and $CH_3S\text{-}P=O^{\bullet+}$ were characterized and differentiated by tandem mass spectrometry. Metastable ion spectra of $CH_3O\text{-}P=S^{\bullet+}$ and $CH_3S\text{-}P=O^{\bullet+}$ ions show that water elimination is the most prominent reaction to yield m/z 74 cyclic product ion $[\text{-}S\text{-}CH=]P^{\bullet+}$. The CBS-QB3 derived mechanism showed that these two isomers communicate via a common intermediate, the distonic ion $CH_2S\text{-}P\text{-}OH^{\bullet+}$, prior to the loss of water.

Finally, in Chapter 4, it was shown that computational chemistry played an integral role in the elucidation of the mechanism for the water elimination from

metastable ethyl acetate ions. Metastable ethyl acetate ions yield ionized methyl vinyl ketone and water. Theory suggests that prior to the water loss, ethyl acetate radical cations rearranges into ionized 4-hydroxy-2-butanone, where it proceeds to lose water.